Bachelorarbeit

zur Erlangung

des akademischen Grades

Bachelor of Engineering (B.Eng.)

"Thermal and Mechanical Investigation of a Preload Release Mechanism for a Space Probe under Laboratory Conditions"

angefertigt im

Fachbereich Maschinenbau und Verfahrenstechnik

Hochschule Niederrhein

vorgelegt von

Christoph Freukes

Matr.-Nr.: 728338

Studiengang: Maschinenbau

Betreuender Professor: Prof. Dr.-Ing. Hader

Krefeld, im April 2013

Hochschule Niederrhein
University of Applied Sciences

Maschinenbau und Verfahrenstechnik
Faculty of Mechanical and Process Engineering

Kurzfassung der Bachelorarbeit

Titel der Arbeit:	Thermale und mechanische Untersuchung eines Vorspannungsabbau Mechanismus für eine Raumsonde unter Labor-bedingungen
Verfasser der Arbeit:	Christoph Freukes
Matr.-Nr.	728338
Betreuender Professor:	Prof. Dr.-Ing. Hader
Zweiter Prüfer:	Prof. Dr.-Ing. Unger
Betreuende Einrichtung:	Deutsches Zentrum für Luft- und Raumfahrt, Institut für Raumfahrtsysteme, Abteilung Explorationssysteme
	Dipl. Ing. Eugen Ksenik (FH)
	MSc, MSc Christian D. Grimm

Kurzfassung der Arbeit:

Der Vorspannungsabbau Mechanismus der Asteroidenlandeeinheit MASCOT soll auf seine Funktionalität untersucht werden. Dazu muss ein Teststand entwickelt werden. Zusätzlich soll der Mechanismus derart verändert werden, dass der Erfolg des Abbauvorganges während des Fluges überprüft werden kann.

Stichwörter zum Thema:

Abgabe der Arbeit: 22.04.2013

Hochschule Niederrhein
University of Applied Sciences

Maschinenbau
und Verfahrenstechnik
Faculty of Mechanical and Process Engineering

Eidesstattliche Erklärung

Ich versichere durch meine Unterschrift, dass die vorliegende Bachelorarbeit ausschließlich von mir verfasst wurde.

Es wurden keine anderen als die von mir angegebenen Quellen und Hilfsmittel benutzt.

Die Arbeit besteht aus 47 Seiten (ohne Anhang).

Krefeld, im April 2013

.....

(Unterschrift

Confidentiality clause

This bachelor thesis contains confidential data of the German Aerospace Center. This work may only be made available to the first and second reviewers and authorized members of the board of examiners. Any publication and duplication of this bachelor thesis - even in part - is prohibited. An inspection of this work by third parties requires the expressed permission of the German Aerospace Center.

Foreword

An dieser Stelle möchte ich mich bei allen Personen bedanken, die mich bei der Erstellung meiner Bachelorarbeit unterstützt haben.

Besonders möchte ich mich bei Herrn Dr. Tim van Zoest für die Möglichkeit bedanken, beim DLR-Institut für Raumfahrtsysteme in Bremen in seiner Abteilung Explorationssysteme diese Bachelorarbeit anzufertigen. Durch die freundliche und engagierte Betreuung hat mir meine Abschlussarbeit viel Freude bereitet.

Außerdem möchte ich mich bei Herrn Dipl. Ing. Eugen Ksenik (FH) und Herrn

MSc, MSc Christian D. Grimm bedanken, die mir im Laufe der Bachelorarbeit immer mit Rat und Tat zur Seite standen und die Arbeit mit guten Ideen und unermüdlichem Einsatz betreut haben.

Mein Dank gilt außerdem allen Mitarbeitern der Abteilung Explorationssysteme sowie den Mitarbeitern des Zarm, die mich während der Erstellung dieser Arbeit fachlich unterstützt haben.

Vor allem bedanke ich mich bei meiner Familie, ohne die mein Studium nicht möglich gewesen wäre.

Table of Content

List of Figures

List of Tables

List of Abbreviations

CNES	Centre National d'Etudes Spatiales (French Aerospace Center)
DLR	German Aerospace Center
ECSS	European Cooperation for Space Standardization
ESA	European Space Agency
Fig.	Figure
GNC	Guidance Navigation Control
HP3	Heat Flow and Physical Properties Package
HSNR	Hochschule Niederrhein
IAS	Institut Aéronautique et Spatial
IR sensor	Infrared Sensor
JAXA	Japan Aerospace Exploration Agency
MASCOT	Mobile Asteroid Surface Scout
MESS	Mechanical and Electrical Support System
NEA	Non Explosive Actuator
PCDU	Payload Command Decoder Unit
PRM	Preload Release Mechanism
ROBEX	Robotic Exploration of Extreme Environments
Tab.	Table

1 Introduction and Purpose

This chapter provides an overview about the Hayabusa-II mission and the therefore developed lander “MASCOT” (Mobile Asteroid Surface Scout), particularly the significance of the Preload Release Mechanism (PRM), which will be investigated and described in this bachelor thesis, as well as the scientific background of the mission. Sources used in this chapter and can be found in Annex: [1], [2] and [3].

1.1 Motivation

The genesis of life on earth is yet to be clarified. To find explanations how simple atoms could develop to higher molecules asteroid missions are of great weight.

Asteroids are small celestial planets of solid material remaining from the earliest epoch of Solar System formation process. They are orbiting the sun and are also called planetoids. They formed from the same protoplanetary disk as the Sun and the major planets a few 4.569 billion years ago and are made from the same material. The formation of the asteroids took only a few million years. Asteroids have never been part of a single planetary parent. They were prevented from aggregating together by the gravitational influence of Jupiter, which pulled the bodies apart. Jupiter is still the major factor which dominates the dynamics and structure of the asteroid belt. Mars plays a lesser but still important role. Asteroids can provide information about the accretion, differentiation and subsequent evolution of the Solar System and its materials. By studying the origin and composition of asteroids we can gain a better understanding of primitive materials that formed the Solar System.

In this respect the advantage of lander-based exploration is that it is less constrained in spatial resolution and temporal coverage than an orbiting spacecraft. The instruments on a lander can take detailed close-up images as well as making a variety of measurements at high spatial resolution or over an extended period of time. Materials can be studied by the lander instruments immediately in theirs natural environment.

Lander-based exploration has taken a major place in the history of Solar System Science since it is the crucial link between remote sensing observations and the analyses of returned samples. Looking back at past missions and looking forward to future ones to Moon and Mars the scientific motivation for all three mission types is justified. In this context the Hayabusa-II mission (see chapter 1.2) with its present configuration of an orbiter, an impactor, sample return and two landers, the micro-rover MINERVA and the mobile asteroid surface scout MASCOT, fit perfectly into the roadmap of the Solar System Exploration. So does the chosen target asteroid (see Fig. 1-1).

Fig. 1-1: Picture of the asteroid 199 JU3 (Ref. [1])

Remote sensing instruments, operated from the orbiting space-craft, will give macroscopic information of the asteroid, describing its overall characteristics and environment and thus enabling the selection of an optimized area where samples can be collected. In-situ information on the object at micro-scale is only accessible by the scientific payload onboard a lander. In this connection the instrument package will have the means to characterize physical properties (e.g. electrical, magnetic, and thermal) of the landing site as well as its surface and subsurface fine structure and composition (elemental, mineralogical, molecular). Therefore combined orbital and in-situ measurements will ensure a thorough characterization of the selected asteroid in a manner never achieved until now. These two types of instruments will provide unprecedented insights in

the composition and properties of a primitive body, from its macroscopy down to its microscopy. By themselves they can ensure a significant mission success.

The uniqueness of the Hayabusa-II (see Fig. 1-2) mission, with respect to the meteoritic studies performed for decades, is its capability to relate the measurements performed on the returned samples to the properties of its parent body. Although, observations from the orbiter can ensure a thorough determination of the surrounding in which the samples are taken. Key questions could be answered such as: Are the returned soils and rocks representative of the bulk of the parent body or are they sampling specific units, made of pristine materials or alteration and/or weathering products? What are the macroscopic physical properties of the terrain from which the samples have been extracted? To which extent did the processes involve in returning the samples have modified at least partly their properties and composition?

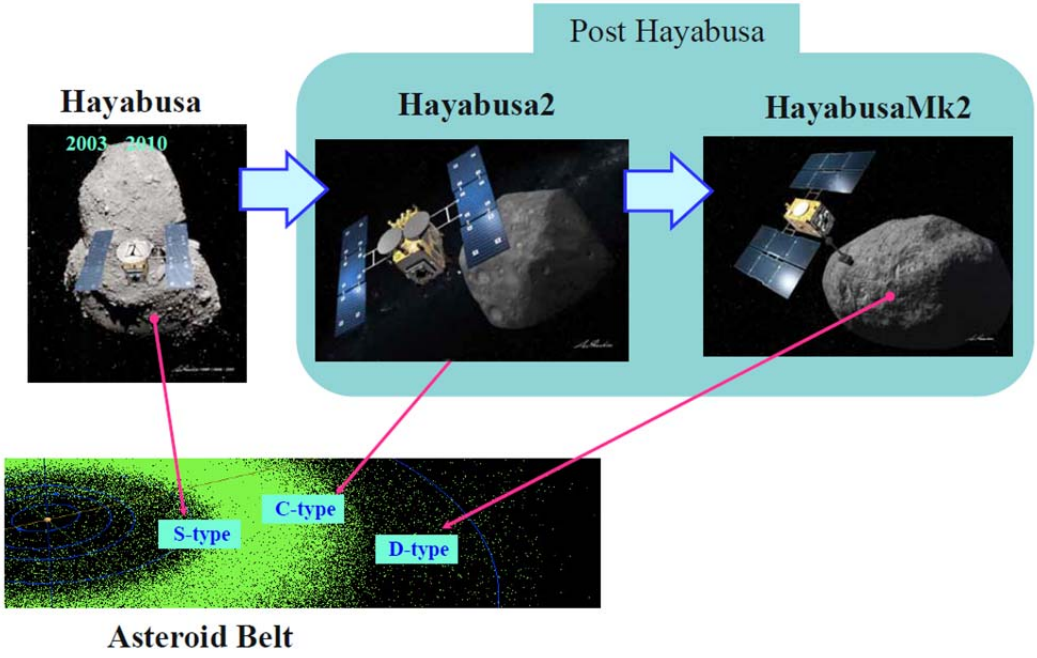

Fig. 1-2: Primitive body exploration program considered in Japan (Ref. [2])

The Lander package therefore is not a complement to be implemented if resources are sufficient: It represents an essential component of the mission, providing unique information that will depart the Hayabusa-II samples from all extraterrestrial ones collected so far. The analyses of the returned samples of the Hayabusa-II can merge two sites with its associated potential for seminal discoveries. With the “extraterrestrial matter” scientists are capable of

deciphering fundamental astrophysical clues from analyses at a grain scale and the “space builders” have acquired an impressive skill in designing and building miniaturized instruments with ultimate performances for in-situ characterization of an asteroid.

1.2 Mission description Hayabusa-II

In this context the Japanese space agency JAXA plans a sample return mission to the asteroid 1999 JU3. The mission is currently named Hayabusa-II and is the successor of the Hayabusa mission. As mentioned its main goal is to bring soil samples of the asteroids surface to Earth. After the Hayabusa mission examined an asteroid of type S (S=Silicate) now, for the first time, a C-Type (C=Carbon) asteroid shall be investigated in such a detail.

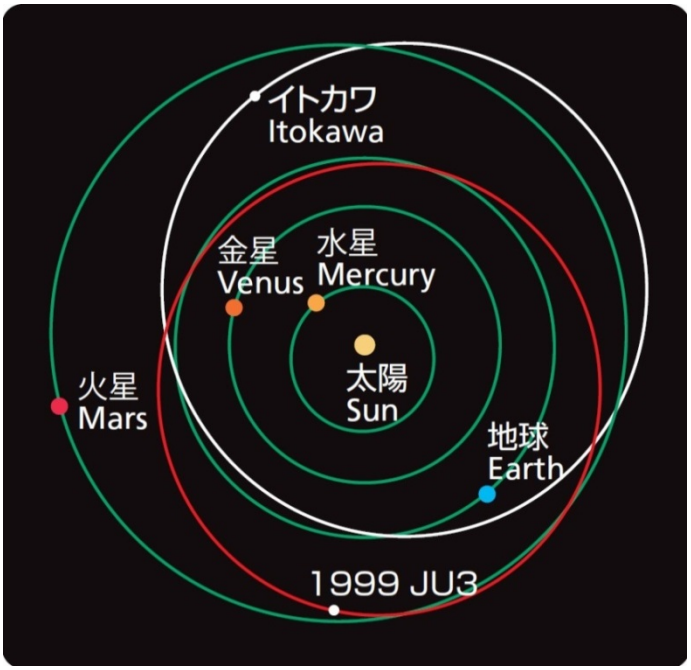

Fig. 1-3: Orbit of the asteroid 1999 JU3 (Ref. [2])

The spacecraft (see Fig. 1-4) shall be launched at the end of 2014 towards the target asteroid (see Fig. 1-3). The arrival is expected at the end of 2018 after four years flight duration. This is enabled with the aid of an ion drive, which are characterized by low energy consumption. After the Hayabusa-II arrived at the target asteroid it will remain about one year in orbit before releasing a small landing package called MASCOT (see chapter 1.3) which carries out in-situ investigations. In the next step soil samples shall be taken by the main

spacecraft with the aid of an impactor. The Hayabusa-II is expected to return to Earth at the end of 2020.

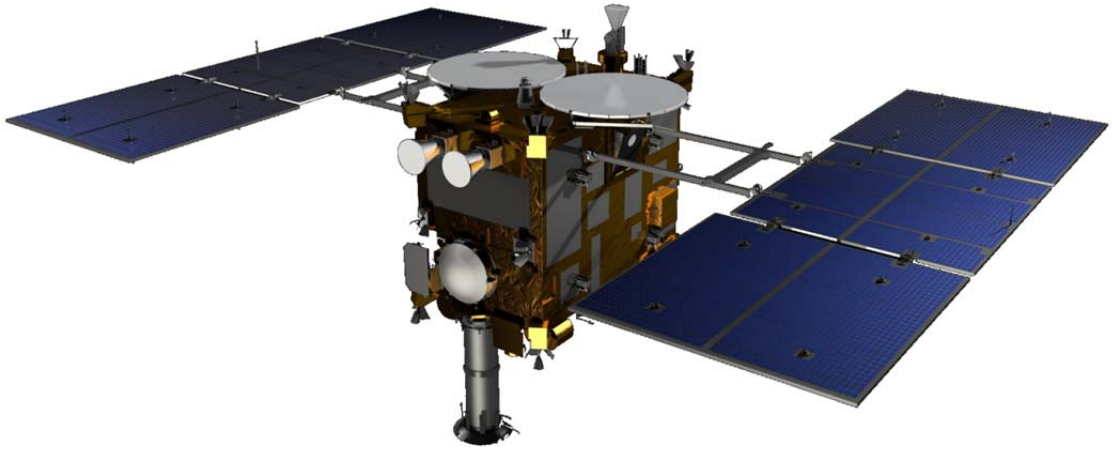

Fig. 1-4: Rendered Picture of the Hayabusa-II (Ref. [1])

1.3 Mobile Asteroid Surface Scout (MASCOT)

The general concept of MASCOT is to provide a small landing module intended to be deployed from the main spacecraft Hayabusa-II (“mothership”) on an asteroid mission. It is specifically designed to be compatible with the Hayabusa-II mission design and the environment given by asteroid 1999 JU3 as chosen target asteroid. It is developed by DLR, IAS, CNES and JAXA.

MASCOT´s has a total weight of 10kg and is about shoebox size. It has a payload of 3 kg (including margins) onboard which consists of a suite of instruments (see Fig. 1-5). These instruments are:

- MicrOmega (1): A near infrared hyper spectral microscope, which is designed to characterize the asteroid surface composition at its grain scale. It is developed by “IAS”.
- MARA (2): A radiometer which shall detect the surface temperature and its mineral composition. It is developed by the “DLR Institute of Planetary Research”.

- Magnetometer (3): The radiometer shall measure the magnetization of the asteroid if it exists. It is developed by the “Technical University Braunschweig”.
- Camera (4): The camera has various tasks. It shall support the movement operations (“hopping”), take panchromatic high resolution images of the landing site. It is although developed by the “DLR Institute of Planetary Research”.

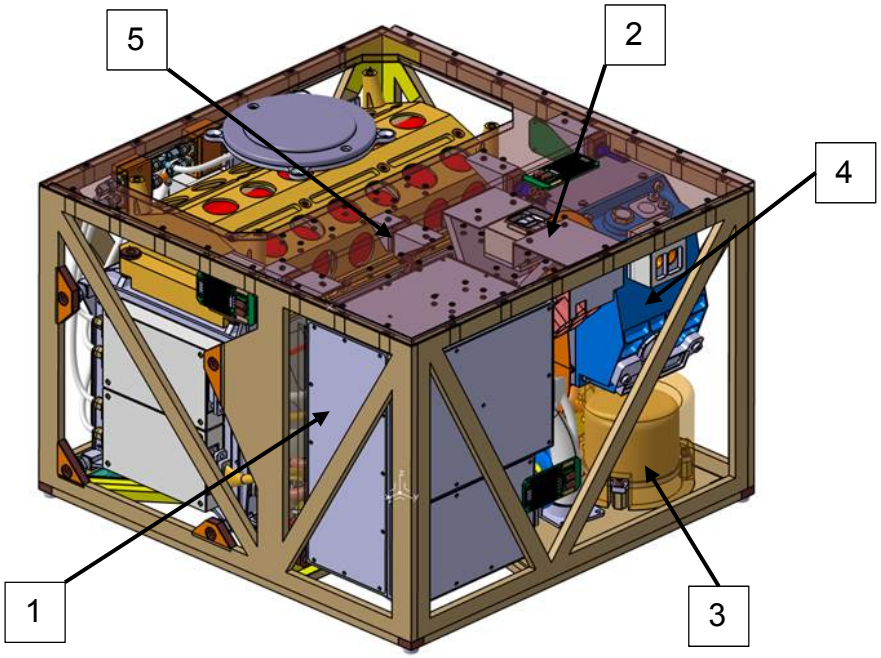

Fig. 1-5: CAD-Model of MASCOT (Ref. [1])

Furthermore MASCOT is equipped with a unique mobility mechanism (see Fig. 1-5 and Fig. 1-6 Nr. 5). By driving an internal eccentric mass to provide a respective momentum MASCOT is enabled to move. With this mechanism MASCOT can fulfill two functions:

- Providing the capability to upright and to correct MASCOTs attitude after landing to enable optimum measurements.
- Relocate MASCOT by hopping to increase the spatial resolution of the measurements and allow several monitoring wells

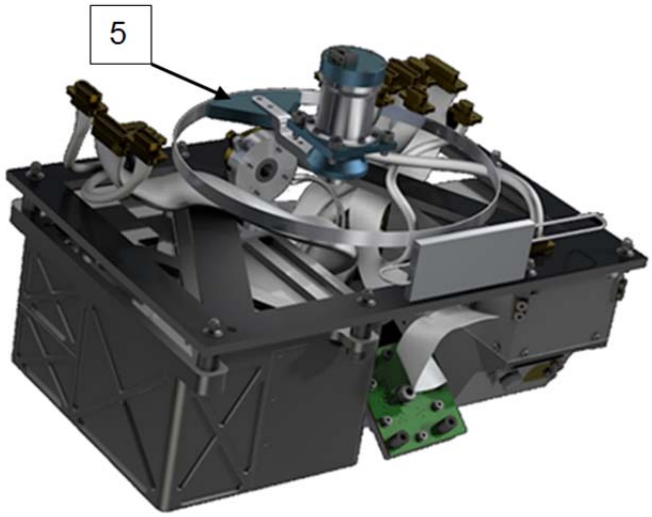

Fig. 1-6: Rendered picture of MASCOT showing the mobility mechanism (Ref. [1])

The operational scenario of MASCOT foresees two hopping and up-righting operations within only 16hrs (two full asteroid day / night cycles) service life. Due to the short lifetime on the asteroid´s surface it is foreseen to conduct all surface operations autonomously, without any intervention from Earth.

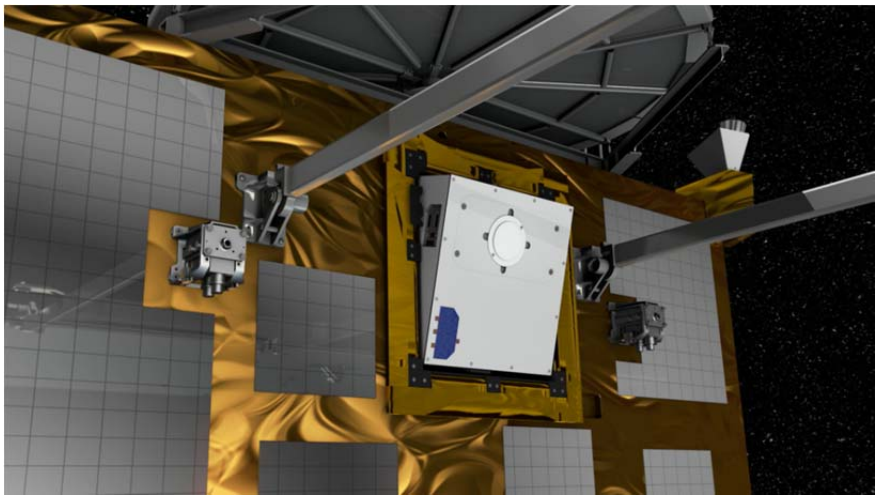

Fig. 1-7: Rendered picture of Hayabusa-II and MASCOT for clarification of the mounting position (Ref. [2])

MASCOT will be integrated in a Mechanical and Electrical Support System (MESS) which serves as interface between the spacecraft Hayabusa-II and MASCOT. It is needed because of the special mounting position (see Fig. 1-7) at the spacecraft. The MESS will be mounted to Hayabusa-II and will remain there even after MASCOT is released.

2 State of the Art

This chapter describes the current state of MASCOT´s separation device. This includes the Separation Mechanism, the Preload Release Mechanism and its components. Sources used: [1], [2] and [3].

2.1 Separation Mechanism of MASCOT

The MASCOT accommodation to the MESS and associated Separation Mechanism is based on four stand-off elements (see Fig. 2-1 for a principal sketch) for lateral guidance, one Non-Explosive Actuator (NEA), a push-off plate as well as a spring for ejection. In this interface design, a required preload force has to be guaranteed to ensure contact in the stand-off elements under all mechanical environments, especially for the launch phase.

When the NEA is activated, a compression spring drives a push-plate, which ejects MASCOT from the MESS into its landing trajectory. The potential energy stored in the compressed spring corresponds to MASCOT's required kinetic energy for ejection (kinetic energy = potential energy). The Separation Mechanism is specially designed to enable a landing speed of 5cm/s.

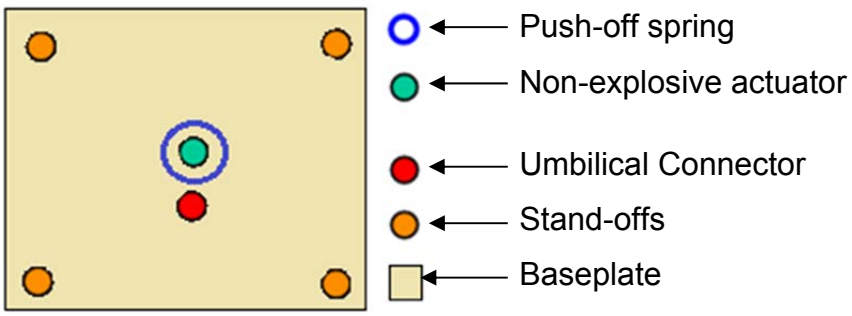

Fig. 2-1: Principle of MASCOT to MESS interface elements (Ref. [1])

A detailed design view of the separation mechanism and its position in MASCOT within the MESS is depicted in the Fig. 2-2 and Fig. 2-3. The design of the push-plate and its linear guidance is done according to ECSS mechanisms design and space tribology. Further it is designed to minimize alignment errors and to avoid cold welding.

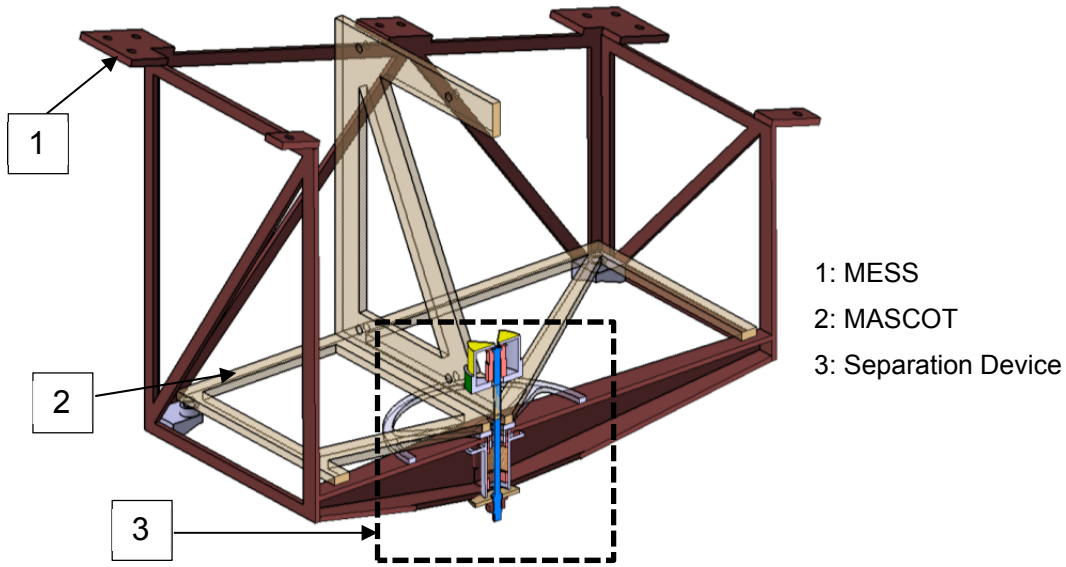

Fig. 2-2: Cut-View of the Push-off Assembly (Ref. [1])

In Fig. 2-3 the separation device is depicted in detail. As can be seen the PRM is not integrated yet. Conceptually, it should be mounted under the NEA within MASCOT, marked by the red border strip. The integration and dimensioning of the PRM is facilitated by several through holes of the NEA.

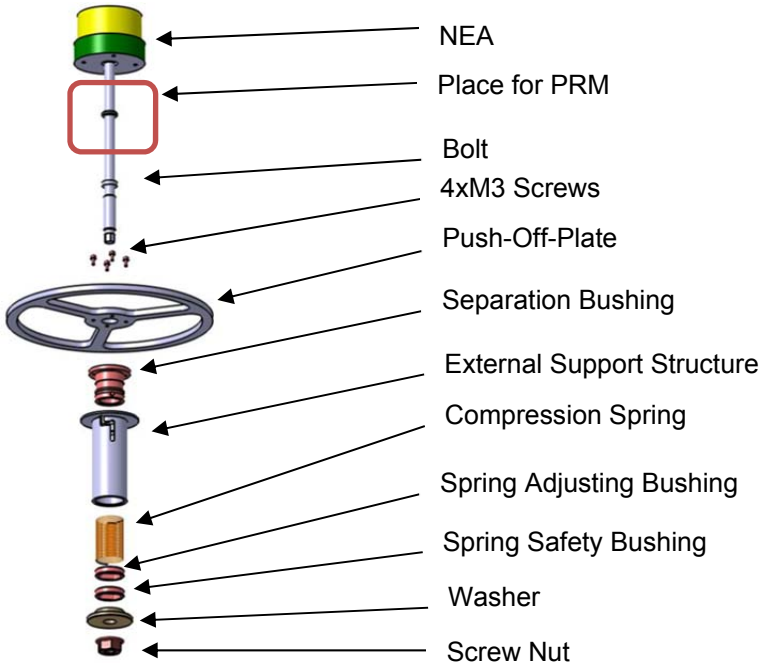

Fig. 2-3: Detailed view of the Separation Mechanism and its components (Ref. [1])

2.2 Preload Release Mechanism (PRM)

The main task of the Preload Release Mechanism (PRM) is to enable MASCOT to controllable decrease the initially stored preload force, which is strongly required during the launch phase. The lander will be fixed with approximately 2500N inside the MESS which is mechanically connected to the Hayabusa-II spacecraft. This 2500N are necessary, to prevent MASCOT from braking away due to vibrations during the launch phase. This preload force is stored inside the structure by elastic deformation.

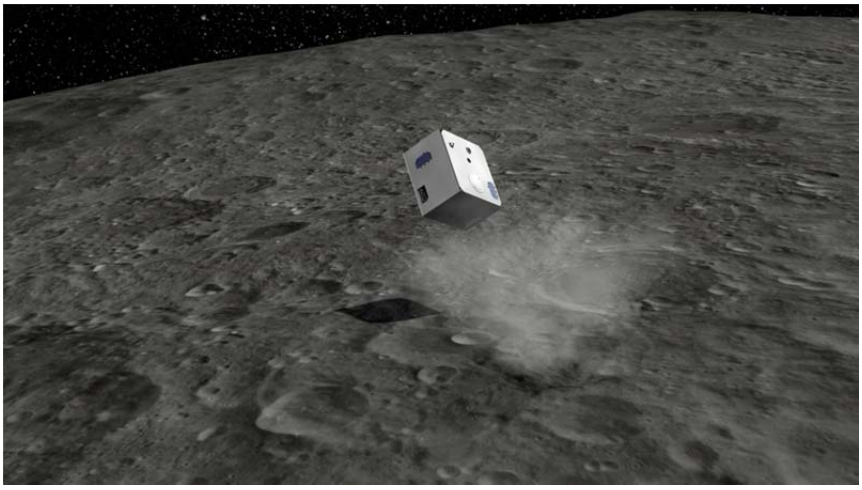

Fig. 2-4: Bouncing of MASCOT at the target asteroid (Ref. [1])

The structure therefor acts also as a spring. The energy stored in the dedicated compression spring is comparably low. This is necessary for a controlled separation with a velocity of 5cm/s. Due to the very low gravity environment of the target asteroid, if separated too fast, MASCOT would bounce (see Fig. 2-4) of the surface back to open space. The preload force shall be thereby reduced until the structure, which is loaded with 2500N, is not sagged anymore. This shall be executed after launch in order to guarantee a safe separation (see chapter 2.1).

The PRM assembly shall be placed inside MASCOT under the NEA as shown in Fig. 2-5 and Fig. 2-6. It consists of two collection pans, two thermoplastic inserts, two mounting pins, a spacer bushing as well as a heating foil.

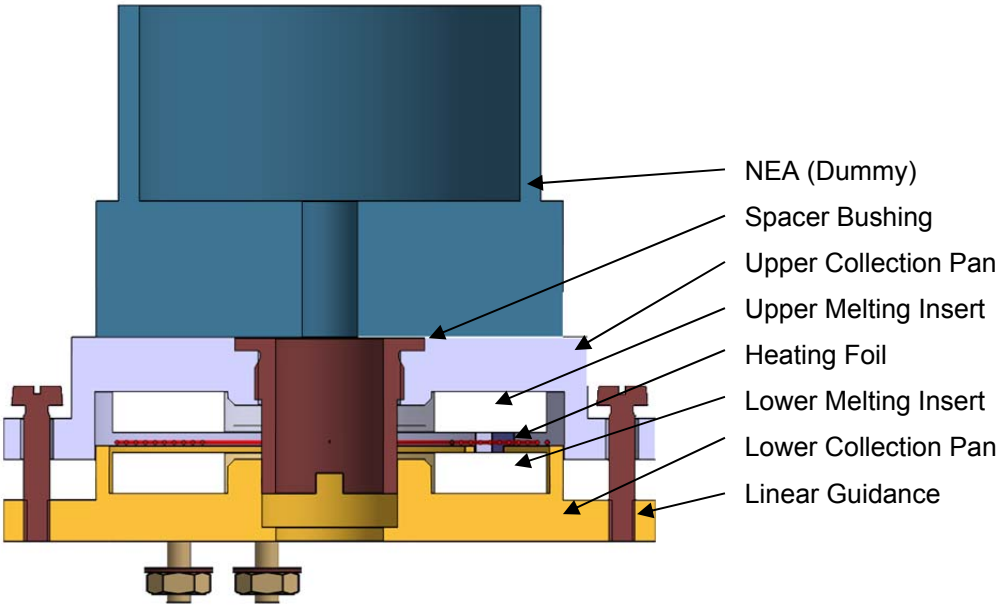

Fig. 2-5: Cut view of PRM CAD Model

The operating mode of the PRM works as follows: After launch the heating foil inside the PRM will be electrical heated up to a temperature higher than the melting temperature of the thermoplastic inserts. Due to the increased temperature both thermoplastic inserts, which are placed on both sides of the heating foil, will be thermally loaded and starts to flow. Initially, highness of thermoplastic inserts is 3mm both. This pulls the collection pans 2mm further apart than the spacer bushing does. While the thermoplastic inserts are thermally treated, they become unable to pull the collection pans apart. Owing to the initial preload force, which is stored in an elastic deformation of MESS and MASCOT, the lower collection pan will move towards the upper one until it is limited again by a spacer bushing (about 2mm covered distance). Caused by specially adapted bolts, which are used as a linear guidance, the lower collection pan should only move linear. The thermally treated inserts meanwhile flow in the collection pans where they are stored. Through this relaxation of the mechanical MESS to MASCOT interconnection, the initial 2500N preload force after the launch phase is reduced for the upcoming separation of the landing module from the Hayabusa-II spacecraft at destination arrival.

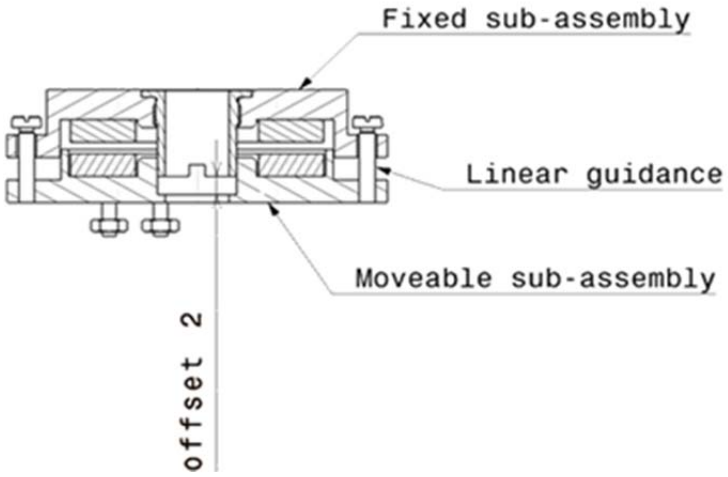

Fig. 2-6: Drafting of PRM (Ref. [1])

2.2.1 Collection pans

The two major parts of the Preload Release Mechanism (see Fig. 2-7) are both collecting pans. These have almost the same internal geometry to guarantee the collection of the thermally deformed thermoplastic inserts as well as to fix them before they are thermally loaded. The external geometry of the upper collecting pan is adapted to the outer size of the NEA´s one, while the upper one is adapted to the lander accommodation. That shall ensure that the PRM has no harming influence on other devices.

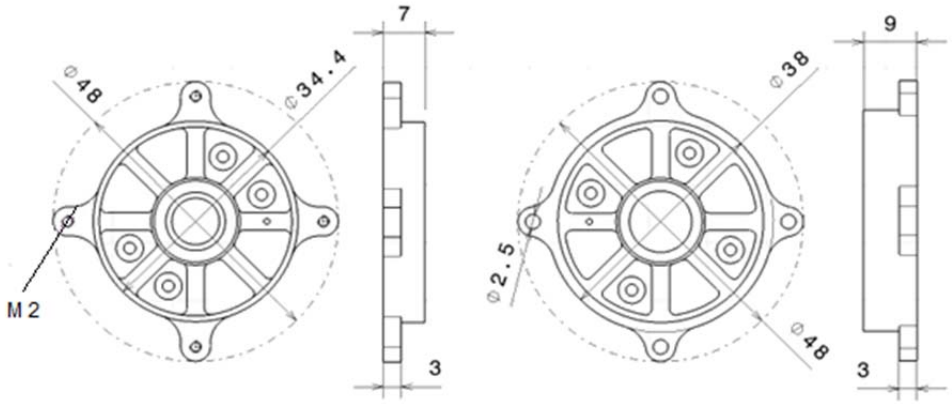

Fig. 2-7: Outer dimensions of both collection pans left the lower one.

The internal shape of the collection pans contains eight identical grooves. The total volume (see Fig. 2-8), which can be used to keep the thermoplastic inserts, is 864mm^3. This is enough space to store the volume of one thermoplastic

insert. The grooves are specially designed to store the thermally deformed melting inserts and allow them to flow inside while they are heated.

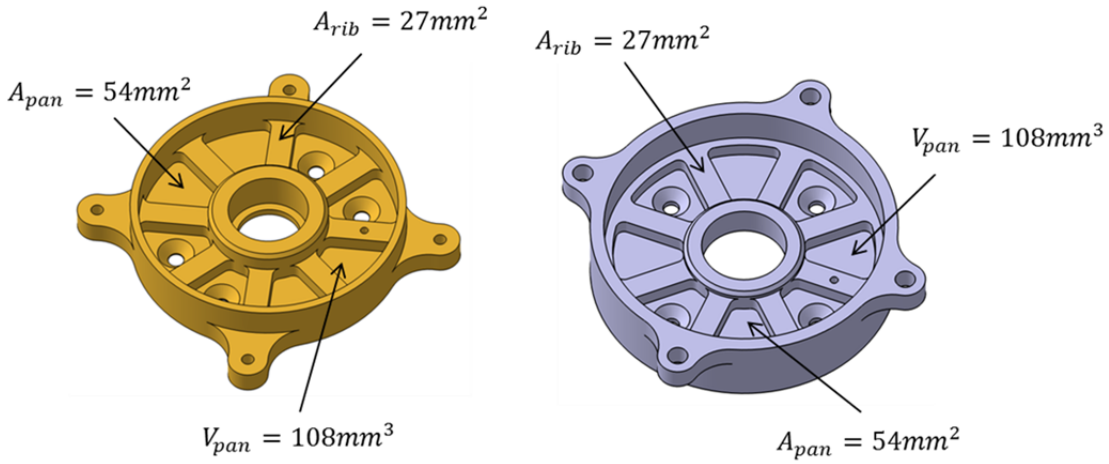

Fig. 2-8: Geometrical properties of both collections pans, left the lower one.

2.2.2 Thermoplastic Melting Inserts

The following Fig. 2-9 shows dimensions of the thermoplastic melting inserts which are made of Polyethylene (PE1000). Polyethylene is chosen as melting material according to the expected temperature in during the flight (approx.-80°C). The low melting temperature of Polyethylene makes it the best suitable choice. The lower the melting temperature of the chosen material the less energy is needed for heating.

As can be seen the shape of the insert is adapted to the collection pan´s geometry and additionally to the ribs of the collection pan to enable them to flow. In order to accelerate the plastic deformation of the thermoplastic melting insert, several round grooves are added. These grooves are placed between the collection pan´s ribs. Each row contains two grooves and is displaced by 45°. The thickness of the insert is 3mm and the thickness of all grooves is approximately 0,5mm.

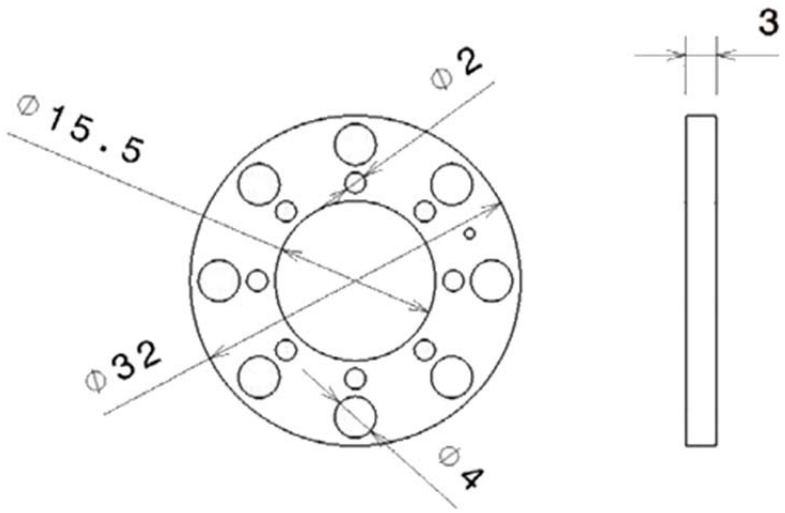

Fig. 2-9: Thermoplastic Insert (Ref. [1])

2.2.3 Heating Foil

The selected Kapton® heating foil has the only shape in the standard range, which can be used within the preload release mechanism due to its fixed geometry. The chosen heating foil offers following specifications:

- Model number: Minco HK5542R84.4L12A
- Dimensions: X=31,75mm, Y=15,24mm
- Electric resistance of the heating foil: 84,4Ω
- Connecting cable: AWG 26, l=300mm
- Effective heating surface: 380mm²
- Temperature range: -200°C to +200°C
- Electrical strength: up to 1000V RMS
- Max. current @ AWG 26: 5A
- Vacuum proof

2.3 Purpose of this Bachelor Thesis

The main purpose of this work is to validate the functionality of the PRM. Therefore, the thermal deformation process and the therewith associated reduction of the preload force shall be verified through testing. Furthermore the creeping properties of the thermoplastic inserts, which are made of Polyethylene 1000 (PE1000), shall be determined.

Further, a new requirement, which is given by JAXA, has to be met. Due to the risk of bouncing, if landing speed is too high, a possibility to check the reduction of preload force shall be implemented. This should reliable advertise if the preload force is reduced or not. Though, the requirements given by the MASCOT design as well as the HAYABUSA-II still have to be met.

3 Functionality Test

The purpose of this chapter is to depict the functionality test of the PRM. It describes how the PRM will be tested, the test set-up, the conducted tests as well as the test results and their evaluation. Sources used: [3], [4], [5], [7] and [8].

3.1 Testing Overview

Testing is an organized process which consists of planning, preparation and execution. This process serves to assure systematically, that a system behaves exact as expected and reassures, that differences between actual and required behavior can be identified as early as possible.

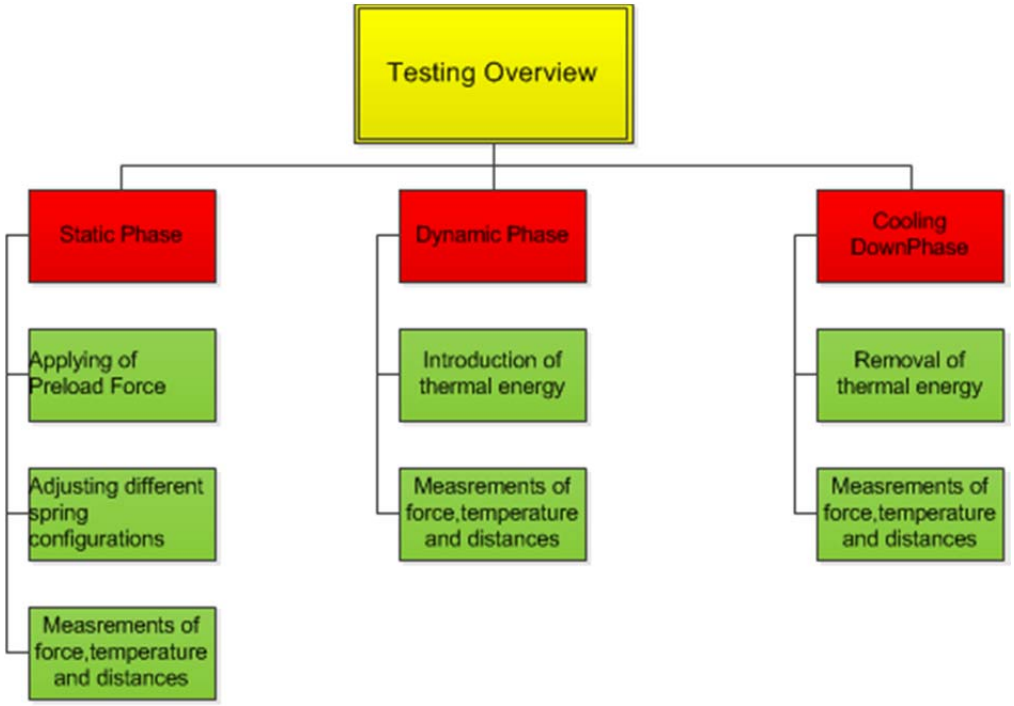

Fig. 3-1: Organogram of the testing overview

This test shall evaluate the functionality of the PRM. To accomplish the testing several items must be assembled and prepared (see Fig. 3-1). These include measurements of force up to 3000N and temperature up to 200°C. MASCOT and MESS stiffness will be simulated by a spring when the preload force is applied. For them, a suitable replacement has to be chosen. Thereby different spring rates shall be adjustable to represent different stiffness of the MASCOT-

MESS system. The test set-up although has to meet safety regulations due to the high preloaded force and the expected high temperatures. For a testing success the reduction of the preload force shall be reproducible. There, the total height of the PRM shall be reduced by 2mm due to thermal deformation of the thermoplastic inserts.

3.2 Basis for Testing

3.2.1 Measurements of Force

Measurements of force shall be enabled through a miniature ring load cell, “Model 8438-6010” from “Burster”. The measured tension and compression force has to be introduced axially and perpendicularly to the entire surface of the inner and outer rings of the sensor in opposite directions to obtain usable results.

The sensor works with strain gauges which changes their electric resistance by strains, even by small ones. So the force sensor converts the acting force into an electrical output signal. This signal is processed by an amplifier, especially “9236-V300” from “Burster” (see Fig. 3-2). The amplifier amplified the analog signal from mv to V. This signal is sent to the CCS, which converts the signal into a digital one. LABVIEW can now display the signal directly in a graphical force output in V.

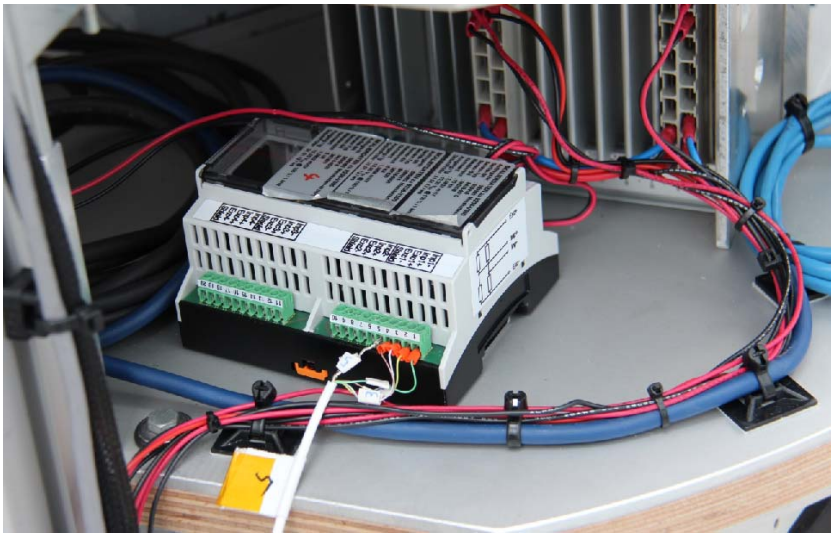

Fig. 3-2: Amplifier used for the ring load cell signal

By calibration with the aid of a second already calibrated force sensor the ratio between voltage and force is determined. The following equation describes it.

$$\frac{V}{F} = \mathrm{C} = 0{,}00122 \qquad \textbf{Eq. 3-1}$$

With V=Voltage in V, F=Force in N and C=Coefficient without dimension.

With the aid of this equitation the diagram in Fig. 3-3 is generated.

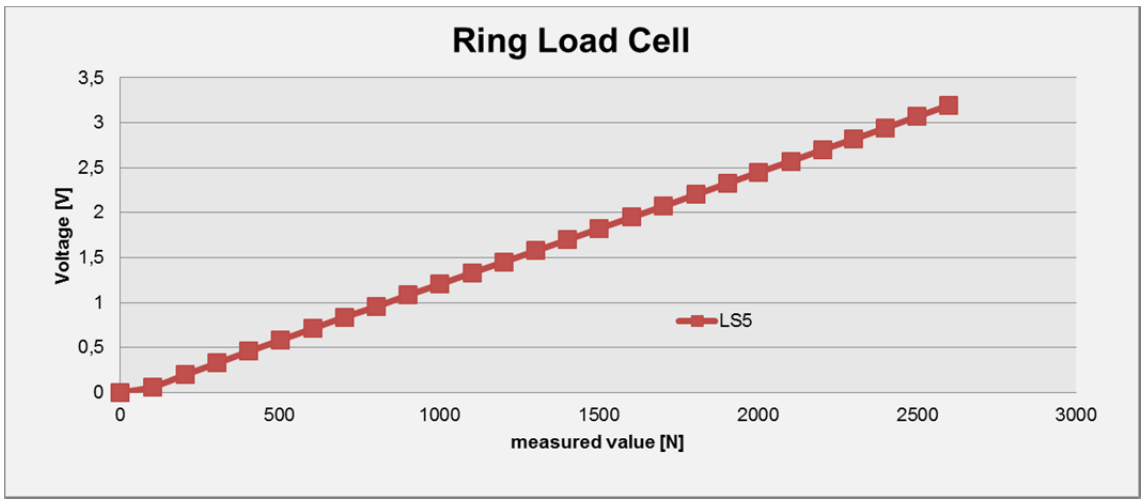

Fig. 3-3: Diagram of measured voltage and corresponding force

Four wire measurement techniques is used to prevent measurement errors By this, one pair of wires carries the excitation current and the other pair connects to the voltage measuring instrument, which, ideally draws no current. Thus any voltage drop on the wires carrying the excitation current is not measured and does not contribute an error.

3.2.2 Measurements of Temperature

The temperature is measured by two thermocouples of Type K (Chromel {90% nickel and 10% chromium} - Alumel {95% nickel, 2% manganese, 2% aluminum and 1% silicon}). These sensors consist of two dissimilar metals bonded to each other, typically by welding. The bimetallic junction generates a small voltage that varies with temperature.

Temperature measurements will be realized with LABVIEW. The program acquires real-time data from both thermocouples. These are directly displayed

in a graphical temperature output in °C. Measured data can be automatically logged for further analyses.

In order to display the signal with LABWIEV special hardware is required. Thermocouples generate only microvolts per degree. The analog output signal (mV) had to be amplified (V). The amplified analog signal must be sent to an analog to digital converter. This signal is displayed by LABVIEW (see Fig. 3-4).

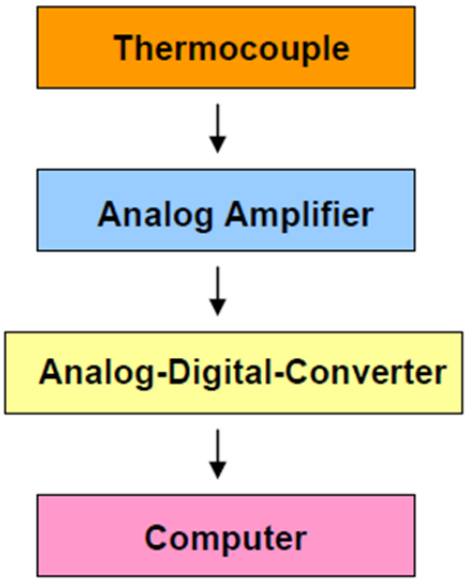

Fig. 3-4: Principle of signal processing from thermocouples

3.2.3 Compression Spring/ Disc Spring

Springs are unlike other machine/structure components in that they undergo significant deformation when loaded; their compliance enables them to store readily recoverable mechanical energy. Springs are common in force, displacement transducers, e.g. in weighing scales, where an easily discerned displacement is a measure of a change in force.

As compensation for the MASCOT-MESS system, in which the preload force is stored, a compressing spring shall be used. This is due to the same working principle. Both, MASCOT-MESS and the spring, are able store potential energy by elastic deformation. The value of stored force depends on the covered distance from unloaded to loaded. This correlation is described in Hook´s law

(see Eq. 3-2). In this is F the force, ΔL the covered distance and c the spring constant.

$$F = c * \Delta L \qquad \textbf{Eq. 3-2}$$

The value of the spring constant depends on the stiffness of the spring. This is also true for the MASCOT-MESS system therefore a spring is used as a replacement.

The spring constant of chosen compression spring is just 90.38 N/mm. At 2mm covered distance this are 180,76N of stored or released. This is far from the required value. For this reason a second type of springs shall be used. Disc springs are the selected ones. Disc springs are conically shaped, washer-type components designed to be axially loaded. Disc springs can be statically loaded either continuously, intermittently or dynamically subjected to continuous load cycling. They can be used singly or in multiples, stacked parallel, in series or in a combination thereof. Therewith different spring constants can be adjusted. In testing different arrangements of springs will be used.

3.3 Material

3.3.1 Appliances

For data sheets see chapter 7.1.2.

For testing several appliances are used. These are listed in Tab. 3-1.

Number	Appliance	Type	Manufacturer
1	Miniature Ring Load Cell	8438-6010	Burster
2	Thermocouples	K1	Heraeus
1	CCS		Zarm
2	Amplifier	9236-V300	Burster
1	Clipper		

Tab. 3-1: Appliance

3.3.2 Mechanical Components

For technical Drawings see chapter 7.1.3 in the Annex.

For testing several components are used. These are listed in Tab. 3-2.

Number	Appliance	Type/Material	Manufacturer
2	Melting Inserts	PE1000	Zarm
2	Insulators	PEEK	Zarm
1	Compression spring	0C1225-192150M	Febrotec
25	Disc springs	0S4251E	Febrotec
1	Spring safety bushing	Stainless steel	DLR
1	Spring forcer	Stainless steel	DLR
3	Spacer Bushings	Stainless steel	Zarm
1	Baseplate	Aluminum	Zarm
2	Shaft	Stainless steel	Zarm
8	Elbow Connector	Aluminum	DLR
1	Casing	Plexiglas	Zarm
1	Rack	Aluminum	DLR

Tab. 3-2: Components

3.4 Test set-up

3.4.1 Rack structure & Baseplate

The first sub-assembly which is mounted and prepared for next steps is the rack structure. Aluminum profiles and fasteners are screwed as shown in Fig. 3-5. Note that the rack structure has the same dimensions as the baseplate with a highness of 140mm.

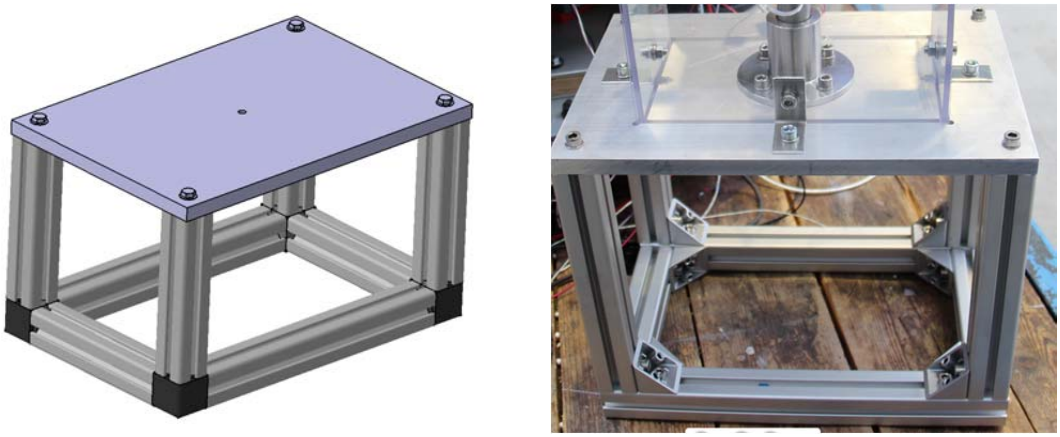

Fig. 3-5: Drafting of the rack-baseplate structure

Next step is screwing of the baseplate on the rack structure. Likewise shown in Fig. 3-5, the baseplate is bolted to the rack structure. The groove is form-close with the end of the shaft to prevent the shaft from overrunning while preload force is applied. The rack structure acts as construction which bears the experimental set up. Also the measuring technique, which will be needed during long term tests (not treated in this work), can be compactly installed inside the structure.

3.4.2 PRM & Insulators

The PRM is divided into two sub-assemblies, the upper and the lower one. The first sub-assembly is the upper collection pan assembly (Fig. 3-6). Note that the polyethylene insert is covered with heat transfer paste, Keratherm® KP92, to accelerate the heating process. A foil made of aluminum will be placed on the melting inset to protect the heating foil.

Fig. 3-6: Upper Collection Pan Assembly with insulator

The second sub-assembly is the lower collection pan assembly (see Fig. 3-7). Once again the melting insert is bushed with the heat transfer paste Keratherm® KP92.

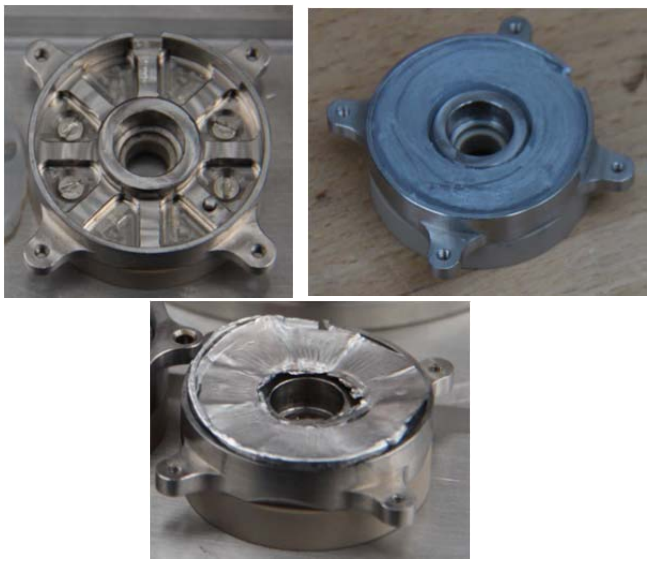

Fig. 3-7: Lower Collection Pan Assembly with insulator

3.4.3 PRM final assembly

After mounting of both sub-assemblies they are connected with each other (see Fig. 3-8). The round heating foil will be placed inside the lower collection pan assembly (14). Then the prepared assembly of the upper collection pan will be fixed with four M2x10 slotted screws. Note that no additional force shall be introduced on the thermoplastic melting inserts from the linear guidance bolts. It shall be still moveable along +/- z-axis.

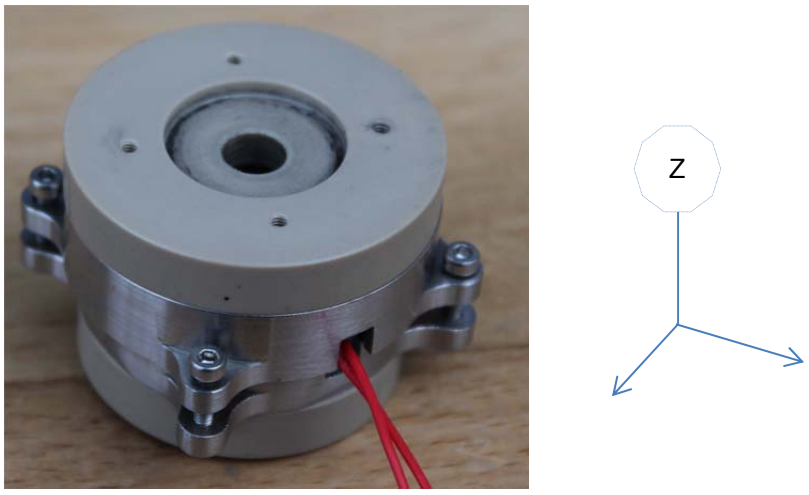

Fig. 3-8: Picture of the PRM assembly

After the PRM assembly is mounted the thermocouples for temperature measurements should be implemented. Therefor two holes are bored with the aid of a brace. They are located in the groove on the collection pan housing for

the heating foil power supply cable, one above the heating foul in the upper melting insert and one under the heating foil in the lower melting insert. The thermocouples are inserted into these bore holes (see Fig. 3-9).

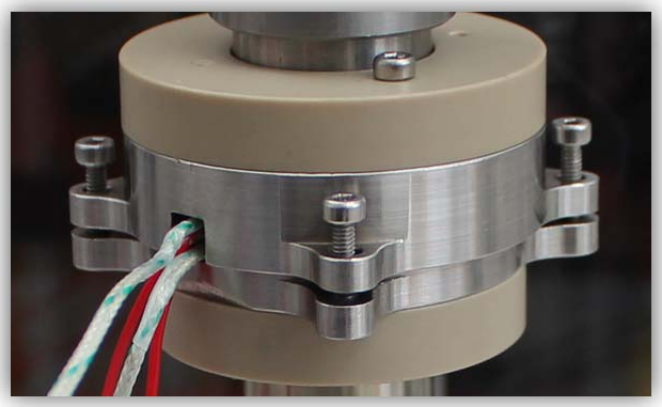

Fig. 3-9: Location of thermocouples in the PRM assembly

Note, that simple DIN 912 screws instead of bolts are used as linear guidance. This should have no effect on the functionality, due to enough clearance between the bore hole in the collection pan and the screw.

3.4.4 PRM Test Arrangement Assembly

In the PRM test arrangement assembly all sub-assemblies will be brought together. First of all the shaft is inserted into the baseplate. Note that the shaft is not fixed yet. At next step the springs are integrated. A test could have a compression spring and always has several arrangements of disc springs.

If the compression spring is used, it shall be mounted first. As second step the spring forcer is lined up on the shaft before the safety spring bushing, which should be screwed to the baseplate, is imposed on both (see Fig. 3-10). The shaft has a fitting for disc springs which are attached in next step (see Fig. 3-11). During the trials there are different arrangements of spring discs to. The compression spring guarantees that there is still force after the thermal deformation process. This is due to its small spring constant and therewith small reduction of force after 2mm reduction of distance. With it the principle functionality is determined.

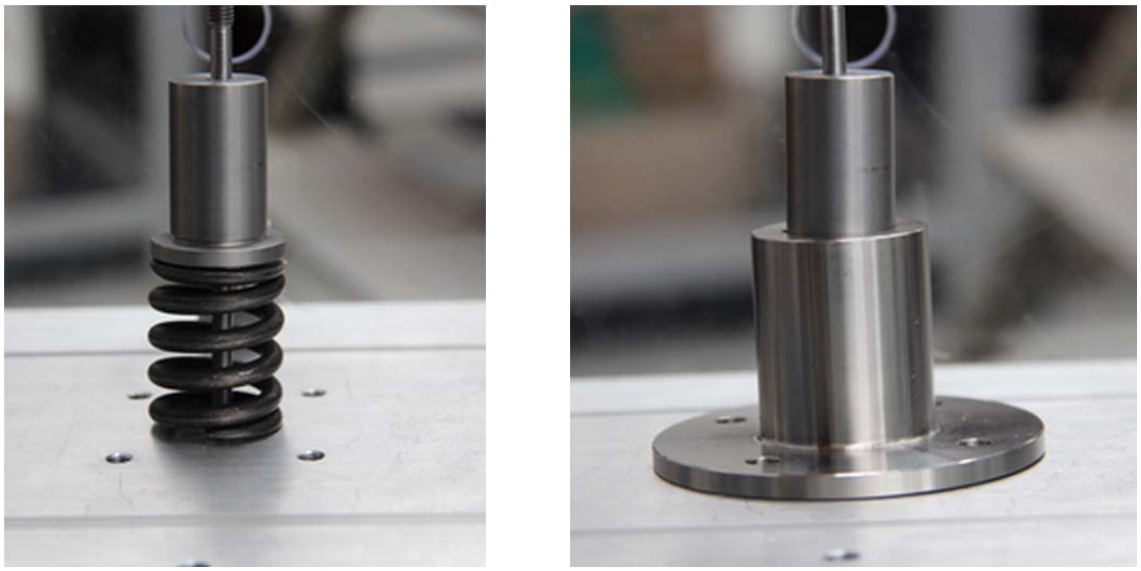

Fig. 3-10: Mounting of compression spring (left), spring forcer and safety spring bushing (right)

Above the spring discs a spacer bushing, which concurrent works as area of support for the disc springs, shall be positioned. Now the ring load cell on the row. The upper area of the ring load cell, in which the force is introduced, requires an area of support too. This is why another spacer bushing is mounted. The PRM assembly with its insulators made of peek is putted on (see Fig. 3-11) next. At least first a further spacer bushing and a M6 screw nut are integrated.

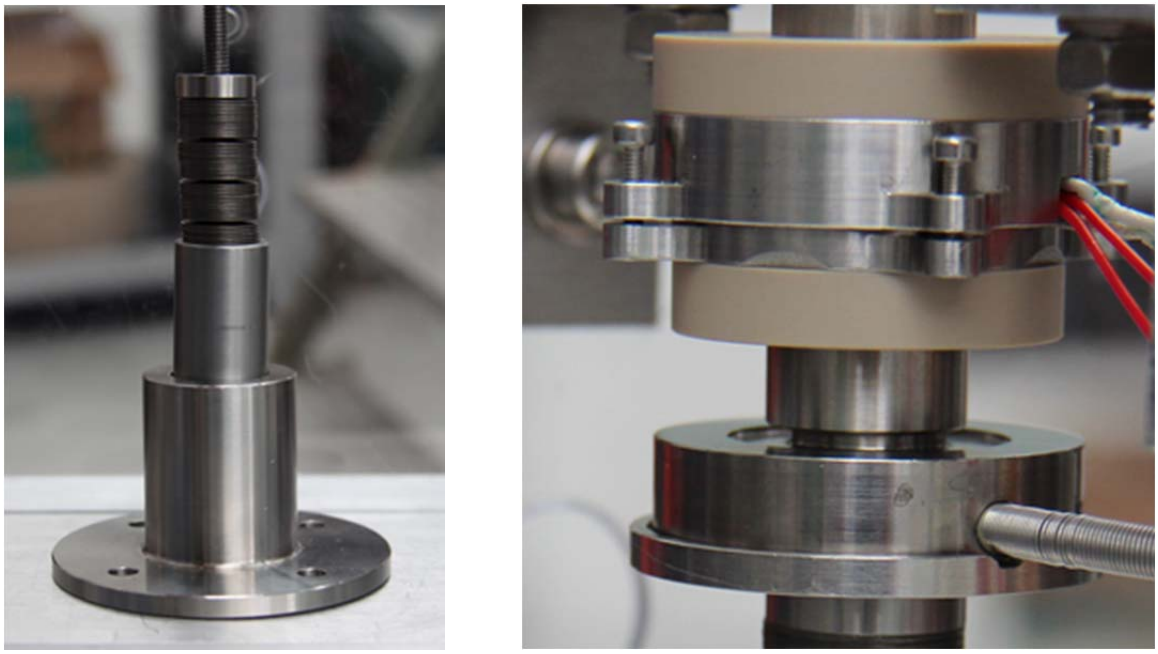

Fig. 3-11: Left, mounting of disc springs and spacer bushing, right of PRM and spacer bushings

For safety reasons, there is a casing made of Plexiglas® screwed on the baseplate and surrounds loaded springs and possibly hot PRM assembly(see Fig. 3-12).

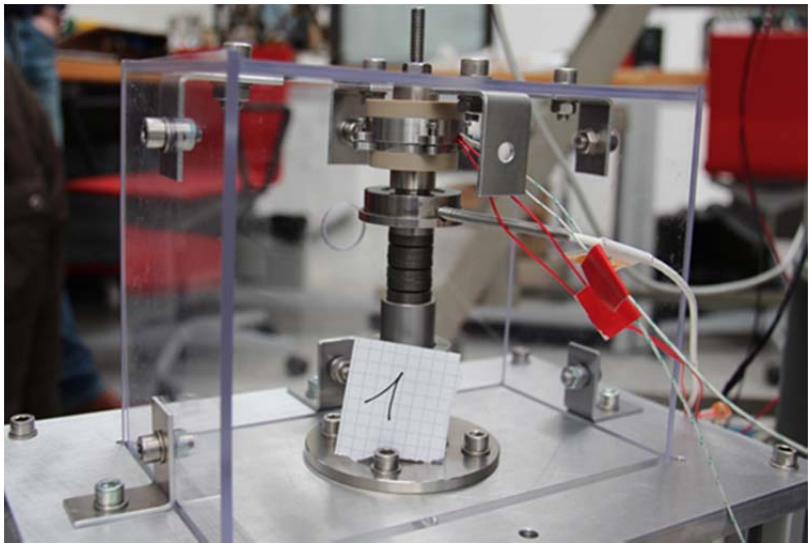

Fig. 3-12 Test set up (Test 1-2) with casing, one side open for better view

Tests, in which no compression spring will be used, have a different construction. In this case the ring load cell is lined up first. Then a space bushing followed by an assignment of disc springs, a spacer bushing, the PRM assembly and the spring forcer (see Fig. 3-13) are lined up. Next a M6 nut is mounted.

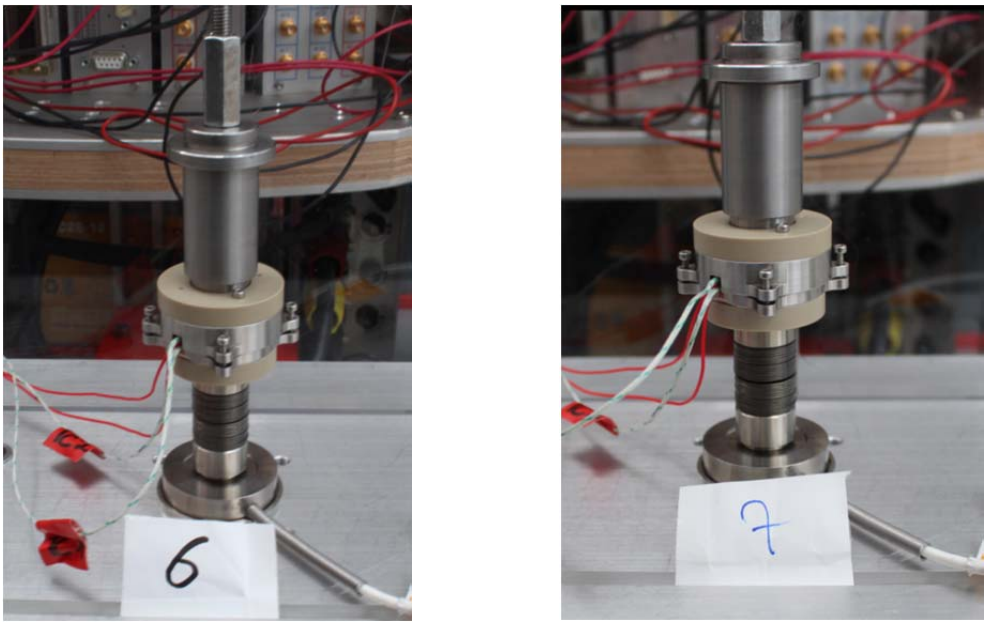

Fig. 3-13: Two experimental set ups without integrated compression spring

3.5 Electrical measurement setup

As can be seen in Fig. 3-14, the electrical set up of the temperature generating and measurement consists of a power source, which will provide a voltage of 24VDC. The voltage will be measured with the aid of a multimeter and processed by a Lab View program. The temperature inside the preload release mechanism will be measured with two identical thermocouples. Their signals will be amplified by an amplifier and processed by LABVIEW. The amplifier and the multimeter are connected with a CCS (Capsule Control System), which converts the analog signals into digital ones. Further it sends all acquired data to a personal computer. On the CCS, which will be remote controlled, a LABVIEW program is running. The program can be found on the data compact disc. While the test will be running, there are screenshots taken from the user interface of LABVIEW. These screenshots will be used in test and data analysis.

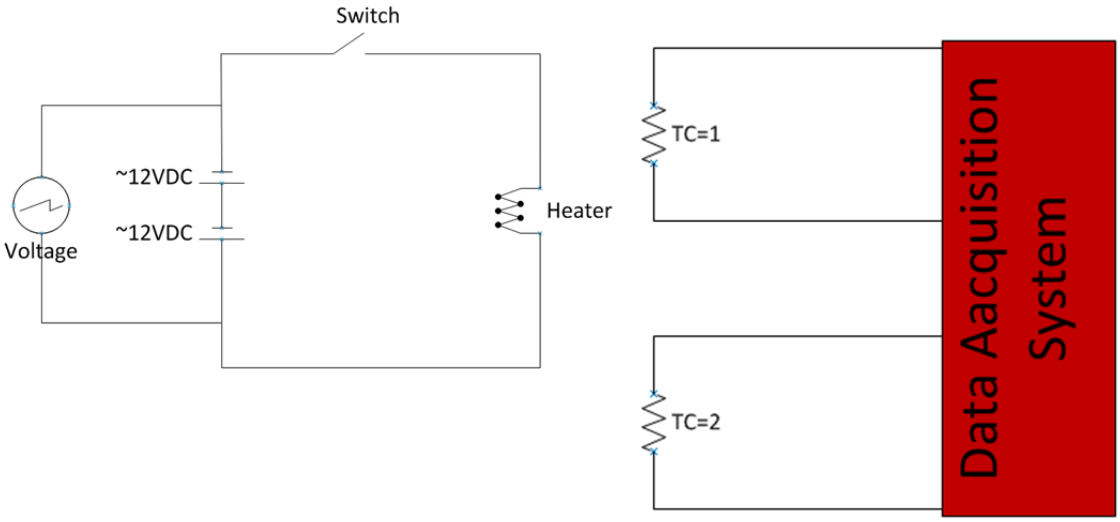

Fig. 3-14: Drafting of the heat generating electrical circuit and temperature measurement concept

3.6 Execution of the Test

The tests are divided into two main phases and a third minor phase. The first main phase is a static test in which the creeping of the thermoplastic inserts, due to the preload force, shall be investigated. The second main phase is a dynamic test in which the heating foil is activated until the melting inserts are

thermally deformed. The third minor phase is a cooling-down phase in which the heating foil is deactivated again and the system cools-down to ambient temperature.

Before the first test phase begins, the distance of the collection pans to each other will be measured with the aid of a caliper. Then, the LABVIEW program, which displays and saves the data from the ring load cell´s amplifier as well as the temperature data, is activated. The M6 screw nut, which fixes the shaft to the baseplate, is tightened up to the required force of 2.5 KN in next step. Therefor a special constructed nut and a nut driver are used. With the aid of the LABVIEW program, which is displaying the signal of the ring load cell, the force is adjusted. After reaching the required force the tools need to be removed. The exact adjusted preloaded force is saved from the LABVIEW program. Now the static test can be started. It ends as soon as no more preload force is reduced based on creeping of both melting inserts. Before and after the test, distance of the collection pans to each other is measured.

To start second test phase, the dynamic one, the power for the heating foil is activated with the aid of the LABVIEW program. During this phase the PRM must not be touched due to the high temperature. The test phase ends as soon as no more preload force is reduced. The heating foil is deactivated. Seamless after the dynamic test phase, third one starts. To accelerate the cooling-down the test set up, especially the PRM, is cooled by compressed air. The phase ends once the PRM reached room temperature. Again distances between the collection pans and the insulators will be taken.

To evaluate the logged data, a program was written to reduce data of the static test. This is due to the long period of time in which data are logged. The program copies the lines from the original .txt document into a new one, but skips a selectable number. If you choose skip range 10 for example, the program copies every tenth line.

3.7 Static Tests

This chapter provides an overview about the 8 static tests executed.

3.7.1 Test 1

To simplify describing of the disc spring assignments, the following acronyms will be used. The number of springs per stack will be “i”=number. The number of stacks will be “n”=number.

Test configuration:

- Compression spring is used
- Disc springs configuration: i=5, n=6
- Preload force is set once to (3,2V) ≙2623N
- Distance top of upper insulator to bottom of lower insulator: 27,8mm
- Distance between linear guidance holes: 2,5mm

Observation:

As can be seen in Fig. 3-15 the applied preload force drops very quickly in the first minutes of the static test. The reduction of the preload force is decelerated over time in a digressive curve. So does the temperature with a more flat characteristic.

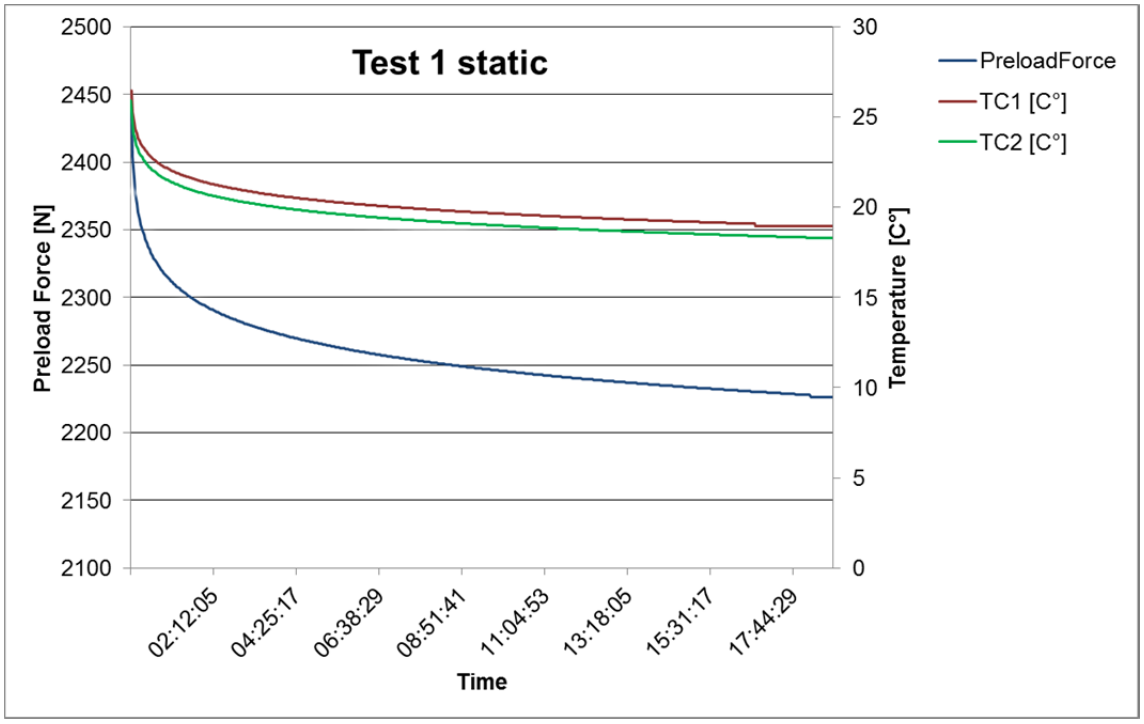

Fig. 3-15: Diagram of test 1 static showing force/temperature over time

At the end of the test there is a preload force of 2,726V≙2234N left (see Fig. 3-16). The value was approximately reduced by 390N. Note that the preload force drops quickly while the force is applied so that the start value is just an approximation.

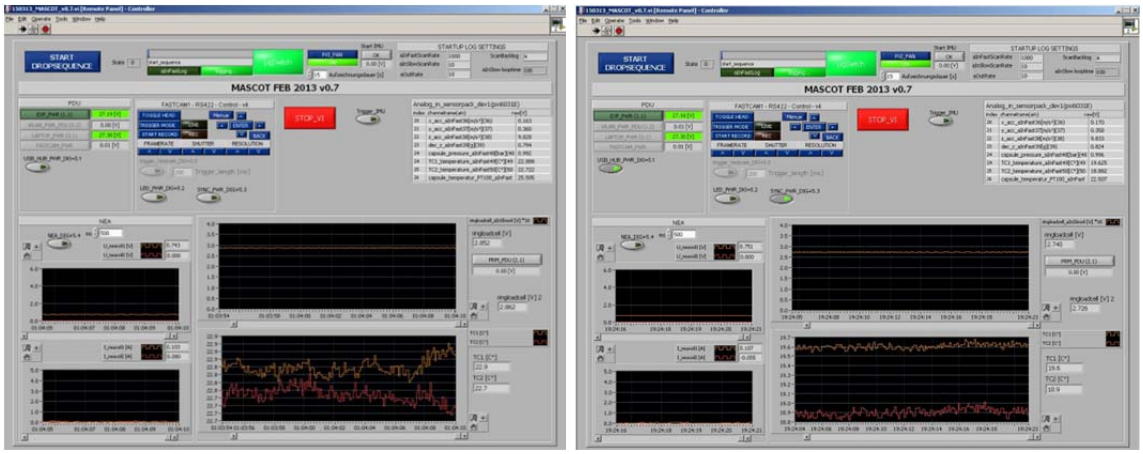

Fig. 3-16: Screenshot of the Lab View program. Left at the beginning and right at the end of test 1

Much more accurate is the measurement of temperature. It goes down from 26C° to 19C°. Note here that the thermocouples have a fault tolerance of +/- 1C° which is still sufficient for the test. Further the before measured distances have become smaller. The distance between the insulators has been reduced to 26.7mm and the one between the linear guidance to 1,5mm to 1,6mm (see Fig. 3-17). Note that the upper collection pane is not straight anymore which results in the 0,1mm difference in guidance holes distances.

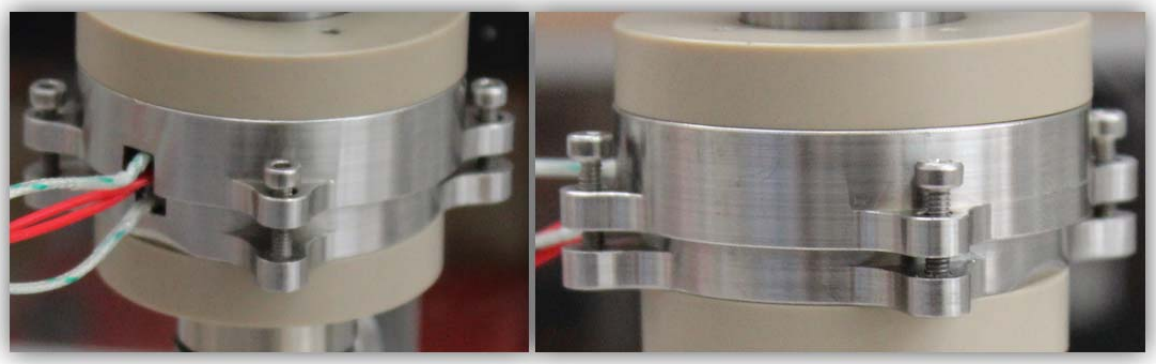

Fig. 3-17: Picture of PRM assembly, left without preload force, right after creeping of thermoplastic inserts

Evaluation:

The reduction of the preload force is attributed to a creeping process of the thermoplastic inserts. The reductions of the distances on the monitoring wells before and after the test prove it. The collection pans have moved 1mm towards to each other. This has the consequence, that the arrangement of spring is also relaxed by 1mm. Out of that results the reduction of preload force.

The monitored sliding of temperature during the static test phase is due to before introduced temperature. Body heat raises temperature of the test set up when it is mounted. This temperature is dissipated until ambient temperature is reached.

The upper collection pan assembly is not straight anymore because of the power supply cable of the heating foil is a little between the melting inserts. This has almost no influence on the preload force but induces a small momentum in the PRM. This has also an effect on the trajectory of MASCOT and must be taken into account. The trajectory of MASCOT after separation shall be straight. Due to the low gravity environment, even little momentums can cause a rotation of MASCOT. If the rotation is too high, MASCOT may hit the wall of MESS. There MASCOT an MESS can become wedged together which has the consequence of no separation.

- Preload force loss: 390N
- Measured distance loss: 1mm

3.7.2 Test 2

Test configuration:

- Compression spring is used
- Disc springs configuration: i=5, n=6
- Preload force is set (3,2V) ≙2,623KN with permanently retightening to the required force
- Distance from top of upper insulator to bottom of lower insulator: 27,8mm
- Distance between linear guidance holes: 2,5mm

Observation:

As can be seen in in Fig. 7-1 the preload force drops very quickly every time the M6 nut is retightened to reach the required preload force. But compared to test 1 the curve of the ring load cell is gentler. At the end of the test, the M6 nut is retightened once again to reach the required 2,5KN. The curves displaying the temperature are almost the same like the once from previous test but with new temperature introduced while the retightening process (see Fig. 7-15).

The distance between the insulators is now 26.7mm and the one between the linear guidance holes is now between 1,5mm and 1,6mm.

Evaluation:

For detailed evaluation see chapter 3.7.1. Note that the values are different.

- Preload force loss: Continuous
- Measured distance loss: 1mm

3.7.3 Test 3

In this test, the preload force should be adjusted to a higher value than the previous tests. This is due to the losses of preload force which is caused by creeping of the thermoplastic inserts.

Test configuration:

- Compression spring is not used
- Disc springs configuration: i=8, n=5
- Preload force is set once to (4V) ≙3278N
- Distance from top of upper insulator to bottom of lower insulator: 27,8mm
- Distance between linear guidance holes: 2,5mm

Observation:

As can be seen in Fig. 7-2 the preload force drops very quickly in the first minutes of the test. Temperature drops to ambient temperature (around 20C°). The preload force is almost constant at a value of (3,315V) ≙2716N which is a loss of approximately 562N preload force (see Fig. 7-16).

The distance between the insulators has been reduced to 26.7mm and the one between the linear guidance to 1,6mm and 1,7mm.

Evaluation:
For detailed evaluation see chapter 3.7.1. Note that the values are different.

- Preload force loss: 562N
- Measured distance loss: 0,9mm

3.7.4 Test 4

Test configuration:

- Compression spring is not used
- Disc springs configuration: i=5, n=4
- Preload force is set once to (3,8V) ≙3115N
- Distance from top of upper insulator to bottom of lower insulator: 27,8mm
- Distance between linear guidance holes: 2,5mm

Observation:
As can be seen in Fig. 7-3 the preload force drops again very quickly in the first minutes of the test. Temperature drops until it reached ambient temperature (around 20C°). The preload force stays constant at a value of (3,163V) ≙2592N which is a loss of approximately 544N preload force (see Fig. 7-17).

The distance between the insulators has been reduced to 26,3mm and the one between the linear guidance holes to a value between 1,6mm and 1,7mm.

Evaluation:
For detailed evaluation see chapter 3.7.1. Note that values are different.

- Preload force loss: 544N
- Measured distance loss: 0,9mm

3.7.5 Test 5

Test configuration:

- Compression spring is **not** used

- Disc springs configuration: i=5, n=5
- Preload force is set once to 3,9V=3197N
- Distance from top of upper insulator to bottom of lower insulator: 27,8mm
- Distance between linear guidance holes: 2,5mm

Observation:

As can be seen in Fig. 7-4 the preload force drops again very quickly in the first minutes of the test. Temperature drops until it reached ambient temperature (around 25C°). The preload force stays changeless at a value of (3,19V) ≙2615N which is a loss of approximately 582N preload force (see Fig. 7-18).

The distance between the insulators has been reduced to 26,3mm and the one between the linear guidance to a value between 1,6mm and 1,7mm.

Evaluation:

For detailed evaluation see chapter 3.7.1. Note that the values are different.

- Preload force loss: 582N
- Measured distance loss: 0,9mm

3.7.6 Test 6

Test configuration:

- Compression spring is not used
- Disc springs configuration: i=6, n=5
- Preload force is set once to (3,8V) ≙3115N
- Distance from top of upper insulator to bottom of lower insulator: 27,8mm
- Distance between linear guidance holes: 2,5mm

Observation:

As can be seen in Fig. 7-5 the preload force drops again very quickly in the first minutes of the test. Temperature drops until it reached ambient temperature (around 21C°). The preload force stays changeless at a value of (2,926V) ≙2398N which is a loss of approximately 717N preload force (see Fig. 7-5).

The distance between the insulators has been reduced to 26,3mm and the one between the linear guidance to a value between 1,6mm and 1,7mm

Evaluation:

For detailed evaluation see chapter 3.7.1. Note that values are different.

- Preload force loss: 717N
- Measured distance loss: 0,9mm

3.7.7 Test 7

Test configuration:

- Compression spring is not used
- Disc springs configuration: i=7, n=5
- Preload force is set to (3,8V) ≙3115N.
- After creeping it is set to (3,85V) ≙3156N
- Distance from top of upper insulator to bottom of lower insulator: 27,8mm
- Distance between linear guidance holes: 2,5mm

Observation:

As can be seen in Fig. 7-6, the preload force drops again very quickly in the first minutes of the test. Temperature drops until it reached ambient temperature (around 24C°). The preload force stays changeless at a value of (2,834V) ≙2323N which is a loss of approximately 833N preload force (see Fig. 7-20). After the preload force is set to (3,85V) ≙3156N again it drops only to a value of approximately 2700N which is a loss of 456N. Overall there is a loss of 1289N

The distance between the insulators has been reduced to 26,3mm and the one between the linear guidance holes to a value between 1,6mm and 1,7mm.

Evaluation:

For detailed evaluation see chapter 3.7.1. Note that values are different.

- Preload force loss: 1289N
- Measured distance loss: 0,9mm

3.7.8 Test 8

Test configuration:

- Compression spring is not used
- Disc springs configuration: i=7, n=5
- Preload force is set to (3,9V) ≙3197N.
- Distance top of upper insulator to bottom of lower insulator: 27,8mm
- Distance between linear guidance holes: 2,5mm

Observation:
As can be seen in Fig. 7-7 the preload force drops again very quickly in the first minutes of the test. Temperature drops until it reached ambient temperature (around 19C°). The preload force stays almost changeless at a value of (2,916V) ≙2390N which is a loss of approximately 807N preload force (see Fig. 7-21).

The distance between the insulators has been reduced 26,3mm and the one between the linear guidance to a value between 1,6mm and 1,7mm

Evaluation:
For detailed evaluation see chapter 3.7.1. Note that values are different.

- Preload force loss: 807N
- Measured distance loss: 0,9mm

3.8 Dynamic Tests

This chapter provides an overview about the 8 dynamic tests executed.

3.8.1 Test 1

During the dynamic test the heating foil is activated. As can be seen in Fig. 3-18 the preload force first raises while the temperature is increased. This is due to thermal expansion of the thermoplastic inserts. But this effect does not take long. After some minutes, the preload force is reduced from the (2,726V) ≙2234N at the beginning to a value around (1,25V) ≙1025N at the end of the heating. This is a reduction of 1209N. The reduction of force is due to a thermal deformation of the thermoplastic inserts. There is still preload force because the springs of the test set up still load the PRM or rather the ring load cell. The temperature at the measurement points rises in a digressive curve. The

temperature rises very quickly at the beginning, about 10 degrees per minute, before the temperature curve becomes more and more flat. The highest reached temperature was 115C°.

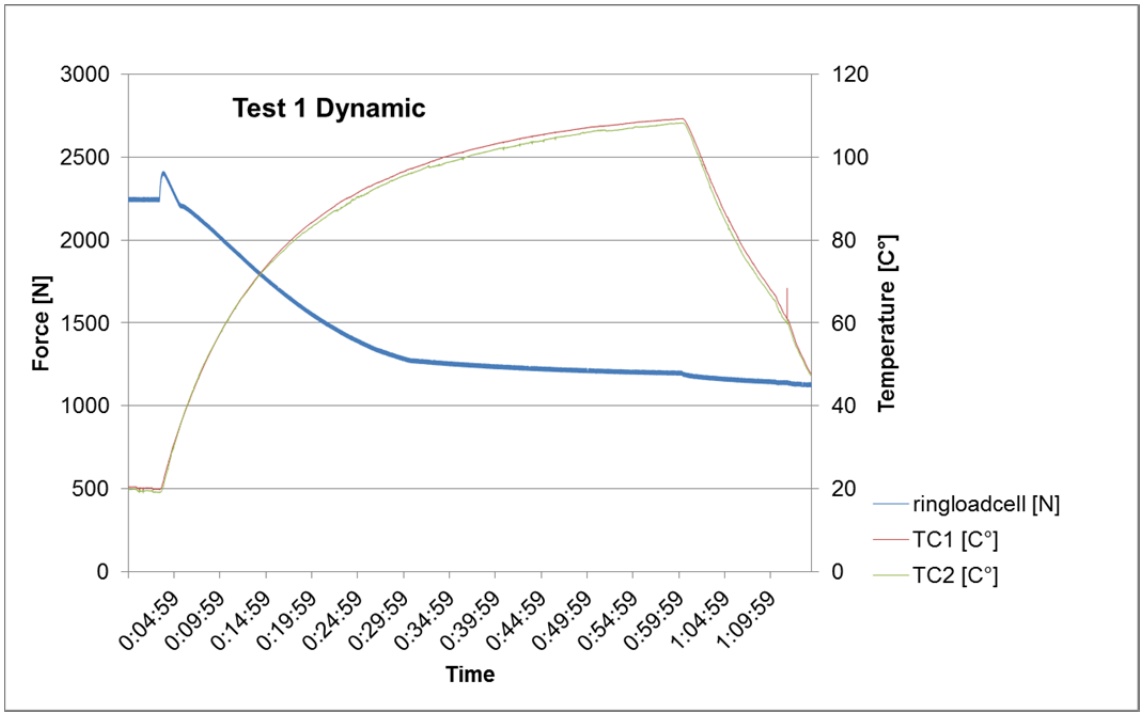

Fig. 3-18: Diagram of test 1 dynamic showing force/temperature over time

As soon as the preloaded force is almost constant, the third phase of the test starts and the heating foil is deactivated again. The temperature falls to ambient temperature again. Note that the preload force decreases its value about 100N while the temperature is decreased. After the cooling phase the distances have changed again. The melting insulator well has now a distance of 25,7mm and the linear guidance holes are now 0,5mm-0,6mm away from each other which corresponds 2mm reduced distance in total.

Evaluation:

The increase of preload force by the time the heating foil is activated is attributed to thermal expansion of the thermoplastic inserts and of the metallic components of the test set up. Due to the different materials used in the MESS-MASCOT spring (mostly carbon) and the therewith connected different coefficient of thermal expansion, the increase and decrease of preload force based on temperature is not comparable. The thermal coefficient of carbon is just 0,1[$^{10\text{-}6}$/K] what is a lot smaller than the one of steel for example which is

about 11,5[10^{-6}/K]. Because of that, this effect should be much weaker in the original system.

Result:

- Reduced distance from the beginning of the dynamic test: 26,7mm-25,7=1mm
- Preload force reduced to: 1025N
- Max. temperature reached: 115C° at a voltage of 24V

3.8.2 Test 2

As can be seen in Fig. 7-8 the preload force raises at the beginning of the test while the temperature is increased. After some minutes the preload force was reduced from the 2590N at the beginning to a value around 1290N at the end of the heating phase, further to 1126N at the end of the cooling down. The reduction of force is due to a thermal deformation of the thermoplastic inserts. The highest temperature reached was 116C°.

Note, that the preload force is decreased by a value about 161N while the temperature is decreased (see Fig. 7-22). After the cooling phase the distances have changed again. The insulator distance has been reduced to 25,7mm and the linear guidance holes to 0,6mm-0,7mm.

Result:

- Reduced distance since start of the dynamic test: 1mm
- Preload force reduced to: 1126N
- Max. temperature reached: 116C° at a voltage of 24V

3.8.3 Test 3

As can be seen in Fig. 7-9 the preload force raises at the beginning of the test while the temperature is increased. After some minutes, the preload force was reduced from the 2716N at the beginning to a value around 1530N (see Fig. 7-23) at the end of the heating and further to 1530N after the cooling down. The reduction of force is due to a thermal deformation of the thermoplastic inserts. The highest temperature reached is 119C°.

The insulator distance has been reduced to 25,7mm and the one of linear guidance holes to 0,6mm-0,7mm.

Result:

- Reduced distance since start of the dynamic test: 0,9mm
- Preload force reduced to: 1530N
- Max. temperature reached: 119C° at a voltage of 25V

3.8.4 Test 4

As can be seen in Fig. 7-10 the preload force raises at the beginning of the test while the temperature is increased. After some minutes the preload force is reduced from the 2592N at the beginning to a value around 1293N at the end of the heating phase and further to 1203N at the end of the cooling down (see Fig. 7-24. The reduction of force is due to a thermal deformation of the thermoplastic inserts. The highest temperature reached is 122C°.

After the cooling phase the distances have changed again. The insulator distance has been reduced to 25,7mm and the one of linear guidance holes to 0,6mm-0,7mm.

Result:

- Reduced distance since the dynamic test start: 0,9mm
- Preload force reduced to: 1203N
- Max. temperature reached: 122C° at a voltage of 27V (increased due to a change of voltage source)

3.8.5 Test 5

As can be seen in Fig. 7-11 the preload force raises at the beginning of the test while the temperature is increased. After some minutes, the preload force was reduced from the 2615N at the beginning to a value around 937N (see Fig. 7-25) at the end of the heating phase further to 820N at the end of the cooling down. The reduction of force is due to a thermal deformation of the thermoplastic inserts. The highest temperature reached is 122C°.

The insulator distance has been reduced to 25,7mm and the one of linear guidance holes to 0,6mm-0,7mm.

Result:

- Reduced distance since start of the dynamic test: 0,9mm
- Preload force reduced to: 820N
- Max. temperature reached: 122C° at a Voltage of 27V

3.8.6 Test 6

As can be seen in Fig. 7-12 the preload force raises at the beginning of the test while the temperature is increased. After some minutes the preload force was reduced from the 2400N at the beginning to a value around 996N at the end of the heating phase further to 931N (see Fig. 7-26) at the end of the cooling down. The reduction of force is due to a thermal deformation of the thermoplastic inserts. The highest temperature reached is 121C°.

The insulator distance has been reduced to 25,7mm and the one of linear guidance holes to 0,6mm-0,7mm.

Result:

- Reduced distance since start of the dynamic test: 0,9mm
- Preload force reduced to: 996N
- Max. temperature reached: 121C° at a voltage of 27V.

3.8.7 Test 7

As can be seen in Fig. 7-13 the preload force raises at the beginning of the test while the temperature is increased. After some minutes, the preload force was reduced from the 2588N at the beginning to a value around 678N at the end of the heating phase further to 567N (see Fig. 7-27) at the end of the cooling down. The reduction of force is due to a thermal deformation of the thermoplastic inserts. The highest temperature reached is 122C°.

The insulator distance has been reduced to 25,7mm and the one of linear guidance holes to 0,6mm-0,7mm.

Result:

- Reduced distance since start of the dynamic test: 0,9mm
- Preload force reduced to: 567N
- Max. temperature reached: 121C° at a voltage of 27V

3.8.8 Test 8

As can be seen in Fig. 7-14 the preload force raises at the beginning of the test while the temperature is increased. After some minutes the preload force was reduced from 2390N at the beginning to a value around 637N (see Fig. 7-28) at the end of the heating phase, due to thermal deformation of the thermoplastic inserts. Further to 564N at the end of the cooling down. The highest temperature reached is 121C°.

The melting insulator distance has been reduced to 25,7mm and the one of linear guidance holes to 0,6mm-0,7mm.

Result:

- Reduced distance since start of the dynamic test: 0,9mm
- Preload force reduced to: 564N
- Max. temperature reached: 121C°

3.9 Evaluation of the Test Results

Static tests showed that the loss of preload force due to creeping of the thermoplastic inserts depends on the spring constant of the system of springs. This is because of the loss of highness (always about 0,9-1mm) caused by creeping. This means the higher the springs rate the higher the loss of preload force. Still unknown is the share of plastic and elastic deformation in this reduced highness. In order to determine this, the creeping properties have to be determined after EN ISO 899. This test procedure was not done because it would have exceeded a bachelor thesis in terms of time and lengths by far. The required equipment was also missing. It is suggested to repeat static tests with the spring constant of the MESS-MASCOT spring system as soon as it is

known or, even more meaningful, to repeat the tests with the real MESS-MASCOT configuration.

Dynamic tests show that the principle of preload force reduction by thermal deformation of thermoplastic inserts works. Yet it is difficult to adjust the value of lost preload force. It depends very much on the spring rate of the force saving system. Further, the value of preload force reduction at a specific spring rate and preload force is fixed. It is possible that the reduction of preload force is not high enough at the original MESS-MASCOT system. Since the spring rate of MESS-MASCOT is fixed and the minimum preload force of 2500N is strongly required, the PRM configuration may need to be changed. Opportunities (see Fig. 3-19) are here a change of the spacer bushing that limits the maximum distance the PRM can reduce, as well as to make the polyethylene inserts thicker to increase reduction way.

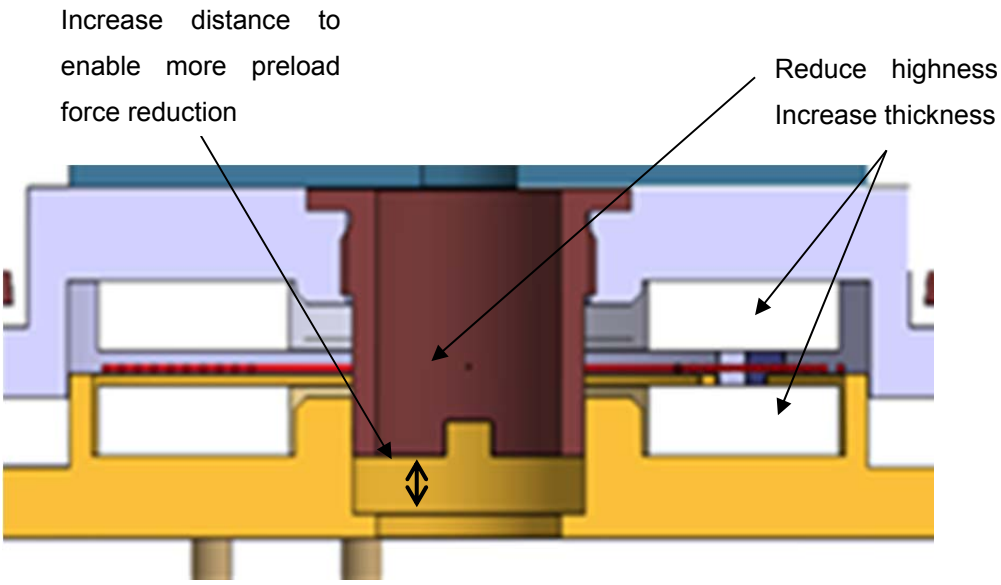

Fig. 3-19: Opportunities of how more preload force can be reduced

It is further suggested to test the device in climate chamber under space conditions as an additional criterion of qualification. The reason is the temperature dependence of the preload force although it will be less in the MESS-MASCOT system.

4 Adaption of the PRM

This chapter provides an overview about the adaptions and changes made at the PRM to meet the new requirements given by the Japanese Space Agency JAXA. They require a mechanism, to control the success of preload force reduction. Sources used [2] and [3].

4.1 Mechanical requirements

- Preload release mechanism assembly should be installable as two single parts for reliable integration into the lander.
- According to the required displacement of 2mm, the PRM shall consist of two main movable parts with little mechanical friction.

4.2 Control of success

The current configuration of the PRM has no possibility to control the success after triggering. This takes the risk of rebounding of MASCOT from the asteroid´s surface if the preload force is yet too high above the required value.

In Tab. 4-1 possible measurements methods are listed as well as an assessment of theirs feasibility and the quality of the gotten information. For further steps of solution finding, possibilities which are not feasible are neglected. From the remaining feasible methods is only one with a high quality of gotten information. The preferred method to confirm the successful preload force reduction by the PRM after launch can be provided from the following table with different feasible options to get the optimum solution. This is the solution with contacts.

	Measurement	Feasibility	Quality of information
Temperature	Temp. sensor	Yes	Low
Movement	Camera/GNC + target	Yes	Moderate (indirect Measurement)

Stress/strain	Strain gauges, Pressure sensor	No (amplifier, etc. would be required)	High
Contact	Electrical contact, Dedicated contact	Yes Maybe (data handle has be to be clarified)	High
Current/voltage	At the PCDU	Yes	Low
Outgassing	Resonating quartz crystal sensors	NO	Low
Displacement	IR sensor	Yes	Moderate

Tab. 4-1: Measurements possibilities and assessment of theirs feasibility and information quality

According to the electrical contacts, the hysteresis effect should be considered precisely. Hence, the available supporting force after the reduced initial force of 2,5kN should be estimated to be still present to close the contacts. As soon as the contacts have contact and an electrical circuit is closed, a visual success display like a diode shall be activated. This signal could be controlled by an integrated camera.

In the present configuration the force is directed through the spacer bushing into the lower collection pan. Due to limited space inside the mechanism, internal cable installation cannot be realized. For this reason the contact has to be outside the PRM. In order to keep the existing configuration of the RPM and internal accommodation inside the lander, three contacts will be preferred. They should be distributed symmetrically around the central axis of the mechanism.

4.3 Proposal of solution

From the four eyelets, which were intended for the linear guidance bolts, three were removed. This modification will provide space for three new eyelets (see Fig. 4-1), with internal screwed contacts. These contacts (see Fig. 4-2) consist of an insulation made of PEEK (Polyetheretherketone). The contact bolt will be

made of aluminum or copper. Finally, the bolt will be screwed inside the insulation.

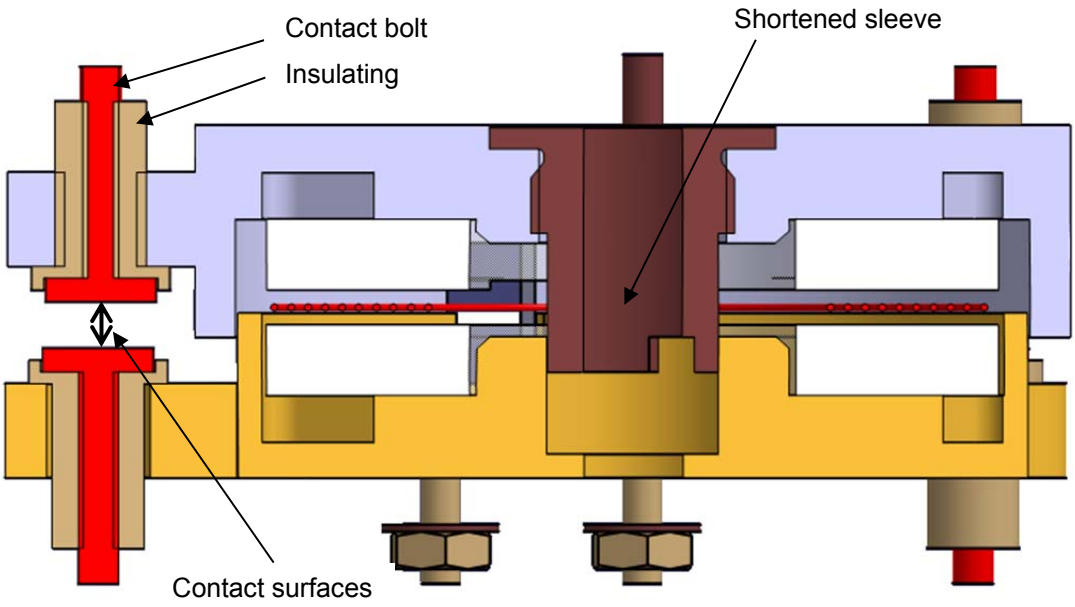

Fig. 4-1: Cut view of the new PRM

The bolts are electrical conductive while the insulating is not. In the same time the former spacer bushing is shorted. Also it is now made of aluminum instead of steel because there will no longer be a force flow through it. Its only task is now to prevent the polyethylene inserts from flowing out of the collections pans while they are heated.

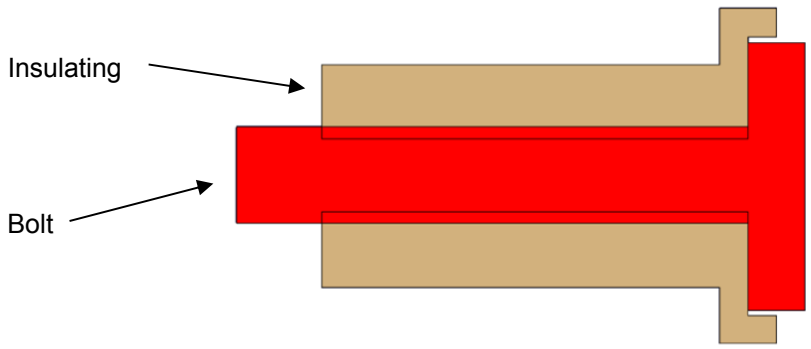

Fig. 4-2: Contact bolt screwed into insulating

From now on the three contacts should direct the force flow. By that the hysteresis effect is of no significance. As soon as the polyethylene inserts are

melted, the upper collection pan moves towards the lower one until it is limited again by the contacts (see Fig. 4-3). The thin end of the contact bolt can be attached with a cable. Together with a source of voltage, a diode and the therefor required circuit a visual success display is realized. As soon as the contact surfaces of the contact bolts are pressed together, the diode will start to glow.

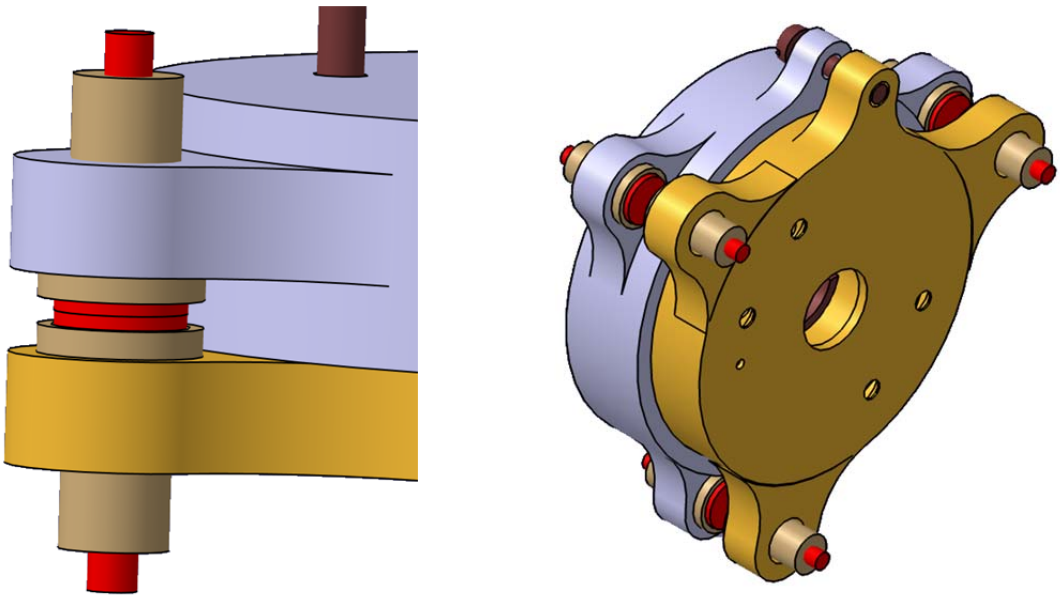

Fig. 4-3: New PRM assembly

The last bolt should secure the upper collection pan, which is screwed with the NEA, from flying away after the separation. This is why the bolt is screwed in the lower collection pan, which is screwed to MASCOT.

5 Conclusion and Outlook

This work focused on the functionality testing of the PRM and the determination of creeping properties of the in this used polyethylene inserts. For these tests of functionality a test set up was constructed, which simulates the conditions, the PRM meets in its mounting position inside MASCOT as far as known. With the test set up the creeping behavior in various spring rate configurations were monitored. During the tests temperature, preload force and distances were taken.

The second part of this work deals with the new requirement, given by JAXA, in which the success of the PRM should be checked in flight. Success means a reduction of the preload force to a specific value. Therefor an investigation of different measurement possibilities was made. These possibilities were rated with respect to their feasibility and the quality of gained information. With the so obtained option, the PRM was adapted. This adaption foresees a visual confirmation during the heating phase as soon as the collection pans are limited again by the contacts.

There still remain unresolved issues in the field of creeping properties. This is due to the still unknown spring rate of the MASCOT-MESS system. The spring rate should be measured empirically with the aid of the manufactured MASCOT-MESS system, especially of the qualification model.

6 Glossary

Abbreviation	Definition
ADC	Analogue Digital Converter
AIV	Assembly Integration and Verification
AOS	Acquisition of Signal
AU	Astronomical Unit (~ 150 mio km)
AVP	Assembly Verification Plan
BEE	Back End Electronics
CAD	Computer Aided Design
CC	Cold Compartment
CDF	Concurrent Design Facility
CDR	Critical Design Review
CFRP	Carbon Fiber Reinforced Polymer
CFT	Cruise Functional Test
CIL	Critical Items List
CM	Compliance Matrix
CNES	French government space agency
CONSERT	Biostatic radar between the orbiter and lander; optional instrument for MASCOT
CUL	Close-up Lens of camera
DDV	Design Development and Verification Plan
DEM	Digital Elevation Model
DH	Data Handling
DHS	Data Handling System
DLR	German Aerospace Center
DMC	Descent Module Composite
DOI	Declaration of Interest
DTC	Drop Tower Campaign

ECSS	European Cooperation for Space Standardization
EGSE	Electrical ground Support Equipment
E-ICD	Experiment Interface Control Document
EID-A	Experiment Interface Document Part A; describes the lander's requirements to the instrument teams
EID-B	Experiment Interface Document Part B; instrument team's answer to the EID-A
E-IRD	Experiment Interface Requirement Document
EQM	Electrical Qualification Model
EMC	Electromagnetic Compatibility
ESA	European Space Agency
ESOC	European Space Operations Centre
ESS	Electrical Support System
FDIR	Failure Detection, Isolation and Recovery
FM	Flight Model
FMECA	Failure Modes, Effects and Criticality Analysis
FOV	Field of View
FPA	Focal Plane Array
FRR	Flight Readiness Review
GNC	Guidance Navigation Control
GRM	Ground Reference Model
GS	Ground Segment
HP3	Heat Flow and Physical Properties Package
HPL	Humboldt Payload, a stationary autonomous package designed to acquire geophysical and environmental data on the Martian surface
HW	Hardware
I/F	Interface
ICD	Interface Control Document
IDD	

IDM	Integrated Data Model
IIT	Initial Integration Test
ILMA	Ion Laser Mass Spectrometer, optional instrument for MASCOT
IR	Infrared
IRD	Interface Requirement Document
JAXA	Japan Aerospace Exploration Agency
LIBS	Laser Induced Breakdown Spectrometer
LOCC	Lander Operations Control Centre
LRR	Launch Readiness Review
LUP	Latch Up Protection
MARA	MASCOT Radiometer
MASCOT	Mobile Asteroid Surface Scout
MASCOT XS	current lander option with reduced/optimised size
MCC	MASCOT Control Center
MER	Mars Exploration Rover
MESS	Mechanical & Electrical Support System
MGS	MASCOT Ground Segment
MicrOmega IR	Microscope (infrared spectrum); optional intrument for MASCOT
MicrOmega VIS	Microscope (visual spectrum) ; optional intrument for MASCOT
MLI	Multi-Layer Insulation
MuO	Memorandum of Understanding
MRD	Mission Requirement Document
MSU	MicrOmega Sensor Unit
MUSC	Microgravity User Support Center
NASA	National Aeronautics and Space Administration
NEA	Non Explosive Actuator
NEA	Near Earth Asteroid

NEO	Near Earth Object
OBC	On Board Computer
OBDH	On Board Data Handling
OP	operational
P/L	Payload
PA Plan	Product Assurance Plan
PAR	Preliminary Acceptance Review
PCBs	Printed Circuit Board
PCDU	Power Control and Distribution Unit
PDR	Preliminary Design Review
Pis	MASCOT payload teams
PIM	Periphery interface module
PLUTO	Planetary Underground Tool
POR	Power On Request
PP	Permittivity Probe
PPI	Planetary Protection Implementation Plan
PPL	Pasteur Payload (specification?)
PRR	Preliminary Requirements Review
QR	Qualification Review
RD	Reference Document
RF	Radio Frequency
RGB	Red Green Blue (Color specification a camera mode)
S/C	Spacecraft
SDD	System Design Document
S/S	Subsystem
SDL	Separation, Descend & Landing
SDR	System Definition Review
SEE	Single Event Upset Error

SEP	Surface electrical properties or also Solar Electric Propulsion
SNR	Signal to Noise Ratio
SRD	Science Requirements Document
SRR	System Requirements Review
SSAs	MASCOT sub-system authorities
STM	Structural and Thermal Model
SW	Software
TB	Thermal Balance
tbc	to be confirmed
tbd	to be defined
tbw	to be written
TC	Thermocouple
TRL	Technology Readiness Level
TS	Technical Specification
TVAC	Thermal Vacuum Test
TVR	Technical Validation Review
UART	Universal Asynchronous Receiver Transmitter
UHF	Ultra High Frequency
URD	User Requirements Document
VCD	Verification Control Document
VIB	Vibration Resonance Check
WAC	Wide Angle Camera, optional instrument for MASCOT
wrt	with respect to
XRD/XRF	X-ray Refractometer
H2A	Launcher for HAYABUSA

7 Annex

7.1 Functionality Test

7.1.1 Evaluation

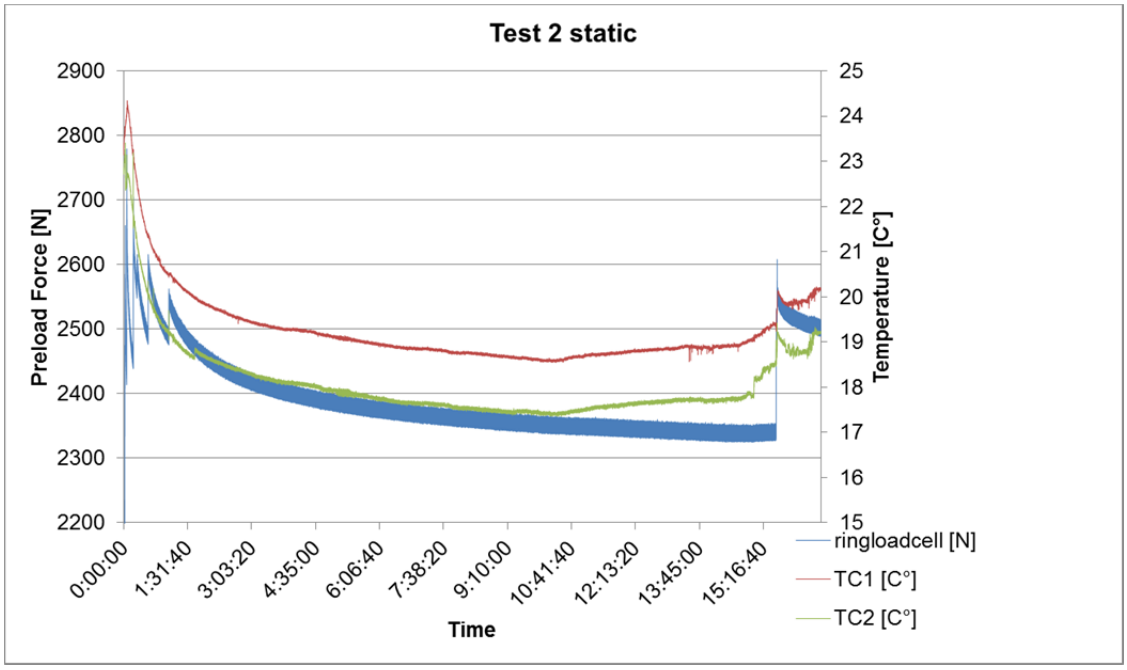

Fig. 7-1: Diagram of test 2 static showing force/temperature over time

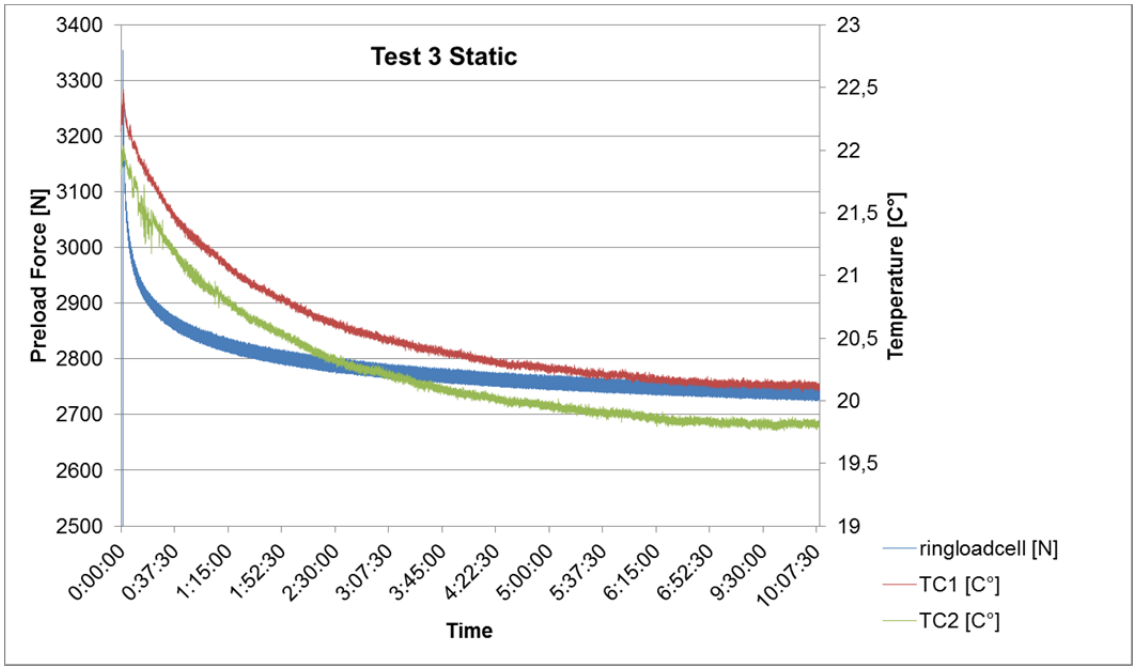

Fig. 7-2: Diagram of test 3 static showing force/temperature over time

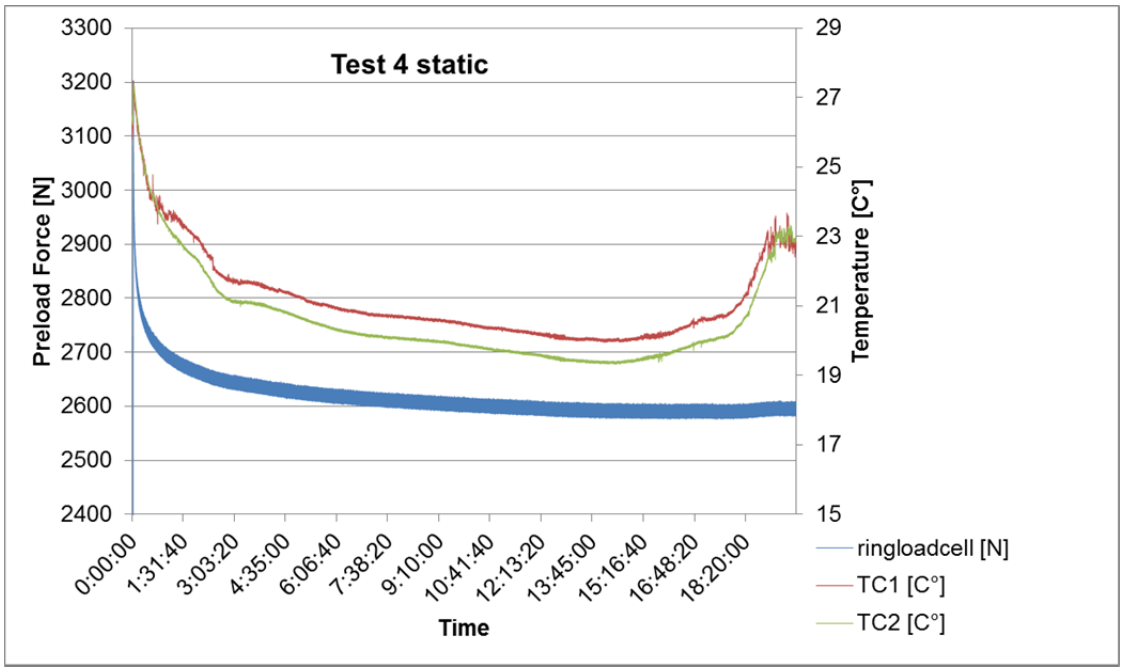

Fig. 7-3: Diagram of test 4 static showing force/temperature over time

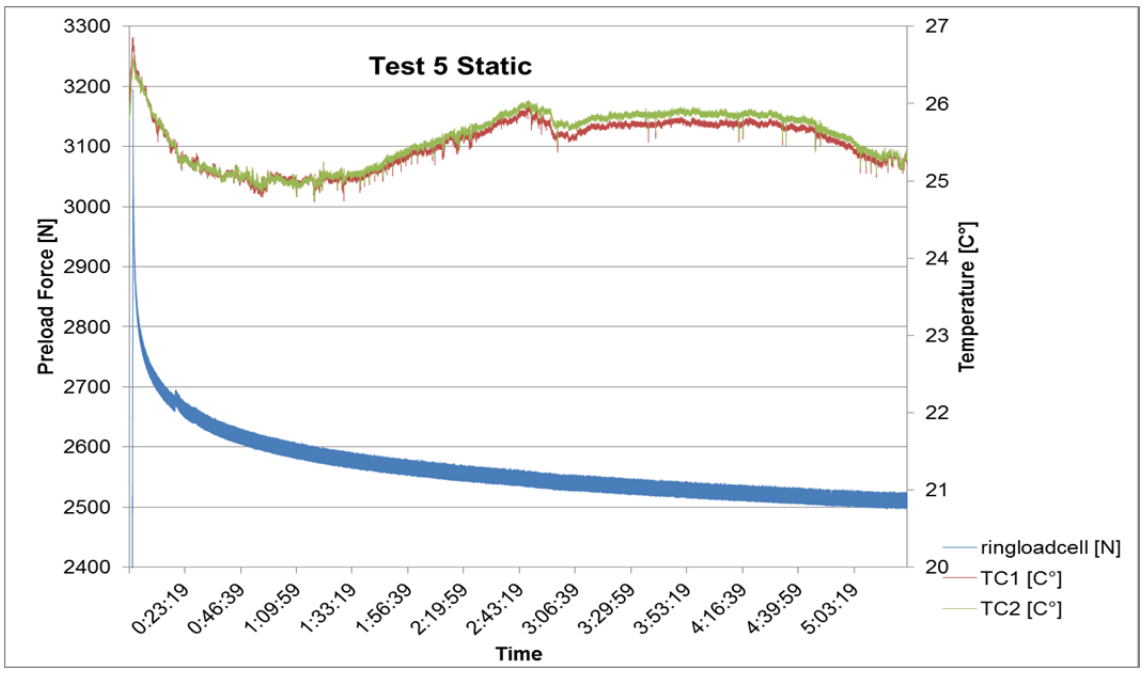

Fig. 7-4: Diagram of test 5 static showing force/temperature over time

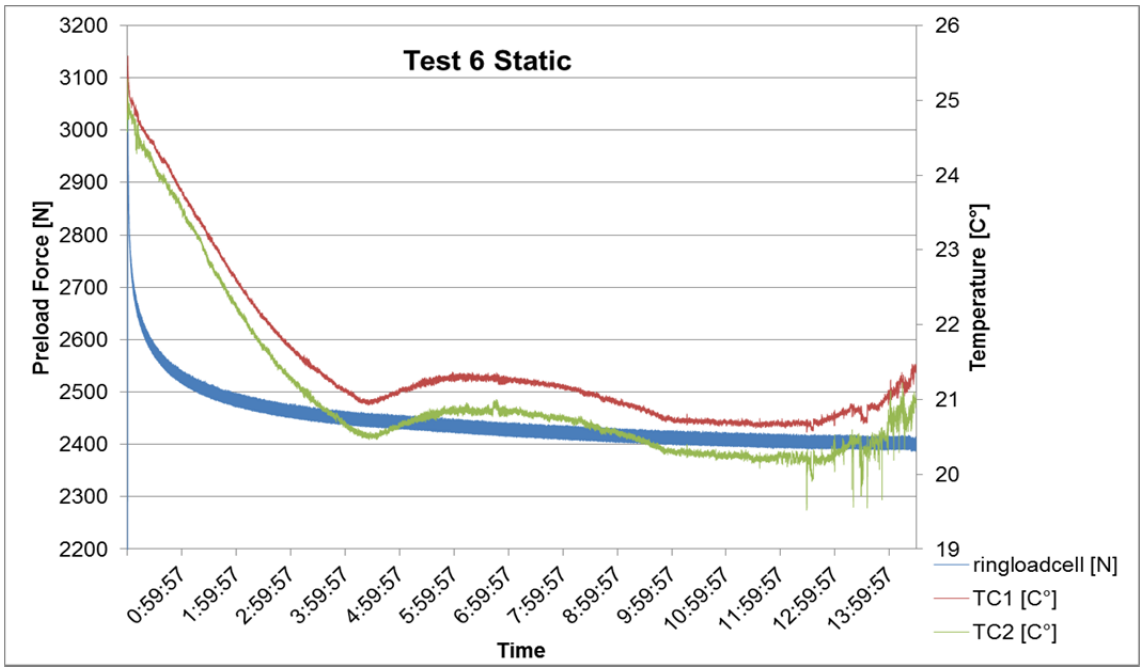

Fig. 7-5: Diagram of test 6 static showing force/temperature over time

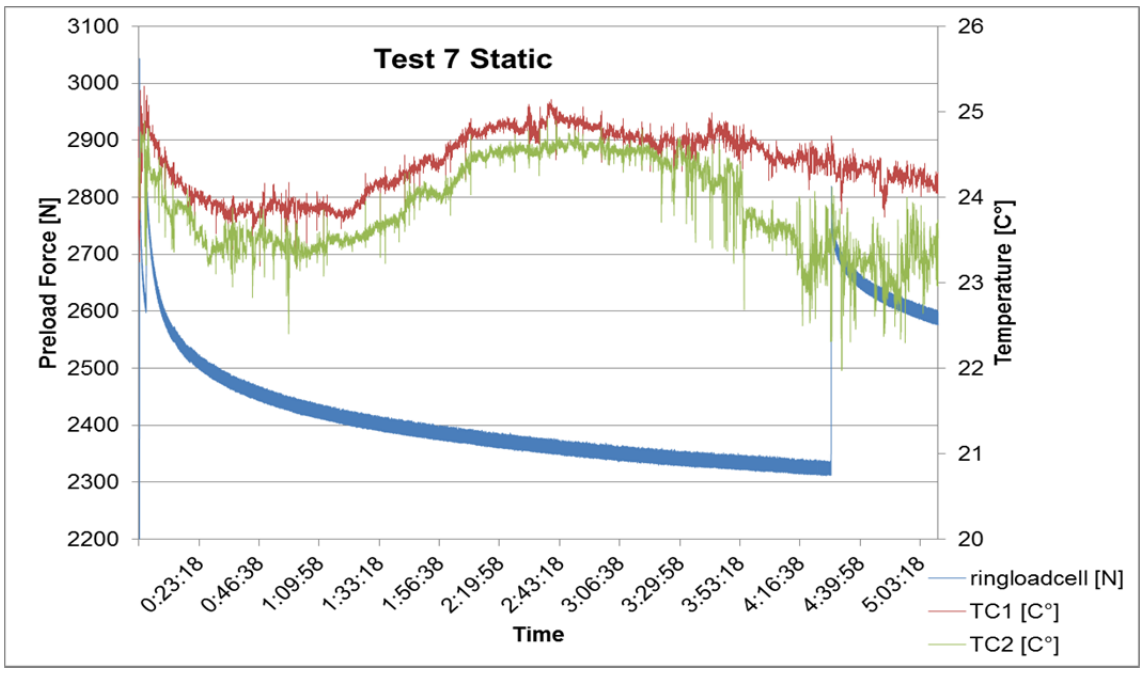

Fig. 7-6: Diagram of test 7 static showing force/temperature over time

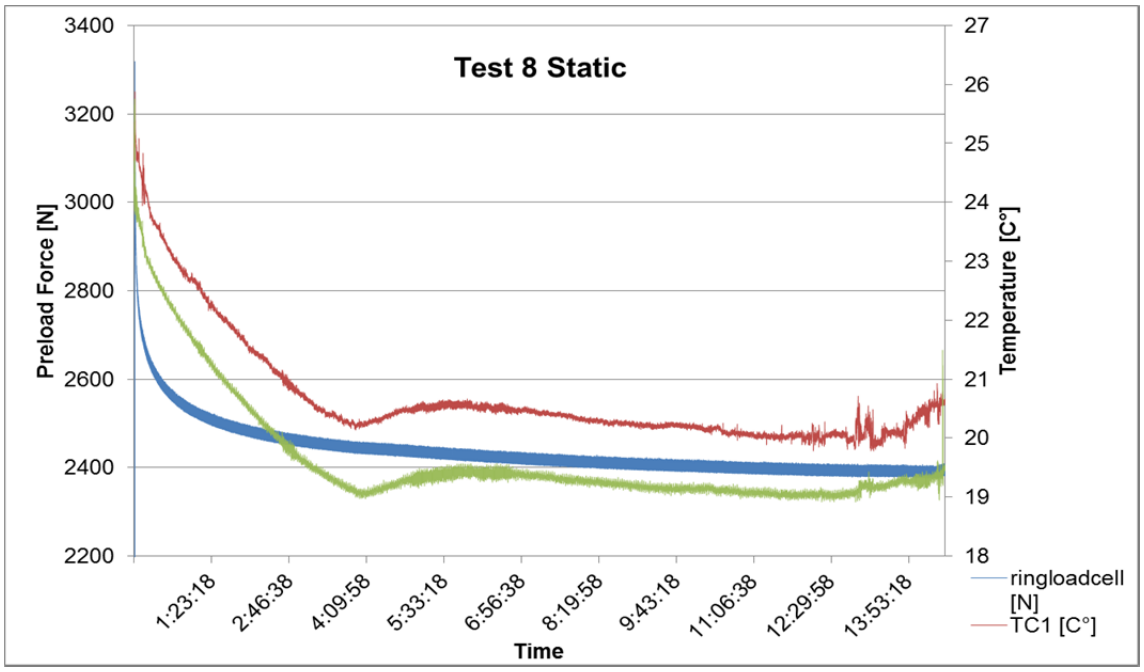

Fig. 7-7: Diagram of test 8 static showing force/temperature over time

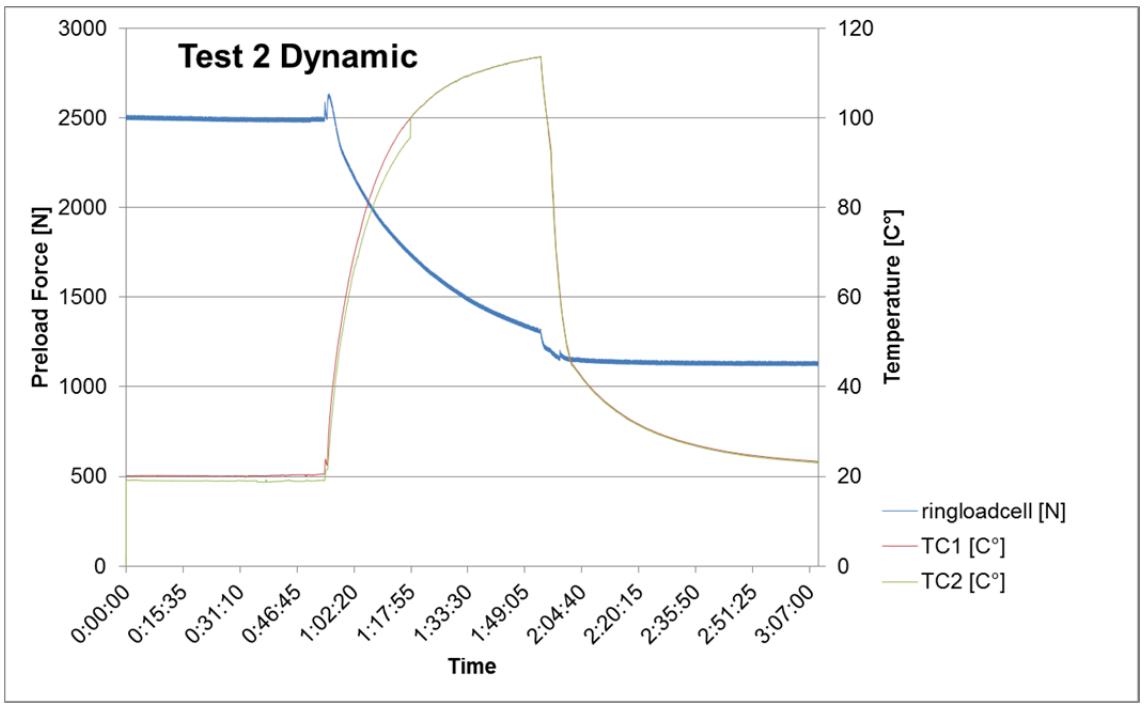

Fig. 7-8: Diagram of test 2 dynamic showing force/temperature over time

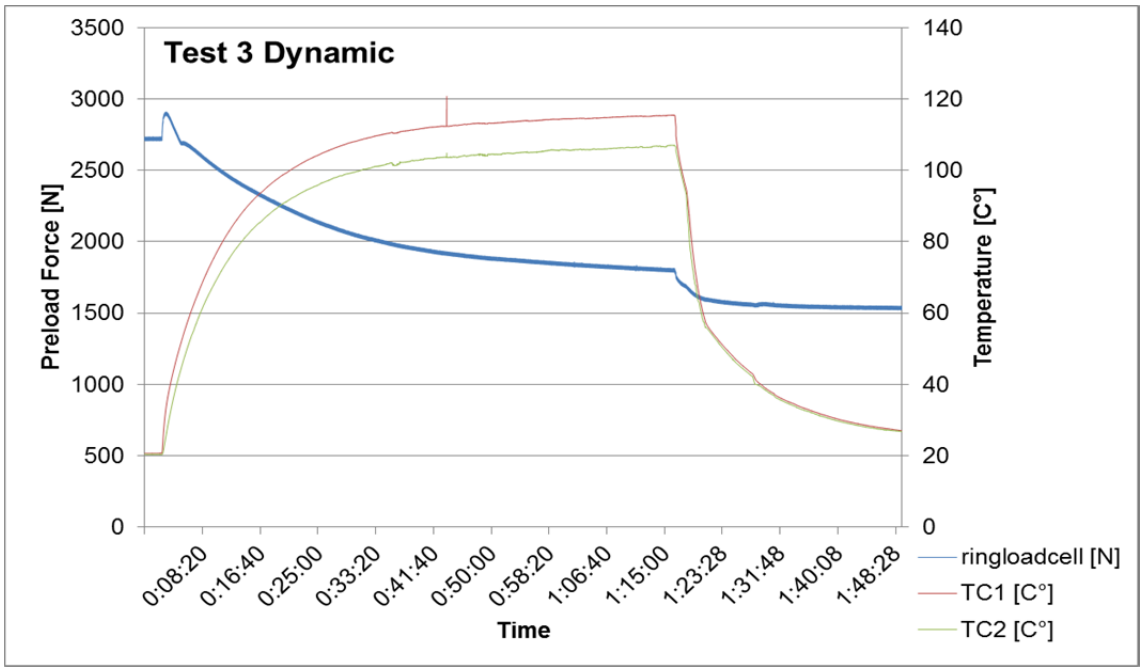

Fig. 7-9: Diagram of test 3 dynamic showing force/temperature over time

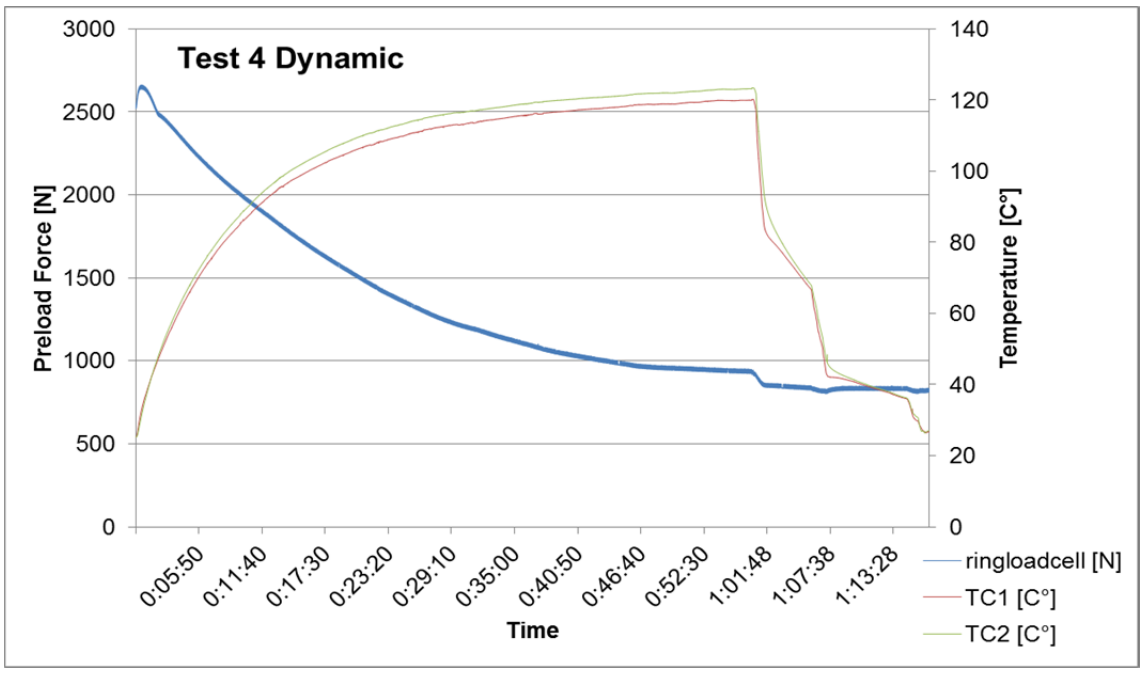

Fig. 7-10: Diagram of test 4 dynamic showing force/temperature over time

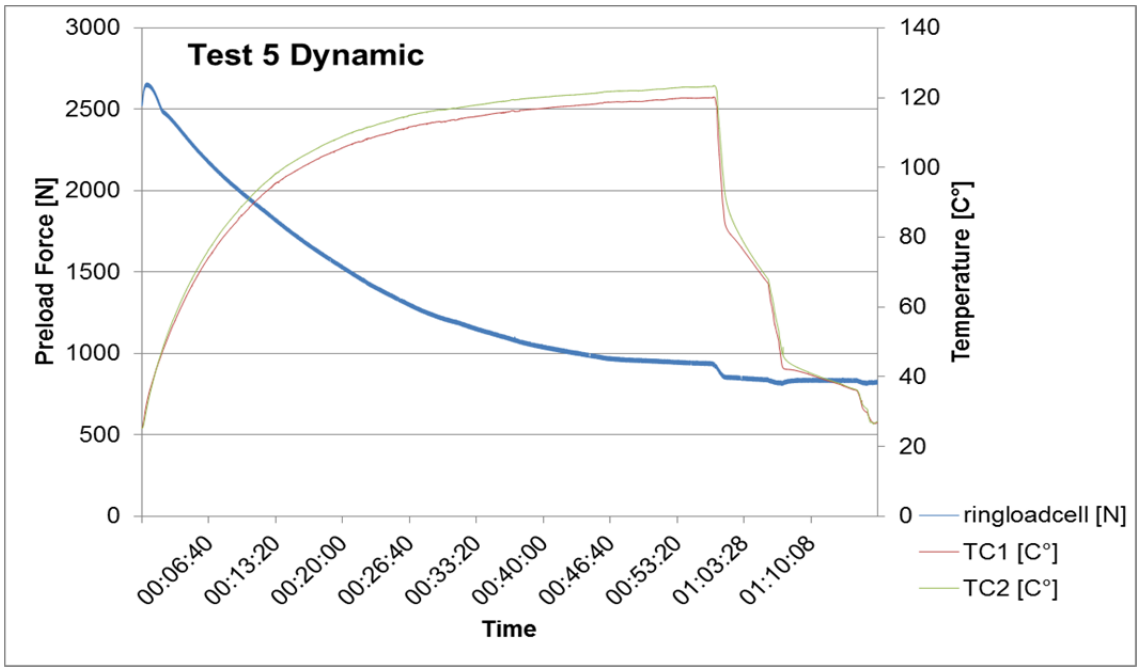

Fig. 7-11: Diagram of test 5 dynamic showing force/temperature over time

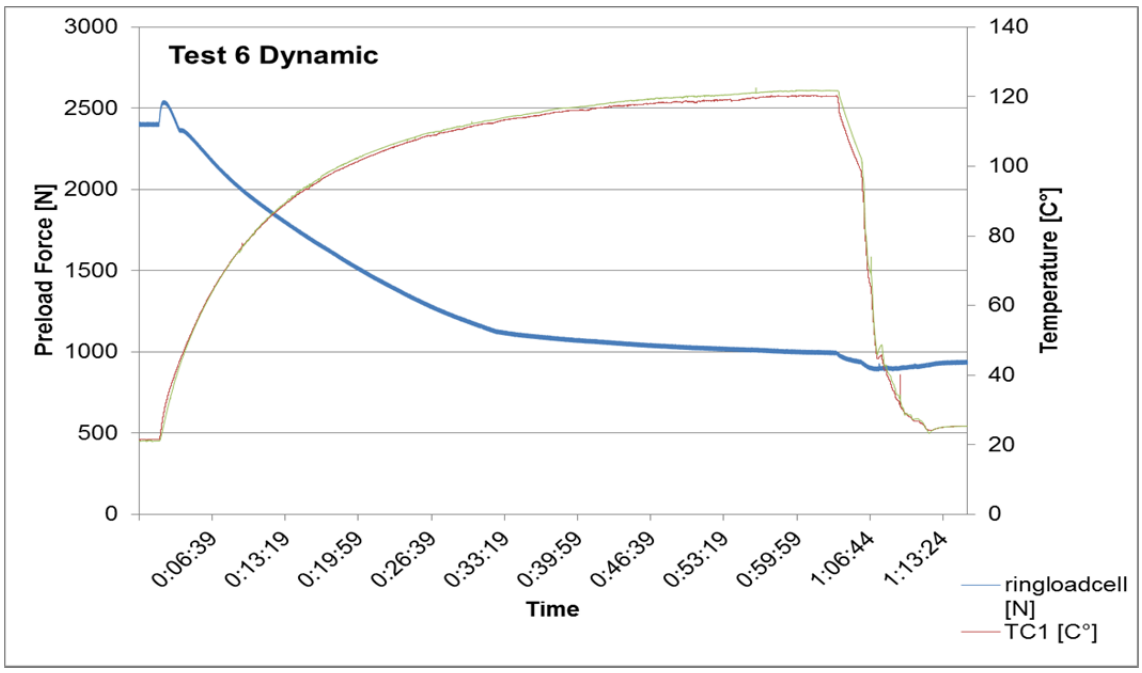

Fig. 7-12: Diagram of test 6 dynamic showing force/temperature over time

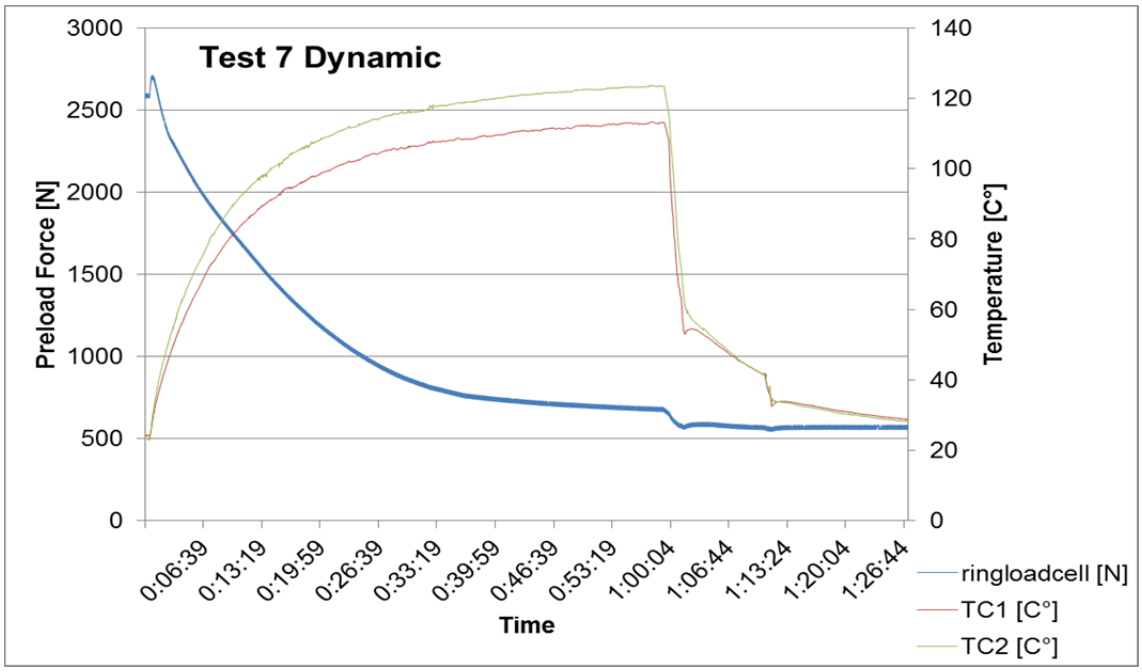

Fig. 7-13: Diagram of test 7 dynamic showing force/temperature over time

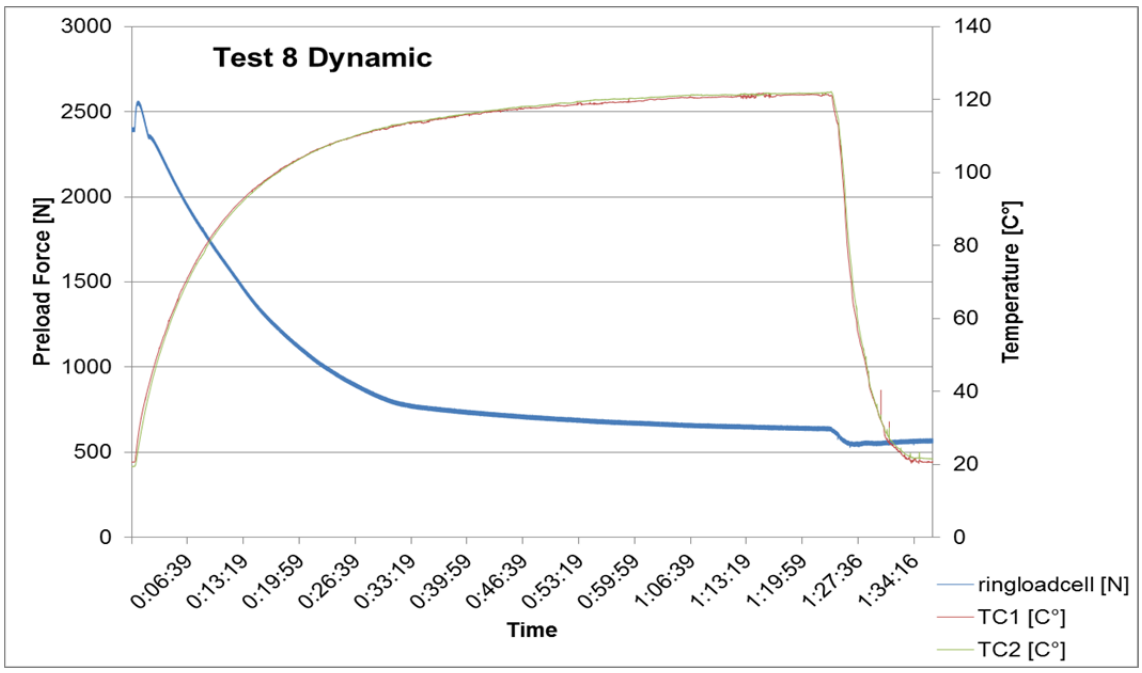

Fig. 7-14: Diagram of test 8 dynamic showing force/temperature over time

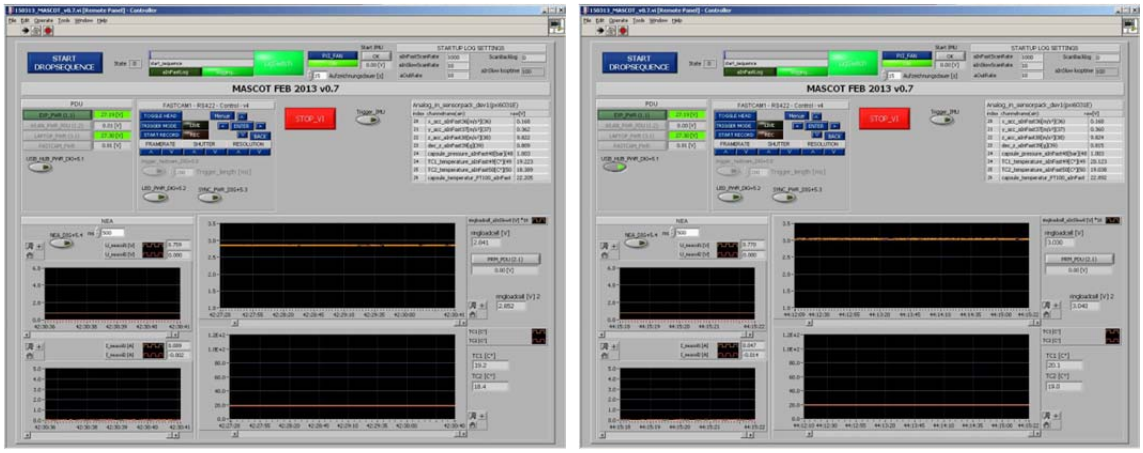

Fig. 7-15: Screenshot of the Lab View program. Left at the beginning and right at the end of test 2

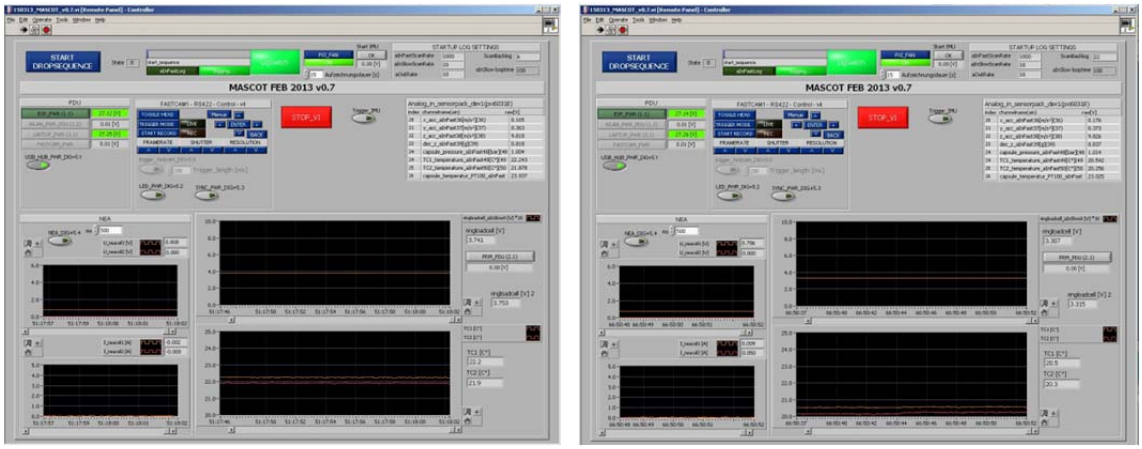

Fig. 7-16: Screenshot of the Lab View program. Left at the beginning and right at the end of test 3

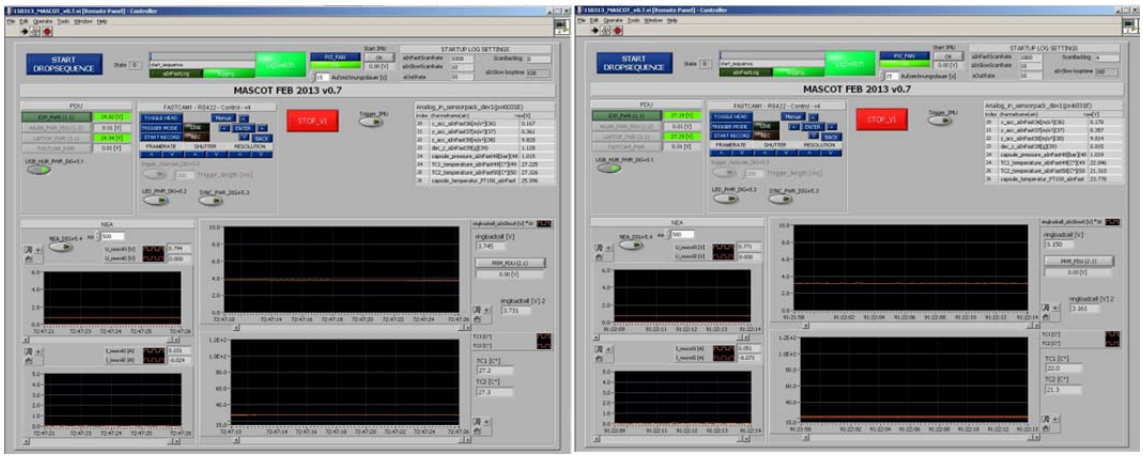

Fig. 7-17: Screenshot of the Lab View program. Left at the beginning and right at the end of test 4

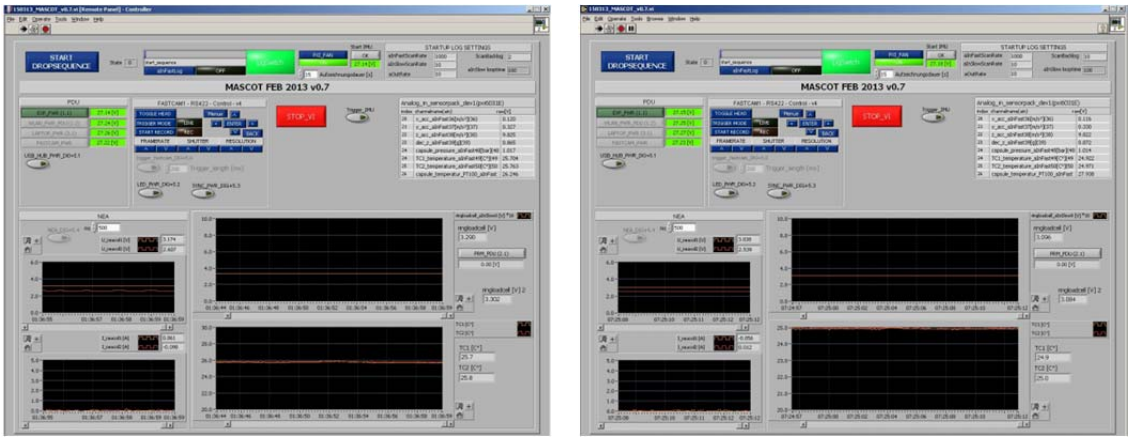

Fig. 7-18: Screenshot of the Lab View program. Left at the beginning and right at the end of test 5

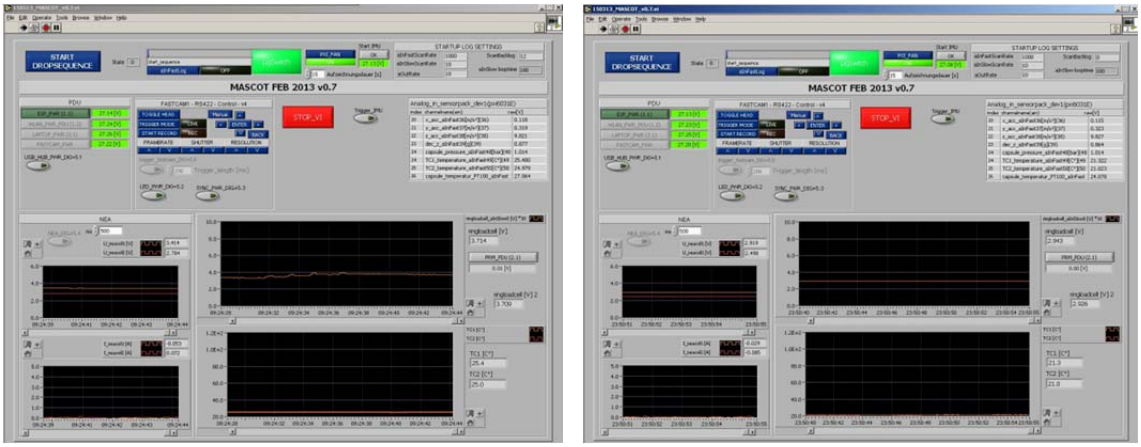

Fig. 7-19: Screenshot of the Lab View program. Left at the beginning and right at the end of test 6

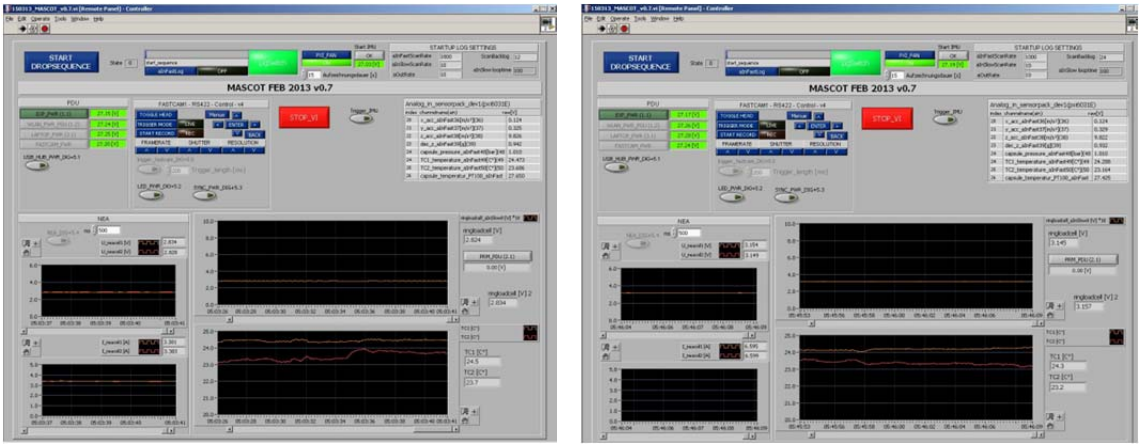

Fig. 7-20: Screenshot of the Lab View program. Left after the first creeping process and right at the second one of test 7

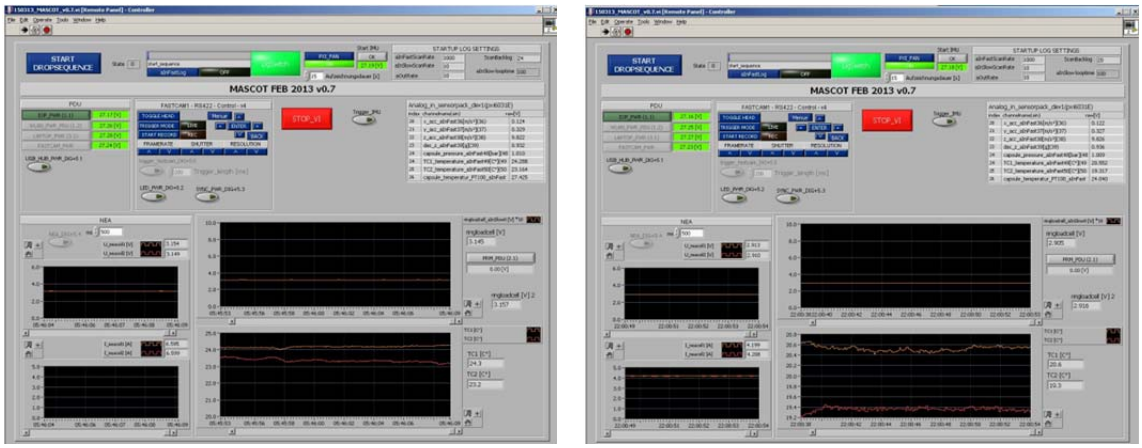

Fig. 7-21: Screenshot of the Lab View program. Left after the first creeping process and right at the second one of test 8

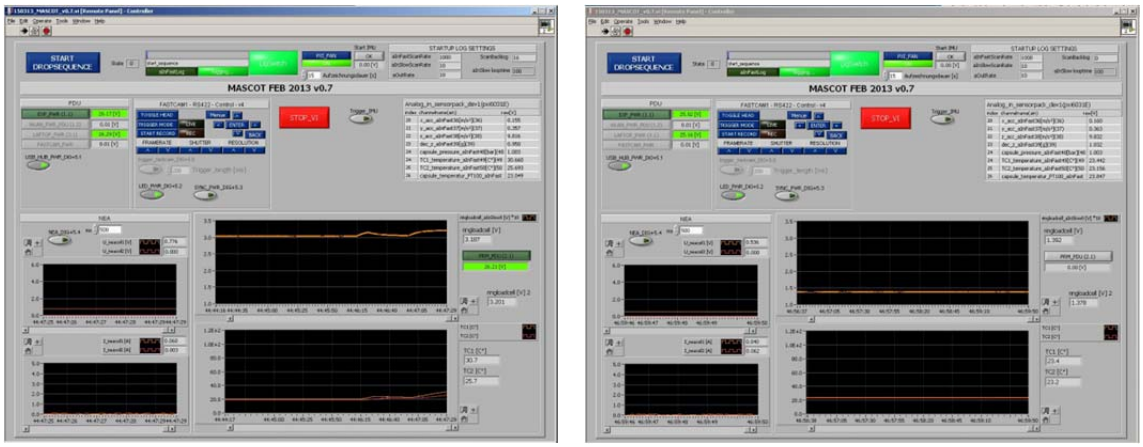

Fig. 7-22: Screenshot of the Lab View program. Left short after the beginning and right at the end of test 2

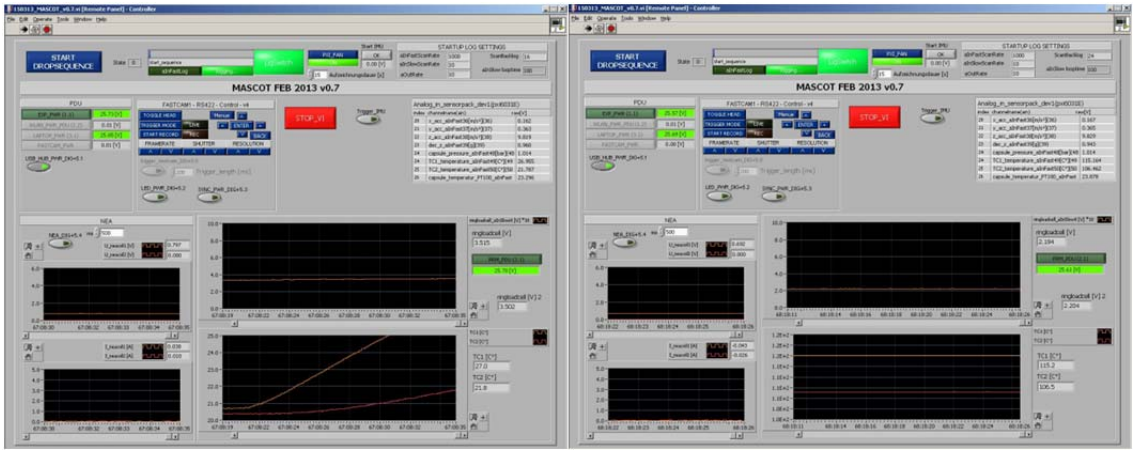

Fig. 7-23: Screenshot of the Lab View program. Left short after the beginning and right at the end of test 3

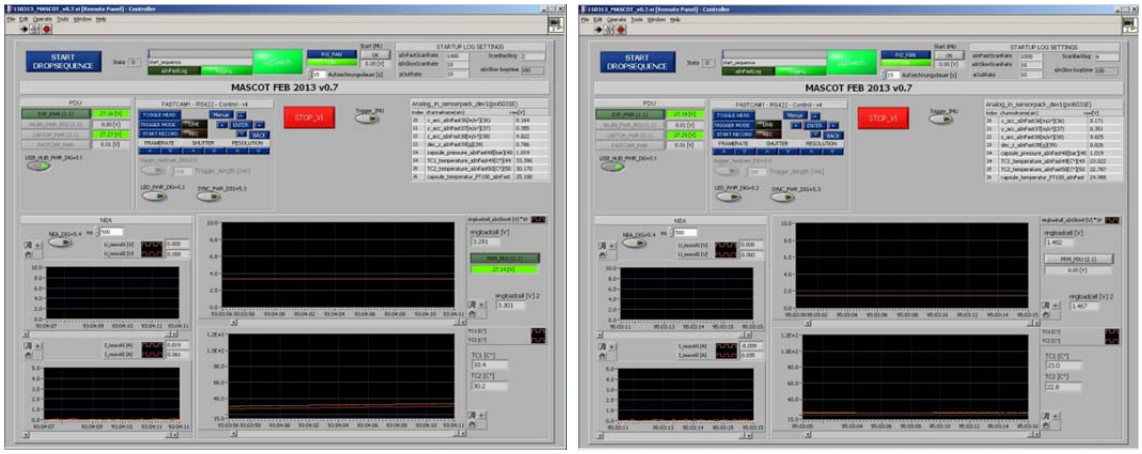

Fig. 7-24: Screenshot of the Lab View program. Left short after the beginning and right at the end of test 4

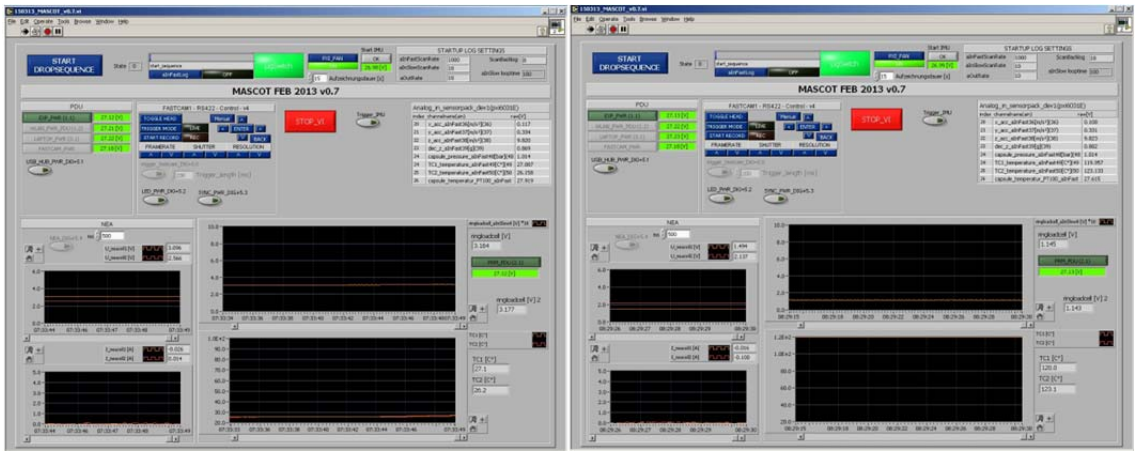

Fig. 7-25: Screenshot of the Lab View program. Left short after the beginning and right at the end of test 5

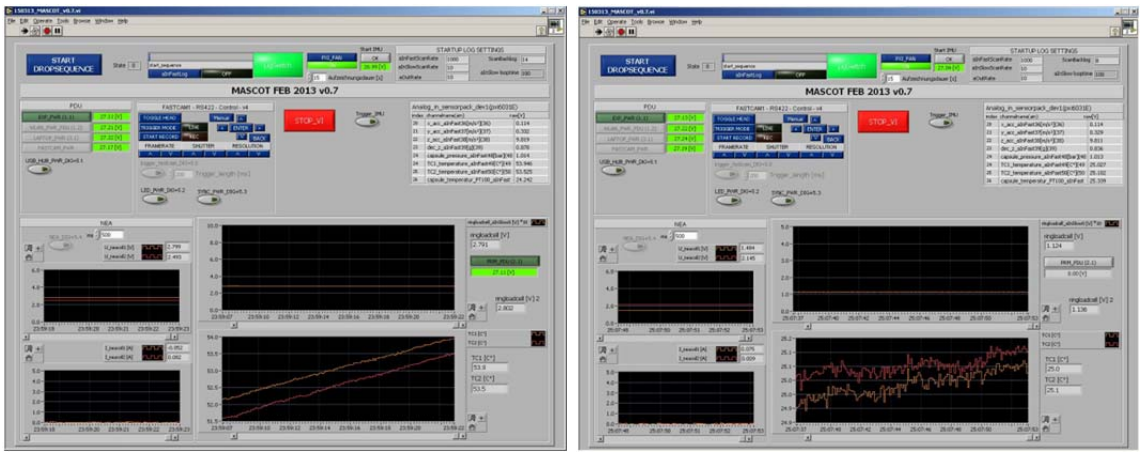

Fig. 7-26: Screenshot of the Lab View program. Left short after the beginning and right at the end of test 6

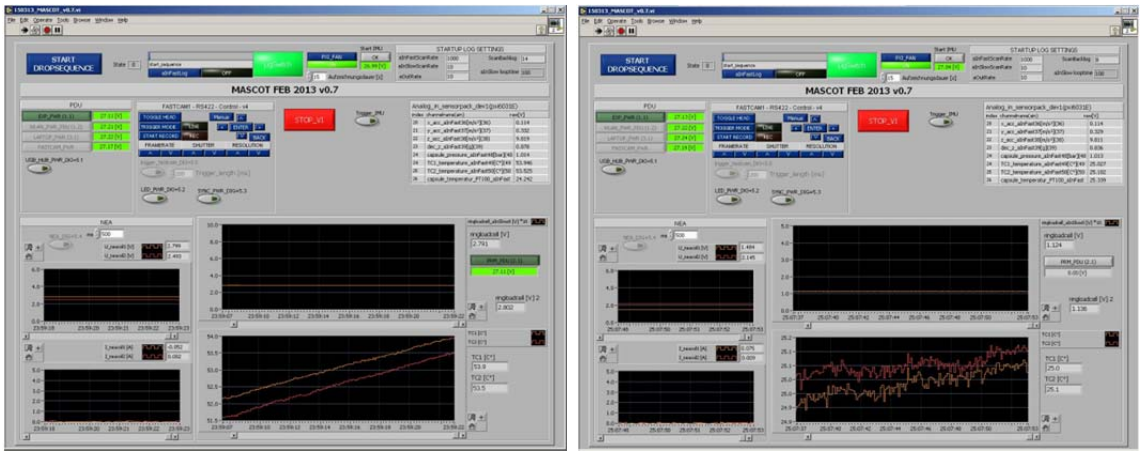

Fig. 7-27: Screenshot of the Lab View program. Left short after the beginning and right at the end of test 7

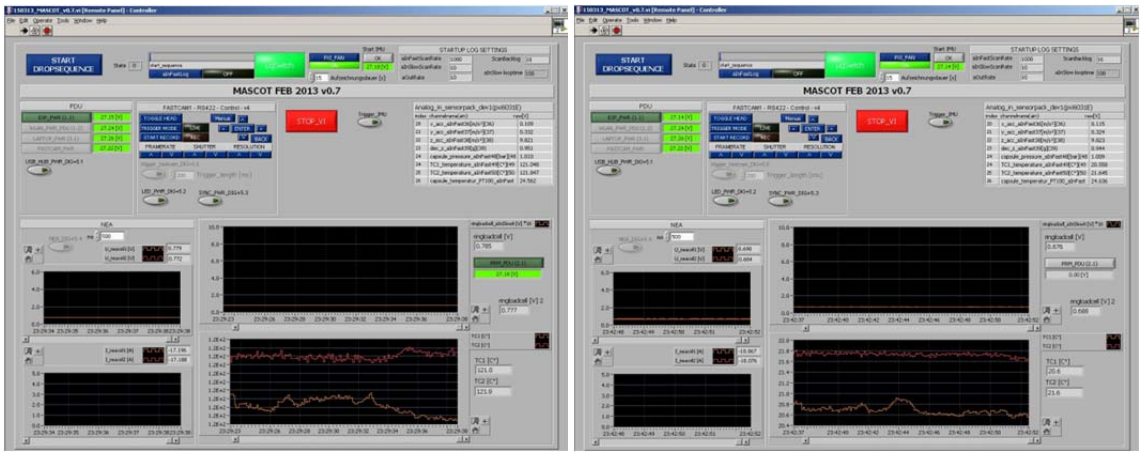

Fig. 7-28: Screenshot of the Lab View program. Left short after the beginning and right at the end of test 8

Grimmomat source code:

“@echo off

title Der Grimmomat

set /p datei="Bitte gewuenschte Text-Datei eingeben: "

echo Die Datei enthaelt folgende Zeilenanzahl:

find %datei% /c /v ""

pause >NUL

set /p var="Bitte gewuenschte Schrittweite angeben: "

```
set /p var3="Bitte geben Sie die Anzahl einzulesender Zeilen ein: "

set var2=1

set cou=1

:loop

For /F "skip=%var2% tokens=1,2,3,4" %%a in (%datei%) do echo %%a %%b %%c %%d>>"Copy of %datei%"&&goto weiter

: weiter

set /a var2=%var2% + %var%

set /a cou=%cou%+1

if %cou% LEQ %var3% goto loop else goto ende

goto ende

:ende

echo Die Programmausfuehrung war erfolgreich. Das Programm wird nun beendet.

pause >NUL”
```

7.1.2 Appliance Data Sheets

burster

Miniature Ring Load Cell

Model 8438

Code:	8438 EN
Delivery:	ex stock/6 weeks
Warranty:	24 months

CAD data 2D/3D for this sensor:
Download directly at www.traceparts.com
Info: refer to data sheet 80-CAD-EN

8438 EN

- **Measuring ranges from 0 ... 5 N to 0 ... 200 kN**
- **Centric throughout hole**
- **Flat disc design**
- **Made of stainless steel**
- **Completely welded sensor body**
- **Nominal characteristic value standardization possible**

Application

The miniature ring load cells of the 8438 series have been specially designed to show-up with small external dimensions. These sensors can be used for a wide range of industrial and laboratory applications due to their small size. The small diameter and height make this miniature ring load cell perfect for installation in structures, in which the measured force is guided directly through the sensor after disconnection.

Examples of this are force measurements on

- Bolts
- Screws
- Plate and cover fasteners
- Bearing contact forces
- Spot welding machines
- Cutting tools

Description

The measured tension and compression force must be introduced axially and perpendicularly to the entire surface of the inner and outer bands of the sensor in the opposite direction. Conversion of the acting force into an electrical output signal is performed by strain gauges connected together in a full bridge circuit. To achieve optimal accuracy, the base of the sensor should rest on a smooth level surface, hardened to at least 63 HRC with sufficient dimensions. The base cover welded to the surface has a stabilizing effect on the sensor element. Lateral forces should be avoided anyway as they distort the measured results.
During installation or operation, ensure that the cable outlet and the sensor cable are not subject to excessively high tensile or bending forces. Strain and bend relief may be necessary for the sensor cable on the machine side.

8438 EN - 2

Technical Data

Order Code	Measuring Range	Dimensions [mm]													Thread	Resonance Frequency
		D1	ø D2	ø D3	ø D4	ø D5	A	H	øC	L	øK	M	B	øT	G	[kHz]
8438-5005	0 ... 5 N	12.7	11.4	10.2	5.1	2.5	3.0	3.8	-	-	1.2	1.2	-	-	-	0.4
8438-5010	0 ... 10 N	12.7	11.4	10.2	5.1	2.5	3.0	3.8	-	-	1.2	1.2	-	-	-	0.7
8438-5020	0 ... 20 N	25.4	21.6	20.6	6.6	5.1	6.4	7.1	4.8	8.0	1.4	3.0	-	-	-	1.0
8438-5050	0 ... 50 N	25.4	21.6	20.6	6.6	5.1	6.4	7.1	4.8	8.0	1.4	3.0	-	-	-	1.1
8438-5100	0 ... 100 N	28.0	25.0	22.0	9.0	5.5 H8	7.0	8.0	2.2	8.0	1.9	2.5	-	-	-	1.2
8438-5200	0 ... 200 N	28.0	25.0	22.0	9.0	5.5 H8	7.0	8.0	2.2	8.0	1.9	2.5	-	-	-	2.0
8438-5500	0 ... 500 N	28.0	25.0	22.0	9.0	5.5 H8	7.0	8.0	2.2	8.0	1.9	2.5	-	-	-	3.7
8438-6001	0 ... 1 kN	38.0	29.0	25.0	13.5	7.0 H8	9.0	10.0	3.6	8.0	3.0	3.0	3.0	33.5	M 2.5x0.45	3.4
8438-6002	0 ... 2 kN	38.0	29.0	25.0	13.5	7.0 H8	9.0	10.0	3.6	8.0	3.0	3.0	3.0	33.5	M 2.5x0.45	5.5
8438-6005	0 ... 5 kN	38.0	29.0	25.0	13.5	7.0 H8	9.0	10.0	3.6	8.0	3.0	3.0	3.0	33.5	M 2.5x0.45	10.0
8438-6010	0 ... 10 kN	38.0	29.0	25.0	13.5	7.0 H8	9.0	10.0	3.6	8.0	3.0	3.0	3.0	33.5	M 2.5x0.45	15.0
8438-6020	0 ... 20 kN	49.0	41.0	35.0	23.0	15.0 H8	15.0	16.0	3.6	8.0	3.0	4.5	3.0	45.0	M 2.5x0.45	14.0
8438-6050	0 ... 50 kN	49.0	41.0	35.0	23.0	15.0 H8	15.0	16.0	3.6	8.0	3.0	4.5	3.0	45.0	M 2.5x0.45	24.0
8438-6100	0 ... 100 kN	78.0	60.0	54.0	42.0	28.0 H8	24.0	25.0	5.6	10.0	5.0	6.5	5.5	69.0	M 4.0x0.7	22.0
8438-6200	0 ... 200 kN	78.0	60.0	54.0	42.0	28.0 H8	24.0	25.0	5.6	10.0	5.0	6.5	5.5	69.0	M 4.0x0.7	37.0

Electrical values

Bridge resistance (full bridge):
- measuring range ≤ 0 ... 10 N semiconductor strain gauge 500 Ω, nominal*
- measuring range ≥ 0 ... 20 N foil strain gauge 350 Ω, nominal*

Excitation:
- measuring range ≤ 0 ... 10 N max. 5 V DC
- measuring range ≥ 0 ... 20 N max. 10 V DC

Nominal sensitivity:
- measuring range ≤ 0 ... 10 N 20 mV/V, nominal*
- measuring range 0 ... 20 N and 0 ... 50 N 2 mV/V, nominal*
- measuring range 0 ...100 N 1.0 mV/V, nominal*
- measuring range ≥ 0 ...200 N 1.5 mV/V, nominal*

* Deviations from the stated value are possible.

Environmental conditions

Range of operating temperature: 0 °C ... + 85 °C
Nominal temperature range: +15 °C ... + 70 °C
Influence of temperature on zero: ≤ ± 0.03 % F.S./K
Influence of temperature on sensitivity: ≤ + 0.03 % Rdg./K

Mechanical values

Non-linearity: ≤ 1.0 % F.S.
Relative hysteresis: ≤ 0.75 % F.S.
Non-repeatability with unchanged assembly position: ≤ 0.25 % F.S.
Deflection full scale: approx. 60 µm
Mounting: measuring range ≥ 0 ... 1000 N
there are three mounting holes on the lower side of the sensor, equally spaced on T diameter with division 120°, one hole is located directly across the cable exit. This kind of mounting is allowed for compression load only.
Operating force max: 150 % of capacity
Dynamic load capacity: recommended 50 % of capacity
max. 70 % of capacity
Material: stainless steel 1.4542
Electrical connection:
- measuring range ≤ 0 ... 500 N: shielded, TPE insulated cable with open ends for soldering, length appr. 2 m. bending radius ≥ 20 mm
- measuring range 0 ... 1 kN to 0 .. 50 kN: additionally equipped with anti-kink protection length appr. 40 mm, bending radius ≥ 30 mm
- measuring range ≥ 0 ...100 kN: additionally equipped with anti-kink protection and adapter for cable holder, length approx. 50 mm, bending radius ≥ 30 mm

Protection class: acc. to EN 60529 range ≤ 0 ... 50 kN IP54
range ≥ 0 ...100 kN IP65
Dimensions: refer to table and dimensional drawing
General tolerance of dimensioning: acc. to ISO 2768-f
Weight: depending on the measuring range, from 5 g up to 900 g
Wiring code: measuring range ≤ 0 ... 50 N / ≥ 0 ...100 N

red	/ with	excitation voltage	positive
black	/ brown	excitation voltage	negative
green	/ green	signal output	negative
white	/ yellow	signal output	positive

Dimensional drawing model 8438

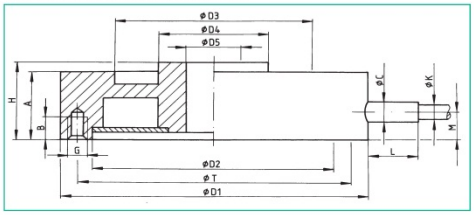

The CAD drawing (3D/2D) for this sensor can be imported online directly into your CAD system.
Download via www.burster.com or directly at www.traceparts.com. For further information about the burster traceparts cooperation refer to data sheet 80-CAD-EN.

Order Information

Miniature ring load cell, measuring range 500 N **Model 8438-5500**

Accessories

Mating connector
12 pins, for all burster desktop devices **Model 9941**
9 pins, for model 9235 and DIGIFORCE® model 9310 **Order Code: 9900-V209**

Installation of a mating connector for main usage of the sensor
- in preferential direction (positive signal for tensile load) **Order Code: 99004**
- only for connection to SENSORMASTER model 9163 desktop version **Order Code: 99002**
- against preferred direction (positive signal for compressive load) **Order Code: 99007**
- only for connection to SENSORMASTER model 9163 desktop version **Order Code: 99008**

Option

Standardization of the sensitivity to 1.0 mV/V ± 1 %, integrated to connector cable only for measurement ranges ≥ 0 ... 20 N **...-V010**

Manufacturer Calibration Certificate (WKS)

Calibration of the load cell separately as well as connected to an indicator is available. Calculation consists of basic costs and additional costs per measuring point. Please mention the requested points. Standard is an 11 point run in 20 % increments up and down.

7.1.3 Test Assembly Drawings

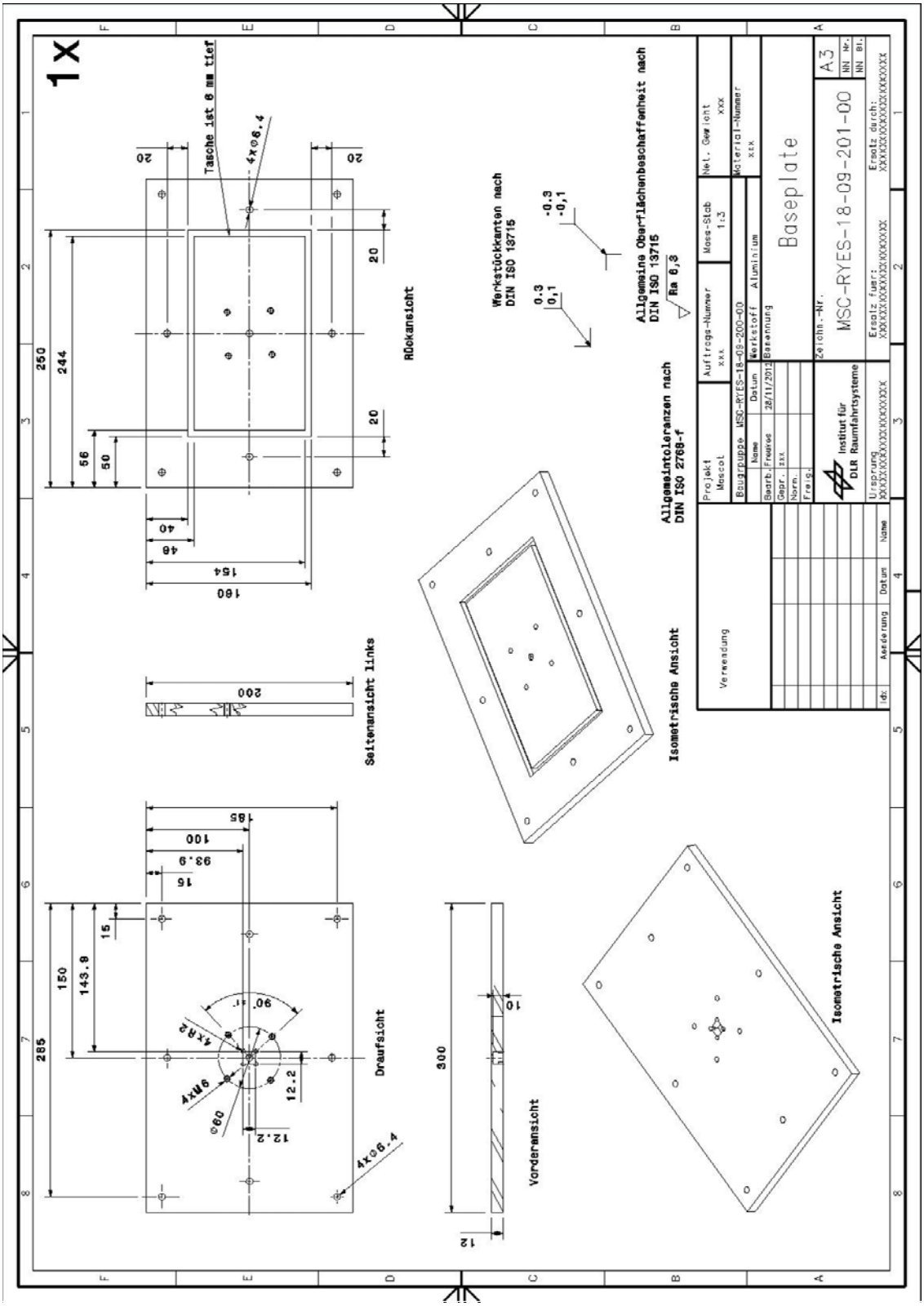

Fig. 7-29: Functionality Test Baseplate Drawing

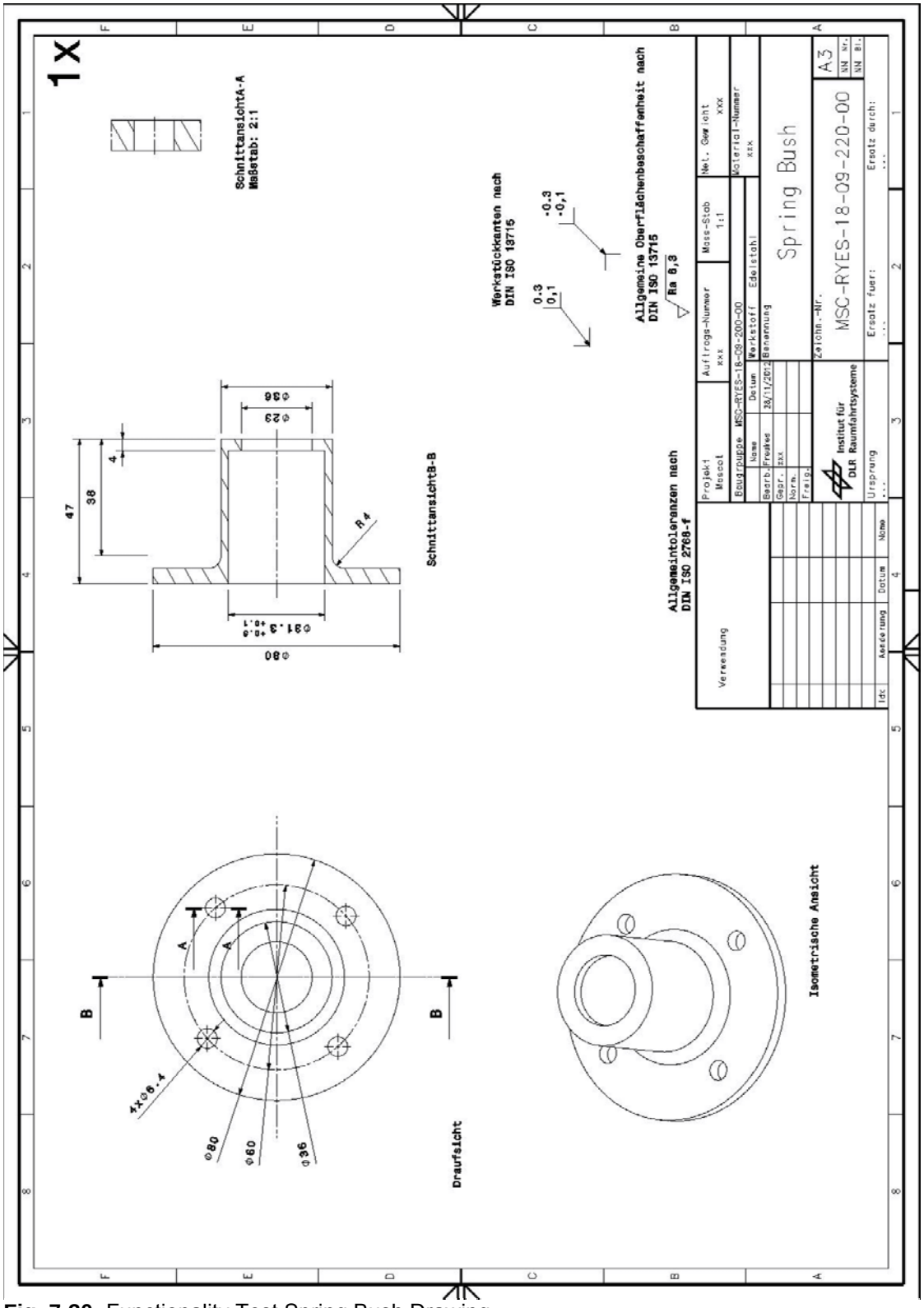

Fig. 7-30: Functionality Test Spring Bush Drawing

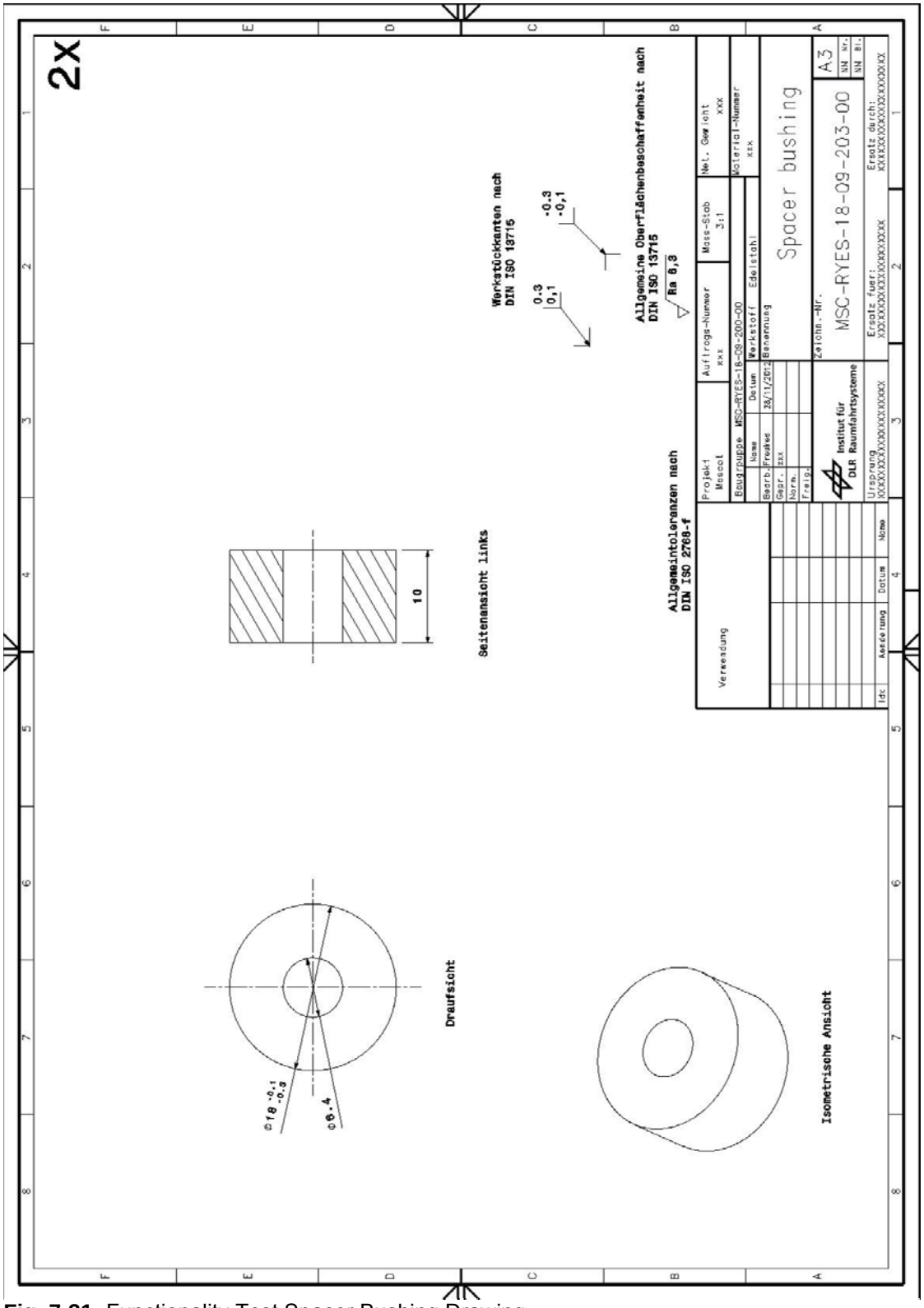

Fig. 7-31: Functionality Test Spacer Bushing Drawing

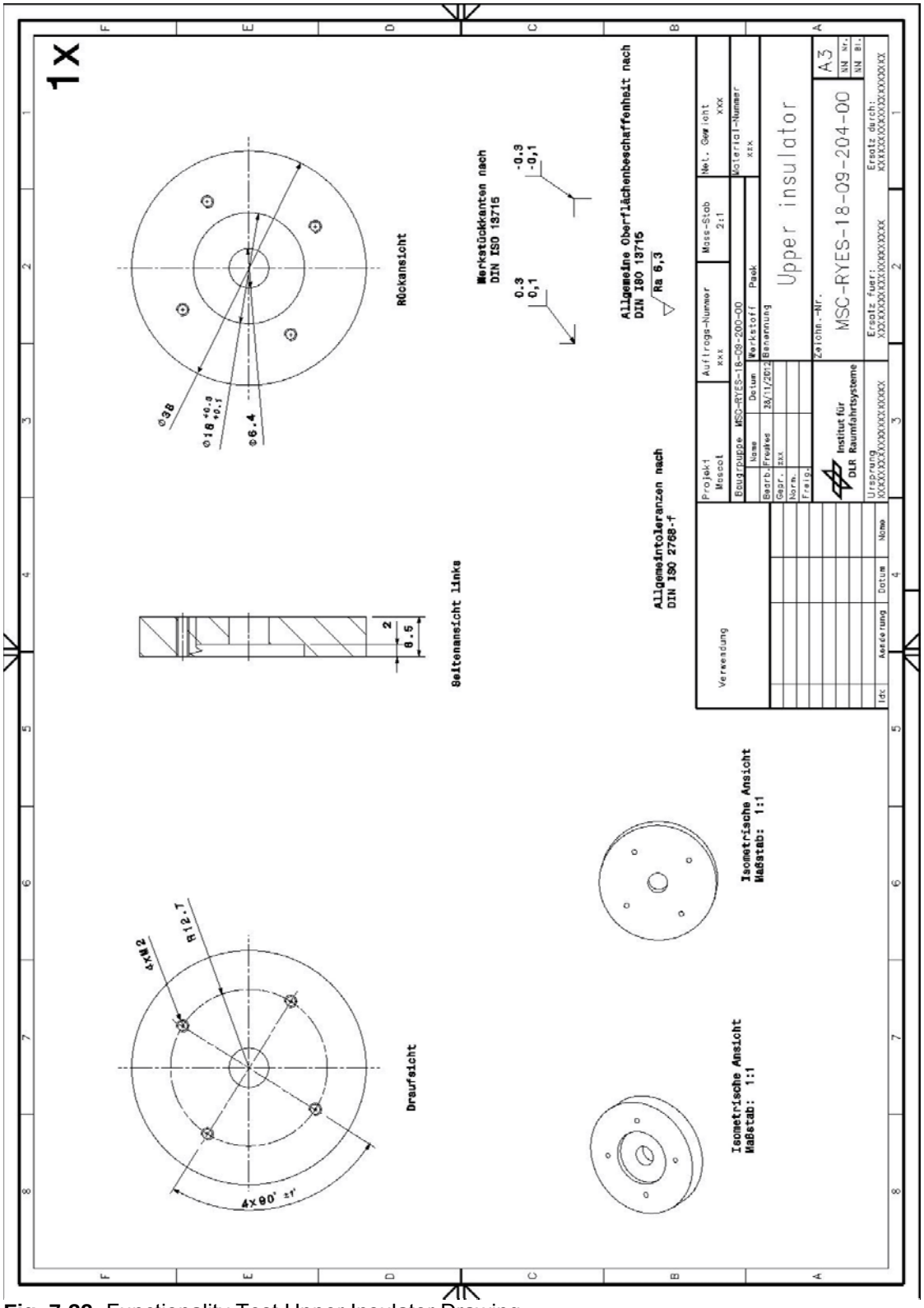

Fig. 7-32: Functionality Test Upper Insulator Drawing

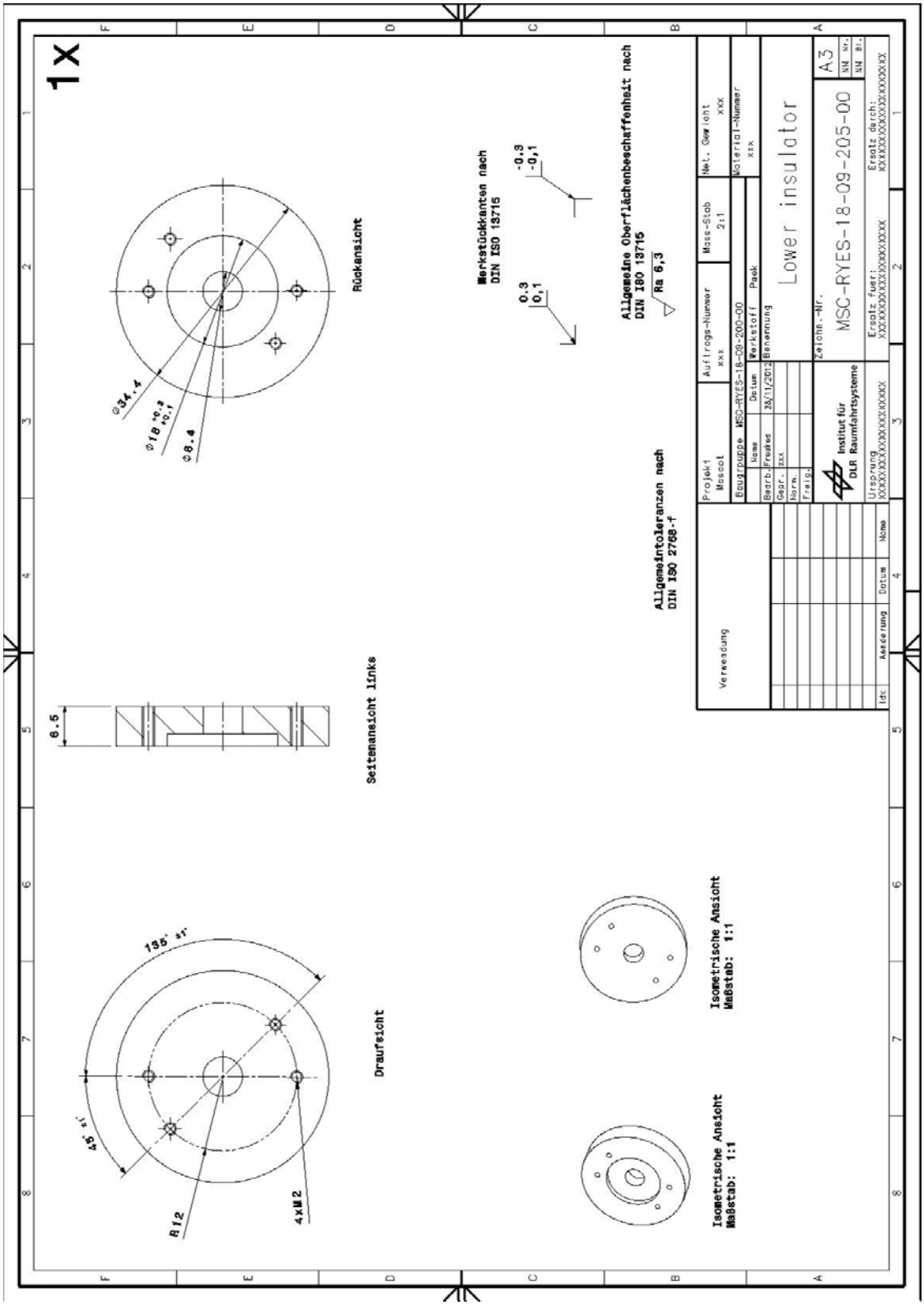

Fig. 7-33: Functionality Test Lower Insulator Drawing

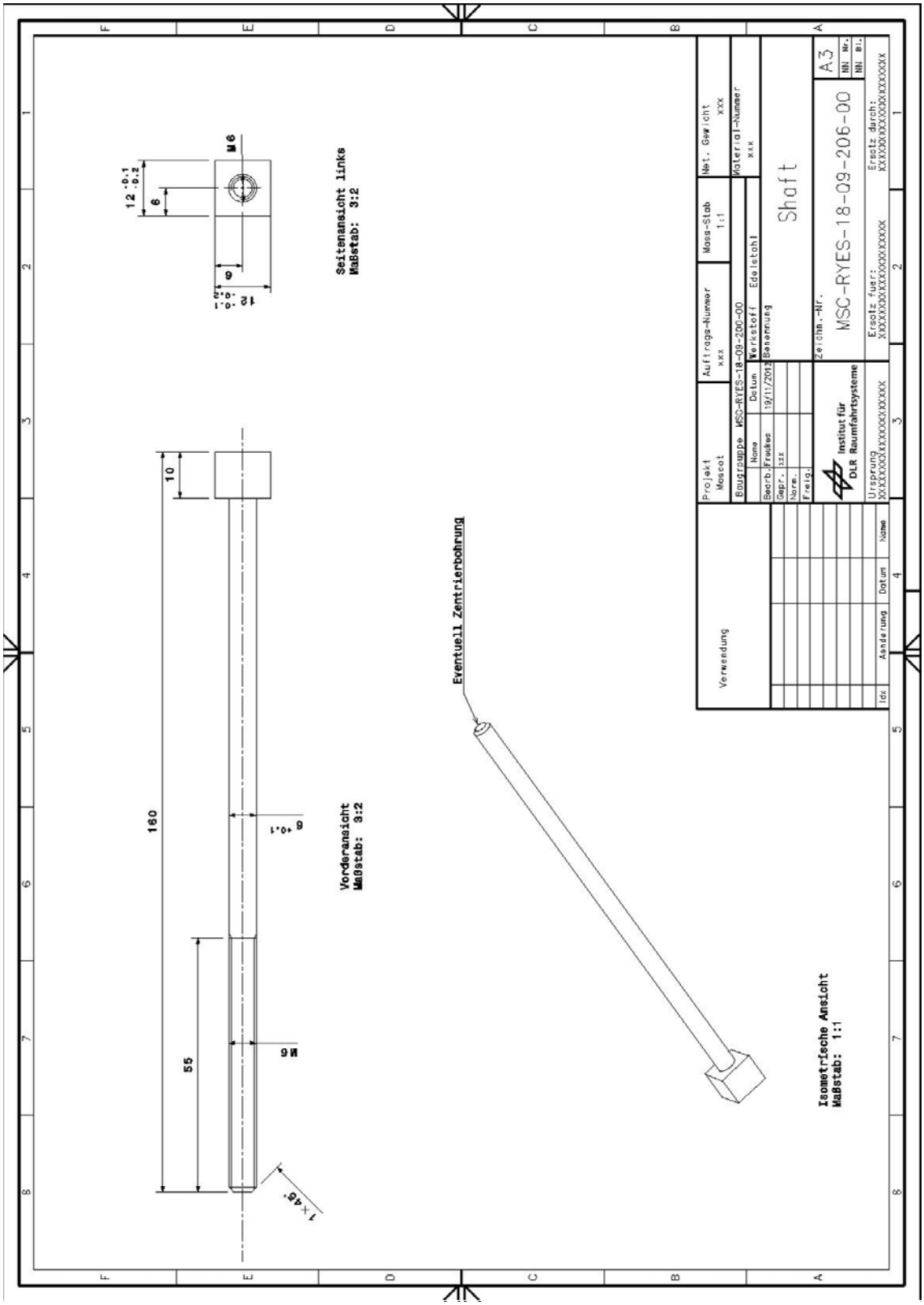

Fig. 7-34: Functionality Test Shaft Drawing

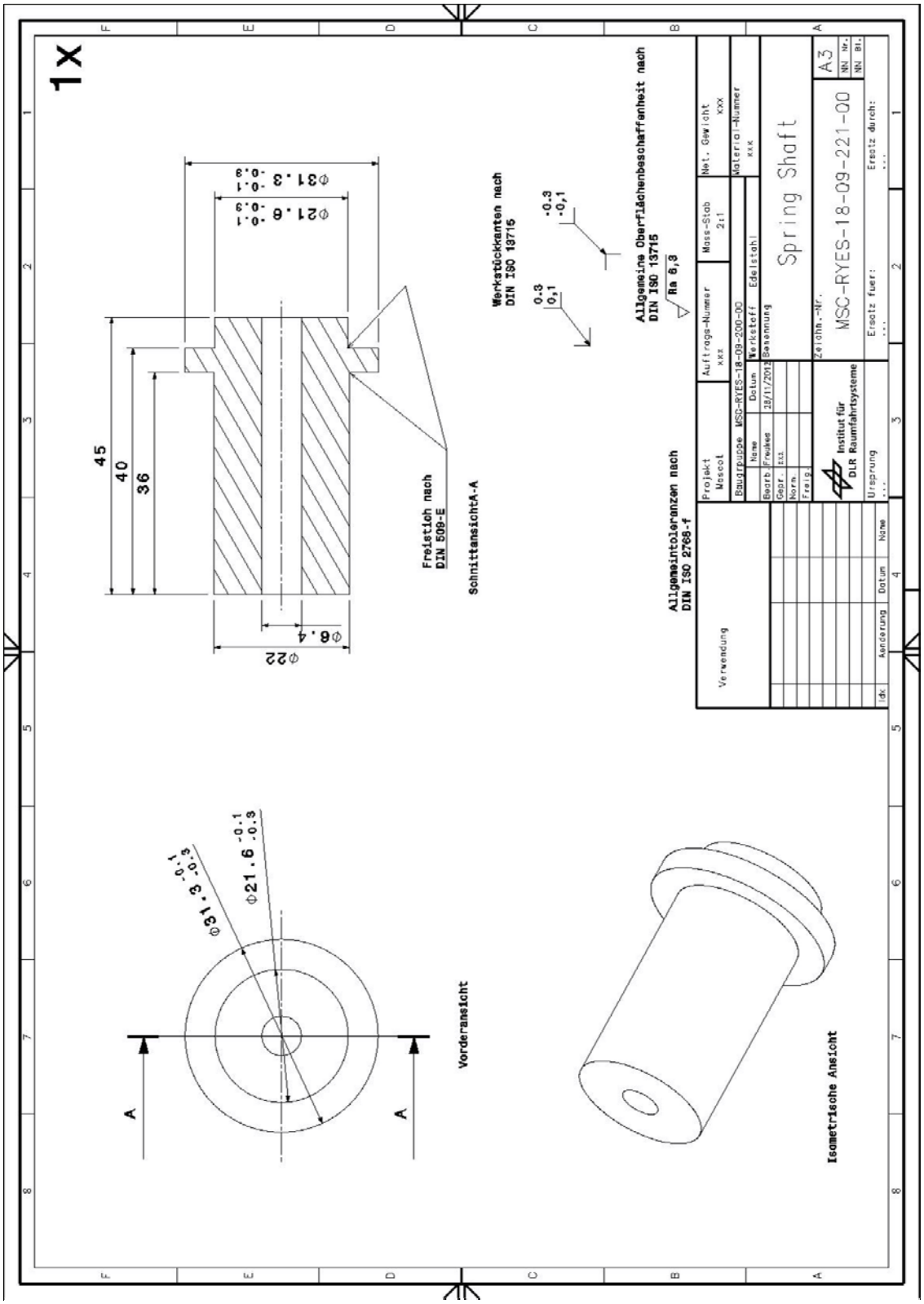

Fig. 7-35: Functionality Test Spring Shaft Drawing

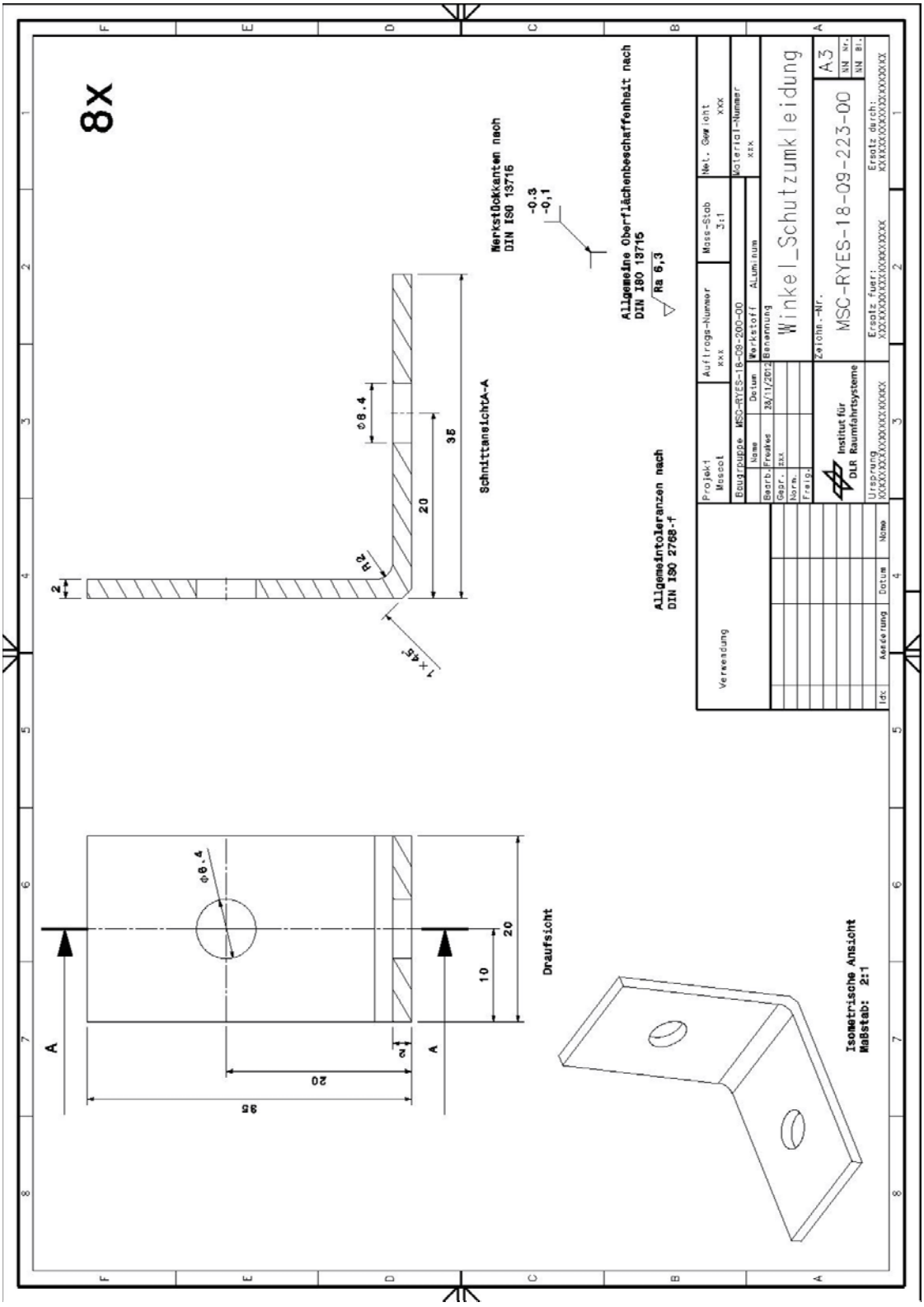
8x
Werkstückkanten nach DIN ISO 13715
Allgemeine Oberflächenbeschaffenheit nach DIN ISO 13715
Ra 6,3
Allgemeintoleranzen nach DIN ISO 2768-f
Schnittansicht A-A
Draufsicht
Isometrische Ansicht
Maßstab: 2:1
Winkel_Schutzumkleidung
MSC-RYES-18-09-223-00
A3
Institut für DLR Raumfahrtsysteme

7.2 Adaption of the PRM

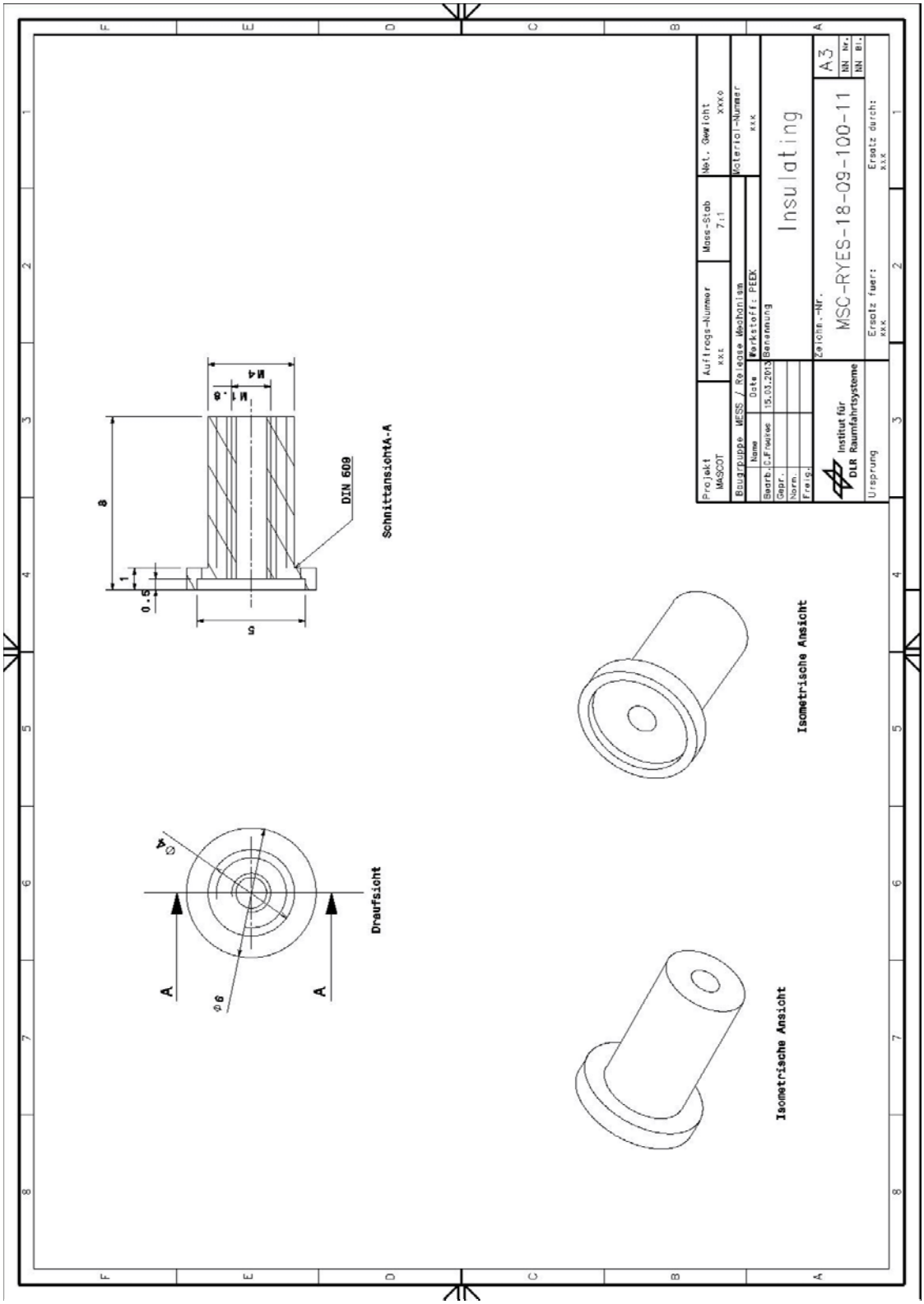

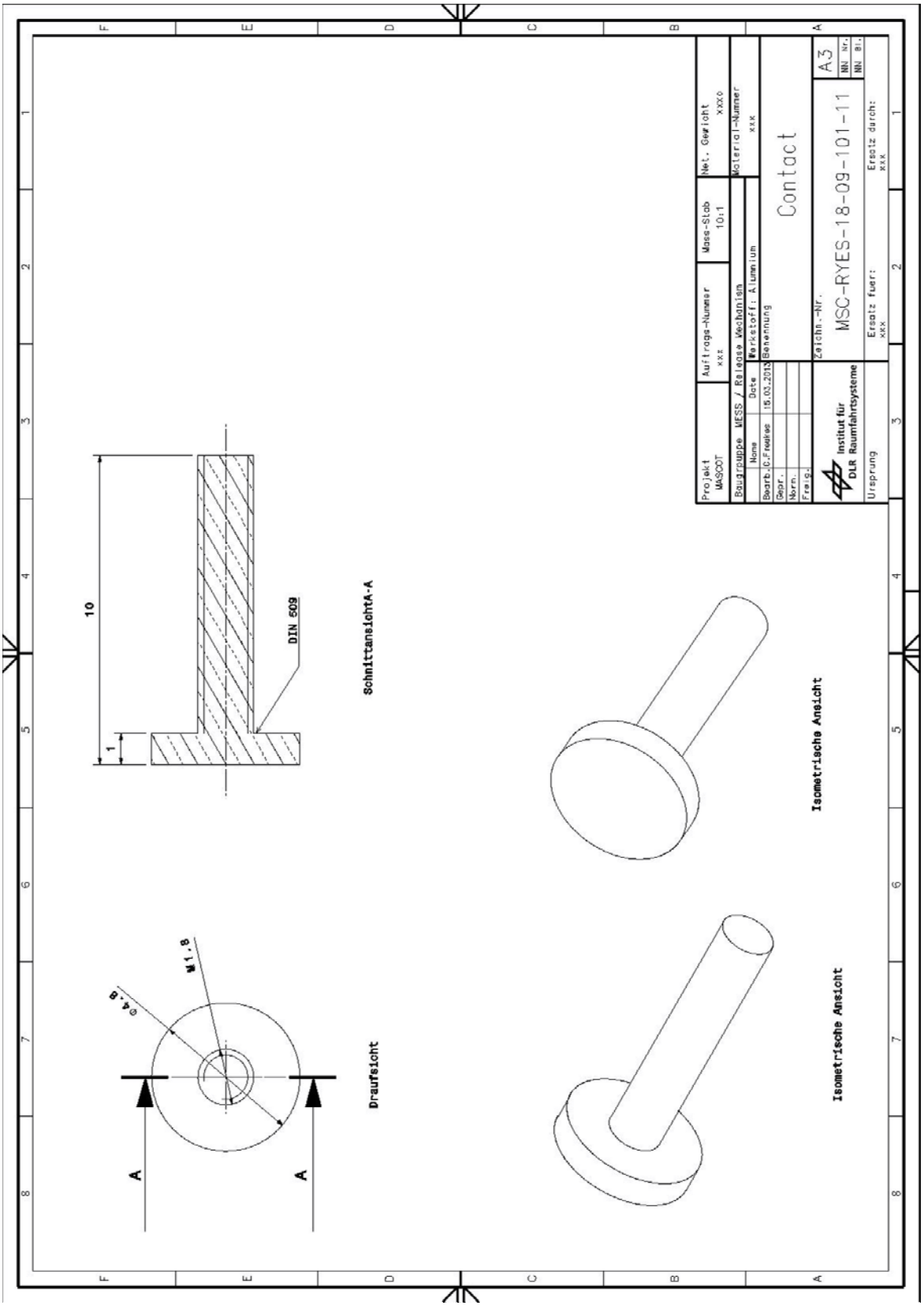
Projekt
MASCOT
Auftrags-Nummer
xxx
Mass-Stab
10:1
Net. Gewicht
xxxg
Baugruppe MESS / Release Wechnion
Material-Nummer
xxx
Name
Date
Bearb. C.Freakes
15.03.2012
Gepr.
Norm.
Freig.
Werkstoff: Aluminium
Bezeichnung
Contact
Institut für
DLR Raumfahrtsysteme
Zeichn.-Nr.
MSC-RYES-18-09-101-11
A3
Ursprung
Ersatz fuer:
xxx
Ersatz durch:
xxx
10
1
DIN 509
Schnittansicht A-A
M1.8
Ø4.8
A
A
Draufsicht
Isometrische Ansicht
Isometrische Ansicht

7.3 Literature/Sources

[1] DLR

[2] JAXA

[3] Intranet des DLR

MSC-INOE-TY-nnn MASCOT Proposal

[RD01] Mascot Science Requirement Document

Preload release mechanism configuration

[4] http://www.thermibel.be/documents/pt100.xml?lang=en

Date:09.01.2013

[5] Department of Mechanical and Materials Engineering

The University of Western Australia Douglas Wright

http://school.mech.uwa.edu.au/~dwright/DANotes/springs/intro/intro.html#top Date: 14.01.2013

[6] http://www.smashinglists.com/top-10-theories-on-beginning-of-life-on-earth/ Date:15.01.2013

[7] http://www.sensorsmag.com/sensors/temperature/temperature-measurement-1030 Date:20.03.2013

[8] http://www.spirol.com/library/main_catalogs/disc_us.pdf

Date:20.03.2013